AD-A044 471 NAVAL AIR PROPULSION TEST CENTER TRENTON N J PROPULS--ETC F/G 21/5
TURBINE ENGINE DIAGNOSTICS DEVELOPMENT PHASE III REPORT.(U)
JAN 77 R T LAZARICK, P WOROBEI, J E ZOOG

UNCLASSIFIED NAPTC-PE-88 NL

1 OF 2
AD A044471

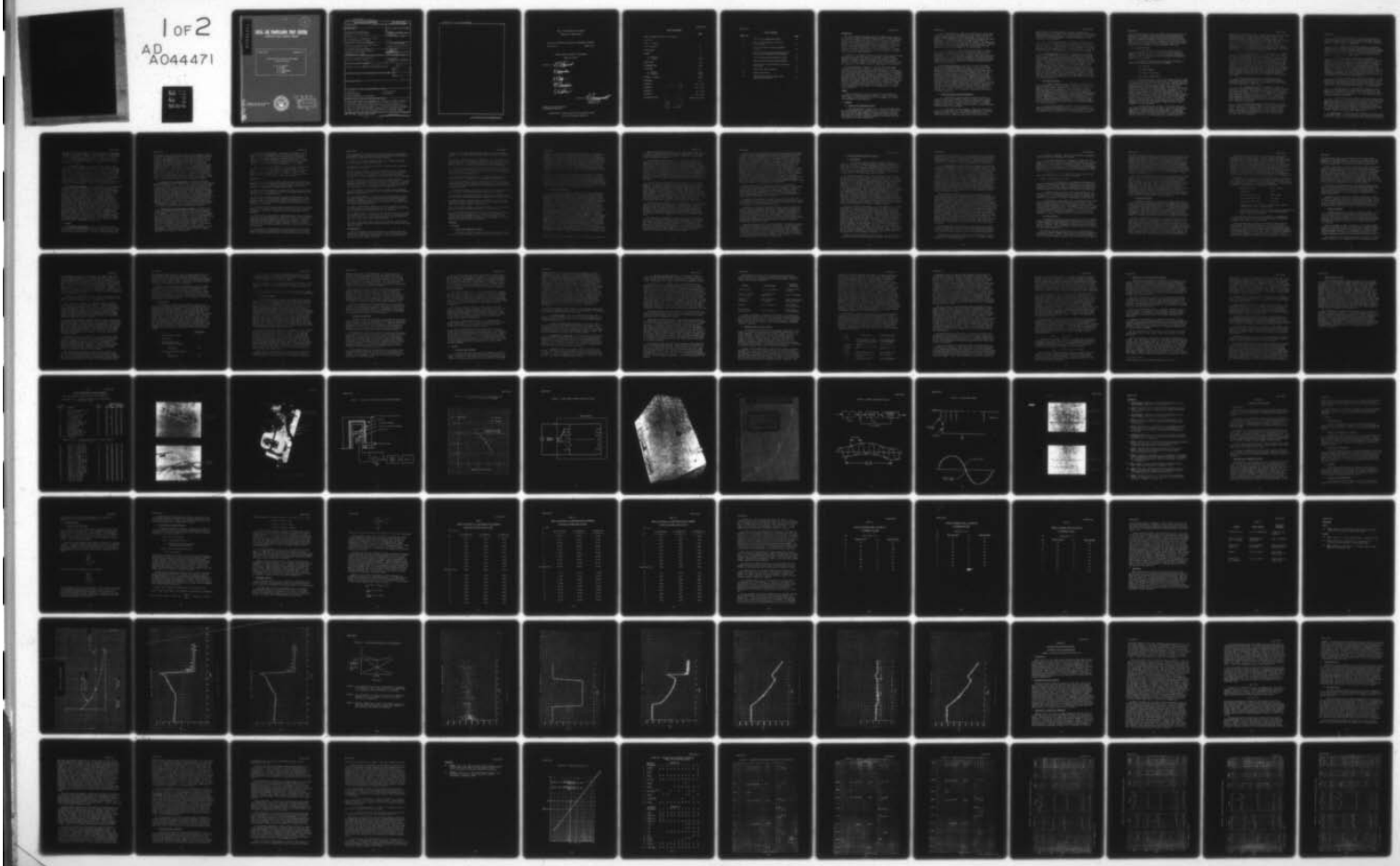

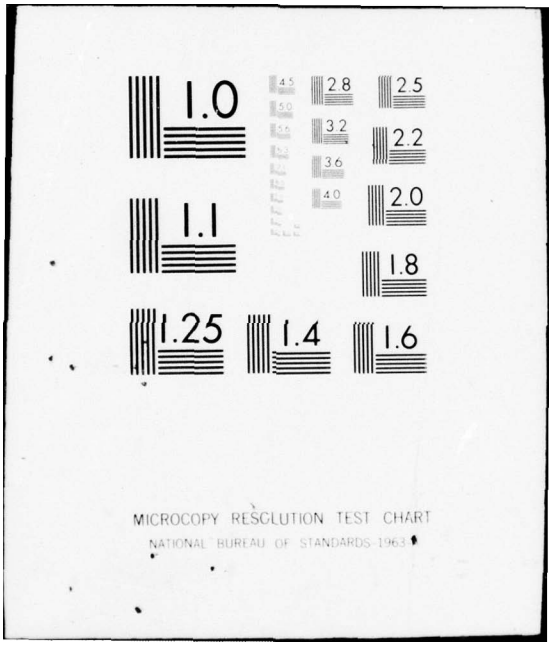
1.0
1.1
1.25
1.4
1.6
1.8
2.0
2.2
2.5
2.8
3.2
3.6
4.0
4.5
5.0
5.6
MICROCOPY RESOLUTION TEST CHART
NATIONAL BUREAU OF STANDARDS-1963-A

(12)
B.S

NAVAL AIR PROPULSION TEST CENTER

TRENTON, NEW JERSEY 08628

NAPTC-PE-88 JANUARY 1977

TURBINE ENGINE DIAGNOSTIC DEVELOPMENT
PHASE III REPORT

By R. T. LAZARICK
P. WOROBEI
J. E. ZOOG
R. E. OBERNDORFER
C. N. SHEN

APPROVED FOR PUBLIC RELEASE;
DISTRIBUTION UNLIMITED

UNCLASSIFIED

SECURITY CLASSIFICATION OF THIS PAGE *(When Data Entered)*

REPORT DOCUMENTATION PAGE	READ INSTRUCTIONS BEFORE COMPLETING FORM
1. REPORT NUMBER: NAPTC-PE-88	2. GOVT ACCESSION NO. / 3. RECIPIENT'S CATALOG NUMBER
4. TITLE *(and Subtitle)*: TURBINE ENGINE DIAGNOSTICS DEVELOPMENT PHASE III REPORT.	5. TYPE OF REPORT & PERIOD COVERED: FINAL rept.
	6. PERFORMING ORG. REPORT NUMBER: NAPTC-PE-88
7. AUTHOR(s): R. T. LAZARICK, P. WOROBEI, J. E. ZOOG, R. E. OBERNDORFER, C. N. SHEN	8. CONTRACT OR GRANT NUMBER(s): NONE
9. PERFORMING ORGANIZATION NAME AND ADDRESS: Naval Air Propulsion Test Center (PE42) Trenton, New Jersey 08628	10. PROGRAM ELEMENT, PROJECT, TASK AREA & WORK UNIT NUMBERS: 62241N, AIRTASK A330330C/ 052B/5F41-433-301
11. CONTROLLING OFFICE NAME AND ADDRESS: Naval Air Systems Command (AIR-330) Department of the Navy Washington, D.C. 20361	12. REPORT DATE: JANUARY 1977
	13. NUMBER OF PAGES: 154 (12) 153p.
14. MONITORING AGENCY NAME & ADDRESS *(if different from Controlling Office)*: Naval Air Propulsion Test Center Trenton, New Jersey 08628 (16) F41433	15. SECURITY CLASS. *(of this report)*: UNCLASSIFIED
	15a. DECLASSIFICATION/DOWNGRADING SCHEDULE

16. DISTRIBUTION STATEMENT *(of this Report)*

(17) WF41433301

APPROVED FOR PUBLIC RELEASE; DISTRIBUTION UNLIMITED

DDC RECEIVED SEP 22 1977 B

17. DISTRIBUTION STATEMENT *(of the abstract entered in Block 20, if different from Report)*

18. SUPPLEMENTARY NOTES

19. KEY WORDS *(Continue on reverse side if necessary and identify by block number)*

DIAGNOSTICS
ENGINE MONITORING
VARIABLE GEOMETRY CYCLE SIMULATION
GAS PATH ANALYSIS
DATA HANDLING

20. ABSTRACT *(Continue on reverse side if necessary and identify by block number)*

Turbine engine diagnostic development was continued in a number of hardware and software areas. New development and/or evaluation work was done on a turbine inlet temperature sensor, Ferrograph iron-in-oil monitor, and vibrating cylinder pressure transducer. Software work included investigation of data smoothing techniques, study of multiple fault gas path analysis applied to TF30-P-408 engine data, development of an advanced variable geometry engine cycle deck, and sensitivity study of the TEDD program.

DD FORM 1 JAN 73 1473 EDITION OF 1 NOV 65 IS OBSOLETE S/N 0102-014-6601

UNCLASSIFIED

SECURITY CLASSIFICATION OF THIS PAGE *(When Data Entered)*

407728

NAVAL AIR PROPULSION TEST CENTER

TRENTON, NEW JERSEY 08628

PROPULSION TECHNOLOGY AND PROJECT ENGINEERING DEPARTMENT

NAPTC-PE-88 JANUARY 1977

TURBINE ENGINE DIAGNOSTICS DEVELOPMENT

PHASE III REPORT

Prepared by: R. T. LAZARICK

P. WOROBEI

J. E. [illegible]

R. E. OBERNDORFER

C. N. SHEN

Approved by: R. K. BRUMWELL
Commander, USN
Director, PE

AUTHORIZATION: NAVAIR AIRTASK 330330C/052B/5F41433301
Work Unit Assignment NAPTC-624

TABLE OF CONTENTS

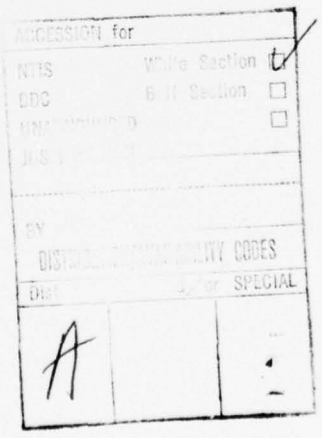

LIST OF FIGURES

INTRODUCTION

The Turbine Engine Diagnostic Development (TEDD) Program began in FY 1972 when the Naval Air Systems Command (NAVAIR, AIR-330) authorized the Naval Air Propulsion Test Center (NAPTC) to develop and demonstrate turbine engine dianostics by full-scale engine testing (reference 1). During FY 1972, NAPTC accomplished Phase I of the program, which consisted of generating and testing a computer program which would track a TF30-P-408 engine operating at sea level conditions and output diagnostic messages in real-time to the test cell operator. A unique vibration monitoring system was used, as well as new type transducers for oil quality and speed sensing.

In Phase II, the computer program was restructured, using new engine operating mode recognition logic and providing for thermodynamic performance analysis. New hardware items used included a radiation pyrometer, internally mounted accelerometer and real-time graphic display. The range of engine testing was extended to include sea level ram conditions. The results of Phase II were reported in reference 2.

With the completion of Phase II in FY 1973, full-scale engine testing was discontinued. However, a large quantity of data was recorded for use in the follow-on software evaluations. It was planned that follow-on TEDD sensor evaluations would be performed in conjunction with other NAPTC engine test programs on a piggy-back basis. Reference 3 authorized NAPTC to continue the exploratory development effort in Task Area WF41.433.301, Advanced Auxiliary/Equipment Systems, in accordance with Work Unit Plan No. NAPTC-624 of June 1973. In TEDD Phase III, this diagnostic development effort was continued in a number of hardware and software areas where further development work was identified. These areas were determined from Phase II test results, as well as from an overall knowledge of future diagnostic requirements and the current state-of-the-art.

SUMMARY

Since the TEDD Phase III effort addressed the development and demonstration of diagnostic elements (sensors, software techniques) rather than a complete diagnostic system, this summary is an item by item description of these efforts.

A. Hardware

1. Turbine Inlet Temperature Sensor

Direct measurement of turbine inlet temperature in modern Navy gas turbine engines is not attempted due to the lack of durability of sensors located in these regions of elevated temperature. If such a measurement was available, diagnostic capability would be improved, particulary in the areas of gas path analysis, hot section life, and overtemperature severity determination.

b. In TEDD Phase III, NAPTC contracted with Tyco Laboratories to develop a turbine inlet gas temperature probe based on the concept of an incandescent immersed sapphire light pipe. The tip of the sapphire, being immersed in the hot gas, becomes incandescent and emits light which is transmitted through the sapphire pipe itself to a photosensor. Since the emission is directly related to the temperature of the probe tip, it is a good indication of that temperature. Sapphire ($Al_2 O_3$) is one of the few materials that can be used in the high temperature, oxidizing environment at the turbine inlet.

c. A prototype probe was fabricated and tested in a burner rig at NAPTC. Although the amount of testing was limited, and the rig temperature was limited to 700°C (1300°F), the results were encouraging. The basic concept that sufficient light will be generated by the probe tip to allow accurate measurement of the temperature was demonstrated, and some indication of mechanical integrity was obtained. Total response time needs improvement, although the response of the probe tip itself is good.

2. Ferrograph Oil Monitor - Iron in oil is one of the prime indicators of problems in bearings and gears. To date, no airborne device can quantitatively identify the amount of iron in oil. The Ferrograph is a device which precipitates magnetic particles from the oil by size through the use of a variable magnetic field. It then measures the optical density of the larger and smaller particles. The ratio of particle densities is then computed and can be related to the health of oil wetted components. NAPTC has contracted with Trans-Sonics, Inc. to take the Ferrograph concept and develop a prototype real-time engine mountable unit for test cell evaluation. A unit was delivered to NAPTC and evaluated on a bearing rig. Preliminary analysis of the rig testing indicated the instrument is capable of detecting incipient bearing failures related to fatigue spalling and abnormal wear. Further evaluation of the unit is being made on a running engine (TF34), and it is planned to develop an airborne unit for flight evaluation.

3. Vibrating Cylinder Pressure Transducer

a. The vibrating cylinder pressure transducer (VCPT) is a relatively new type of pneumatic pressure transducer which utilizes natural vibration modes of a metal cylinder to generate a frequency output as a function of applied pneumatic pressure. Its frequency-modulated output makes it immune to noise and drift to which amplitude-based transducers are susceptible

b. A VCPT manufactured by Hamilton Standard was evaluated at NAPTC during TEDD Phase III. The transducer evaluated is an absolute pressure unit with a range of 0-350,000 newtons/m^2 (0-50 psia). Unlike conventional transducers, the output of the VCPT is a non-

linear function of applied pneumatic pressure. Therefore, the measured pressure is calculated from a manufacturer supplied polynomial which relates frequency output to the applied pressure. An additional manufacturer supplied temperature compensation polynomial is also utilized in the calculation.

c. The evaluation consisted of laboratory calibrations and installation on a J52 engine. Laboratory calibrations before and after the engine test determined the transducer accuracy to be better than 0.2% full scale. The repeatability of the transducer, after more than 200 hours of on-engine use, was determined to be well within the uncertainty limit of the laboratory standard (± 0.07% of reading).

4. Oil Debris Monitor - The K West oil debris monitor utilized during the TEDD Phase I and II tests was installed on a TF30-P-412A engine undergoing afterburner lighting tests. This device consists of a polyester insulating screen interwoven with stainless steel conductors. When conductive particles are trapped on the surface of the screen, an electrical "short" occurs, causing a decrease in total resistance at the sensor terminals. The unit was installed in the scavenge oil line for main bearings no. 4, 4 1/2, 5 and 6 on the TF30-P-412A engine for a total of 65 hours test time. There was no change in the output reading during the test, indicating the integrity of the oil system components. This agrees with the results of SOAP samples for this engine. Thus, no unsatisfactory operation has been noted with the K West unit during any of the TEDD phases, but it has not been subjected to an engine problem situation where its effectiveness could be evaluated.

5. Hot Section Analyzer

a. A Howell Instrument Computer Recorder was installed on a TF30-P-412A engine which was undergoing a 150 hour accelerated cyclic endurance test at NAPTC. This unit, also referred to as a Time Temperature Recorder and Integrator (TTRI), has inputs of turbine inlet temperature (indirectly measured) and high rotor speed, and provides a cumulative Hot Section Factor Count based on the integrated time-temperature exposure and the hot section metallurgical characteristics of the engine. It also displays Hot Section Factor Time (1015°C, 1900°F and above), time above 1177°C (2150°F), total engine time, and maximum temperature, and has three overtemperature flags and one overspeed flag. The unit performed satisfactorily throughout the duration of the test.

b. This type of diagnostic analysis has the potential of impacting maintenance philosophy, that is to perform maintenance "on-condition" rather than at the current fixed time intervals. In order to accomplish this, a correlation of Hot Section Factor Counts and

hot section deterioration must be determined from a large sampling of engines in fleet service. This unit, which is limited because of the number of parameters measured, may not obtain sufficient information to generate a reliable correlation for hot section condition. However, this approach, expanded to include low cycle fatigue, thermal shock and other hot section distress mechanisms, offers the potential for significant improvement in engine maintenance philosophy.

6. Vibration Analyzer

a. The vibration analyzer was built by General Electric Company, Binghamton, New York, for the TF34-GE-2 and subsequently adapted for computer control. There was no problem in using it on the TF30-P-408 since the system is easily converted to any engine by changing ratios and limits.

b. The analyzer contains signal processing electronics to evaluate four classes of malfunctions in an engine.

(1) Bearings

(2) Mass unbalance

(3) Gears - local defect

(4) Gears - gross defect

c. Digital Comb Filter - In the latter three processes, signal extraction is done by the digital comb filter. The digital comb filter is a time-averaging device of 256 discrete points. The time-averaging feature tends to cancel noise on the signal. The comb filter is synchronized with a rotating member so that each of 256 points examines the same point on a rotating member. The filter has responses at its tuning frequency and integer multiples (harmonics) of it. Any signals or noises which are not exactly integer multiples of the tuning frequency will be rejected. The significance of this type of filtering can be seen when a vibration signal from a gearbox is applied to the filter. This signal will consist of the sum of all gearbox shaft and meshing vibrations. By tuning the filter to a gearshaft frequency, only the shaft and its gear meshing vibration are passed through the filter, since its frequency (number of teeth x shaft frequency) is a shaft harmonic.

d. Bearing Malfunction Processor - The bearing malfunction discriminant processor evaluates the Impact Index of the acceleration signal from a bearing housing. The Impact Index is a normalized dimensionless quantity whose value is indicative of the incipient bearing malfunction. The Impact Index value is one-half the ratio of the peak signal level to its average level. An Impact Index for a

normal bearing will range from two to three and during spall initiation, from three to four. As the spall increases in size (but is still relatively small), the Impact Index may increase to eight to ten. Beyond this, with increasing spall size, the Impact Index will decrease due to the increase in average acceleration. The Impact Index discriminant for normal bearings is not a function of engine speed; i.e., it will remain between three and four over the entire engine operating range. For a bearing with malfunction, the Impact Index may increase by up to 30 percent with increasing engine speed. Full scale on the indicator is an Impact Index of 10.

e. Mass Unbalance Processor - The mass unbalance discriminant processor is a narrow band tracking filter which selectively filters vibration energy associated with the mass unbalance of a rotor system. The output is displayed as a displacement on a meter calibrated from 0 to 100 percent full scale, where full scale is equal to 2.54×10^{-3}m (10 mils) double amplitude. The signal is first filtered to accept frequencies in the 10 Hz to 400 Hz band. It is then filtered by the digital comb filter, which is tuned to either once per fan or core frequency. The output of the comb filter now represents the acceleration associated with the rotor mass unbalance. A double integration then yields the displacement associated with the rotor mass unbalance. To obtain a signal suitable for display, the displacement signal is average detected and displayed on a meter calibrated to read peak-to-peak values.

f. Local Gear Defect Processor - The local gear defect discriminant processor evaluates the Impact Index associated with a given gear mesh vibration signature. Local defects on a gear consist of spalled, deformed, or cracked teeth.

(1) A normal gear in mesh will generate a sinusoidal vibration at the gear meshing frequency. When a local defect is present on a tooth of the gear, a transient vibration will be generated each time that tooth meshes. The level of the transient will be considerably higher than the normal meshes. This type of signal can easily be discriminated by an Impact Index measurement. Since, in practice, a single gear mesh vibration is mixed with other mesh vibrations and noise, this mesh must be extracted from the total signal before its Impact Index can be evaluated.

(2) The gear discriminant is implemented by tuning the digital comb filter to the shaft frequency of the gear being analyzed. At this frequency, only harmonics will be passed through the comb filter. The harmonic of interest will be the nth harmonic corresponding to the gear under analysis which has "n" number of teeth. After the gear mesh has been isolated, the signal is evaluated for its Impact Index and displayed.

g. Gross Gear Defect Processor - The gross gear defect discriminant processor evaluates the modulation of gear mesh vibration due to its shaft frequency. A gross gear defect includes misaligned, loose, or eccentric gears on a gearshaft.

(1) A normal gear in mesh will generate a sinusoidal vibration due to its shaft frequency. When a gear has a gross defect, the gear meshing vibration will be modulated by the gearshaft frequency. Since this signal is normally mixed with other gear mesh vibrations and noise, the characteristic gear mesh vibration signature must be extracted from the total vibration signal.

(2) The discriminant measurement is implemented by tuning the digital comb filter to the gearshaft frequency of interest. This will allow integer multiples of the shaft frequency to pass through the filter while rejecting all other signals. The modulation will be passed through the filter. The measurement which is then made on the signal is the ratio of the modulation amplitude to the carrier (gear mesh) amplitude yielding the modulation index, which ranges from 0 to 100. This is a dimensionless parameter. To normalize the ratio, an automatic gain control (AGC) is used. The AGC is a variable gain amplifier that is electronically controlled to boost low level signals up to levels that may be detected.

(3) The AC portion, which contains the modulation, is low pass filtered to allow only the modulating frequency to pass. The low pass filter is programmable so that the filter cutoff may be set for various gears and various engine power settings. The output of the low pass filter is then peak detected and displayed on the output meter.

(4) The section of the analyzer of interest for this phase of the TEDD program was the gross gear defect processor. The analyzer gave unsatisfactory readings for the TEDD engine, and experiments were conducted to determine why. Part of the problem was due to the method of speed measurement.

(5) To provide a speed signal for the gear box experiments, the signal is taken from a tach generator mounted on the gear box. The signal has modulation on it due to gear back lash and play in the gear mesh, which looks like speed changes to the analyzer. A percent modulation can be measured by comparing the period changes that occur to a steady signal of the same frequency. In addition to the problems from the modulated tachometer signal, additional filtering was required to smooth the digital comb filter output.

7. Speed Sensor - In conjunction with the vibration analyzer effort in Phase III, a study of various methods of speed sensing was conducted. The gear box mounted tach used on the TF30 proved to be insufficient for

for vibration analysis due to gear backlash and play, creating signal modulation. The primary emphasis of this study was the determination of signal modulation as a function of pickup location. The locations investigated were the gear box, the nose cone and a direct shaft pickup. A blade passage technique was also investigated, and this technique offers acceptable modulation characteristics for use with the vibration analyzer.

8. Radiation Pyrometer - The Solar radiation pyrometers used during TEDD Phase II engine testing exhibited signal characteristics which required further investigation. This Phase III study addressed particularly the noise in the analog output circuit. Discussion with other users of radiation pyrometers revealed the relationship between signal noise and probe location. Locating the probe such that the flame cannot be viewed (i.e., behind the blade row looking forward or looking radially) resulted in reduced noise levels. Another method of reducing the noise which was investigated is the use of the vibration analyzer filter circuitry to remove the noise. The filtering technique also shows promise for improving the pyrometer output.

9. Internal Accelerometer - One of the reasons vibration monitoring techniques are quite complex is the communication path between the vibration sources and the vibration pickup. An accelerometer which is not closely coupled to the bearing (or other vibration source) which is to be diagnosed will pickup vibration from other sources. This requires the analyzer to "sort out" the vibrations, making the technique complex. Therefore, reduction in analysis complexity can be realized if accelerometers are directly mounted to the bearing to be monitored. There are some common problems associated with this task that have been under design consideration for several years. These problems are the environmental restrictions on the accelerometer, signal lead routes, and bearing housing accessibility, which places restrictions on the design of the engine. The problem of limited life for the accelerometer makes it necessary that it be accessible without engine disassembly. One approach is to place the accelerometer at the bearing through a "dipstick". This requires a suitable engine design, but places the accelerometer and lead in a position of accessibility. This approach is well suited to rigidly mounted bearings; soft-mounted bearings (such as intershaft bearings and other bearings not rigidly mounted to the engine frame) are not conducive to close coupled accessible accelerometer installation.

B. Software

1. Data Smoothing Techniques - During the TEDD Phase II test program, a limited moving average smoothing technique was used to improve the stability of the mode detection routine and reduce the scatter in the performance analysis results. The moving average technique means

the parameter used in the diagnostic logic is the average of the last n values of that parameter (n in TEDD Phase II was adjustable between 1 and 4). This technique (for $n > 1$) will reduce the noise level of the smoothed parameter and will reduce the rate of response. It was recognized that further investigation was required in the area of data smoothing, and especially the consideration of exponential smoothing. Exponential smoothing is a method of estimating each new parameter value in a time series of data by letting the new smoothed value be equal to a fraction $(1 - \alpha)$ of the previous smoothed value, plus a fraction (α) of the new parameter value. α is defined as the weight given to the new parameter value. A study of data smoothing was made during TEDD Phase III, using data recorded during Phase II and also from another NAPTC engine test program. As a result of this study, it was shown that the exponential smoothing technique is better suited to TEDD applications than the moving average technique.

2. Multiple Fault Gas Path Analysis - The NAPTC steady-state performance analysis used in TEDD Phase II was designed to detect single gas path performance faults. However, both single and multiple fault conditions were tested and recorded. This actual test data, acquired at known fault level conditions, provided a means of evaluating the Hamilton Standard "Parameter Interrelationships" approach to multiple fault steady-state performance analysis. During TEDD Phase III, NAPTC contracted (Contract No. N00140-74-C-0582) with the Hamilton Standard Division of United Technologies Corporation to apply and demonstrate their methods, using the TF30-P-408 engine data recorded during Phase II testing. The results of this program verify the capability of this approach to identify and quantify single and multiple gas path performance faults. A further study is being conducted by NAPTC in-house to determine the sensitivity of this approach to "time series" data, i.e., continuous real-time steady-state performance analysis.

3. Diagnostics on Variable Geometry Engines - The need for the capability to simulate the performance of a gas turbine engine with variable geometry arose from the consideration of gas path analysis as one element of a diagnostic package for a 1980-85 aircraft. During the period from January 1974 through March 1975, a variable geometry engine cycle deck was developed at NAPTC. The first application of the data from this cycle deck was to provide variable geometry data to the Hamilton Standard Division of United Technology Corporation for study using the parameter interrelationships method of gas path analysis. The purpose of this study was to identify unique problem areas associated with diagnosing variable geometry engines. Additionally, this study identified critical instrumentation accuracy requirements. This work was conducted under Contract No. N00140-75-C-0049, from 1 April to 1 October 1975.

4. TEDD Sensitivity Study - The ability of diagnostic logic to perform its intended task is limited by the accuracy and/or repeatability of the incoming data. The characteristics of candidate sensors must be viewed with respect to their application, that is, can the sensor perform adequately for the logic using that parameter. Sensitivity studies establish the relationship between sensor performance and the diagnostic logic requirements for that sensor.

During Phase III, a sensitivity study was performed utilizing the gas path analysis technique developed during TEDD Phase II. The results of this study can be used to determine the sensor characteristics required for a given level of confidence in the gas path analysis results. Another aspect of the study considered the sensor characteristics required for hot section life computation.

CONCLUSIONS

1. Initial rig testing of a prototype sapphire light pipe turbine inlet temperature sensor has demonstrated the feasibility of the basic concept to 705°C (1300°F) and has shown encouraging results with respect to sensitivity, strength and potential time response.

2. Analysis of data acquired on a bearing rig indicates that the engine mountable real time Ferrograph is capable of detecting abnormal wear and bearing failure in each case tested.

3. The vibrating cylinder pressure transducer operated satisfactorily and is superior to the conventional diaphram-type transducer in terms of accuracy, stability, repeatability and ease of operation. Its major drawbacks are its relatively slow response and its sensitivity to variations in gas composition.

4. The K West oil debris monitor has been installed on three TF30 engine tests and has performed satisfactorily. However, it was not subjected to an engine oil system fault situation where its effectiveness could be evaluated.

5. The Howell Hot Section Analyzer (Time Temperature Recorder and Integrator) operated satisfactorily on a TF30-P-412A engine, but more extensive operational experience would be necessary as an end item to verify the potential maintenance benefits for any particular engine. It should be noted that the TTR&I does not record LCF cycles or LCF rupture interactions nor has a correlation between TTR&I output and hot section distress been developed.

6. Installation of a filter before the automatic gain control successfully eliminated noise caused by the digital comb filter of the General Electric vibration analyzer; however, at high engine speeds, gear gross

defect experiments were still over limits due to frequency modulation on the tachometer signal, indicating that blade passage speed data would be satisfactory for use with the GE vibration analyzer.

7. Noise in the radiation pyrometer output can be reduced by placing the probe where it cannot view the flame.

8. Circuitry in the GE vibration analyzer could be used to process and analyze pyrometer signals.

9. The problems of mounting internal accelerometers can be overcome if they are addressed during initial engine design. Where the bearing is soft mounted, there is a communication problem between bearing and accelerometer if the accelerometer is not coupled directly to the bearing.

10. The exponential data smoothing technique is better suited for diagnostic system application than the moving average technique. To apply exponential smoothing in a diagnostic system, it is necessary to have predefined separate α's for steady state and transient modes, depending on the response and accuracy requirements for each parameter.

11. The capability of the Hamilton Standard multiple fault diagnostic approach to identify and quantify single and multiple gas path performance faults has been verified.

12. The variable geometry cycle deck developed for diagnostics studies on advanced engines is a very flexible deck with many potential uses in addition to diagnostics, such as the study of the effects of advanced technology on cycle performance, and the evaluation of performance quotes in an engine development proposal.

13. When a non-dimensional technique is used for diagnosis, such as in the TEDD Steady State Performance Analysis, the repeatability of the data is more important than the absolute accuracy of the data.

14. The TEDD turbine life computations are extremely sensitive to turbine blade temperature error. Calculated erosion life will be in error by 10% for a 5.6°C (10°F) error in gas temperature while creep life shows 35% error for a 5.6°C (10°F) error in gas temperature.

15. High and low rotor speeds (N_2 and N_1) are the most sensitive parameter in the TEDD Steady State Performance analysis at the sea level static condition studied.

RECOMMENDATIONS

1. Further development, test and evaluation of a sapphire light pipe turbine inlet temperature sensor should be pursued to determine the sensor's accuracy and response characteristics, and rig testing should be extended up to the limits of the probe.

2. The real time Ferrograph should be further evaluated on running engines in a test cell, and work should continue to develop an airborne unit.

3. A number of possible failure mechanisms should be investigated for engine hot section life diagnostics, including creep, low cycle fatigue, thermal shock and erosion, because current analytical approaches do not provide sufficient accuracy for successful on-condition maintanance.

4. Additional vibration analyzer analysis should be done with data that has a tachometer signal with less than 0.8% modulation, to resolve the question of frequence modulation versus lack of communication, to provide valid gear-gross experiment results.

5. For future vibration analyzer use, a blade passage speed pickup should be used for the high speed rotor and gear box experiments.

6. Pyrometer development should be continued for use in future engine diagnostic systems, with careful consideration given to proper placement of the probe in new engine designs so as to minimize inaccuracies due to reflected radiation.

7. If internally mounted accelerometers are used where the engine bearing is soft mounted, they should be mounted directly on the bearing.

8. Exponential data smoothing should be considered for incorporation in all future NAPTC diagnostic and general transient data reduction procedures.

9. Exponential data smoothing should be considered for use in future diagnostic systems because of its ability to reduce signal noise while maintaining adequate response characteristics.

10. A study should be made to determine the sensitivity of the Hamilton Standard multiple fault diagnostic approach to real time data.

11. Investigation should be made of the Hamilton Standard multiple fault diagnostic approach as applied to an advanced variable geometry gas turbine engine to determine the impact of variable geometry on the analysis complexity, storage requirements, and instrumentation accuracy/repeatability characteristics requirements.

DISCUSSION

A. Hardware

1. Turbine Inlet Temperature Sensor

The ability to directly measure turbine inlet temperature would be a very valuable diagnostic tool as well as being useful as a control

parameter. In TEDD Phase III NAPTC contracted with Tyco Laboratories to develop a turbine inlet gas temperature probe based on the concept of an incandescent immersed sapphire light pipe. The tip of the sapphire, being immersed in the hot gas, becomes incandescent and emits light which is transmitted through the sapphire pipe itself to a photosensor. Since the emission is directly related to the temperature of the probe tip, it is a good indication of that temperature. Sapphire (Al_2O_3) is one of the few materials that can be used in the high temperature, oxidizing environment at the turbine inlet. The high strength and hardness of the sapphire should permit the probe to operate at temperatures up to 1371°C (2500°F).

A prototype probe (Figure 1) was fabricated and tested in a burner rig at NAPTC. Although the amount of testing was limited, and the rig temperature was limited to 705°C (1300°F), the results were encouraging. The basic concept that sufficient light will be generated by the probe tip to allow accurate measurement of the temperature was demonstrated, and some indication of mechanical integrity was obtained. Total response time needs improvement, although the response of the probe tip itself is good. This development effort is further described in reference 4.

2. Ferrograph Oil Monitor

Oil analysis has long been recognized as an effective method of determining the health of engine oil wetted parts as shown by the Spectrometric Oil Analysis Program (SOAP). This approach requires periodic sampling of the oil, the delivery of the sample to an analyzer, and the subsequent reporting of the analysis results to the maintenance personnel responsible for that engine. This approach has at least two drawbacks: (1) samples are taken as a function of engine hours rather than an indicated need for analysis and, (2) the time elapsed between sampling and reporting of the analysis results may exceed the time available to perform effective preventive maintenance. These drawbacks are inherant in any non-real time, non-airborne analysis approach. Chip detectors are a real time, airborne approach currently being used which are limited by the large particle size required to indicate an impending (? already present) failure. Another real time, airborne approach has been formulated by Trans-Sonics, Inc. utilizing their Ferrograph concept. The Ferrograph (Figure 2) is a device which precipitates magnetic particles from an oil sample and deposits them by size through the use of a variable density magnetic field. It has been determined by Trans-Sonics that the progression of many gear and bearing failure mechanisms is directly related to the rate of increase of the presence of large[1] particles in the oil (reference 5). The Ferrograph consequently optically measures the density of the deposited large and small particles and is thereby capable of indicating the presence of a failure mechanism, that is an incipient failure.

---

[1]Large in this instance means between 2 and 10 microns in major dimension.

NAPTC contracted with Trans-Sonics, Inc. under Contract N00140-73-1065 to take the Ferrograph concept and develop a prototype real time engine mountable systems for test cell evaluation. Reference 5 is the Final Report concerning this contract.

For convenience of operation in a test cell, the Real Time (RT) Ferrograph System consists of three units: (1) RT Ferrograph to be mounted on an engine above the oil tank; (2) a pump which is normally mounted below the tank; and, (3) a Control/Indicator designed to be mounted on the wall of the control room so that the indications may be viewed and recorded during engine operation. The RT Ferrograph operates by passing a fixed volume of the engine's lubricating oil through a precipitator tube located in the field of an electromagnet. As the oil flows slowly through the tube in the electromagnet's field, the wear particles are deposited on the inside surface of the tube. The large particles precipitate first and the particle size grades continuously as a function of distance along the tube.

In order to indicate the density of particles of a selected size, a light beam is passed across the tube and the attenuation of the light is measured. The light is conducted from a common lamp assembly to three positions on the tube by means of a trifurcated fiber optic bundle. The first position is a reference and is external to the magnetic field. Light crossing the tube is conducted by a fiber optic bundle to a reference photo resistor. If the color of the oil changes from light to dark, the lamp intensity is automatically increased so that the intensity of light reaching the photo resistor remains constant, independent of color. Light from the same lamp is also conducted to two other positions on the precipitation tube by branches of the trifurcated fiber optic bundle.

The second position, close to the point where the oil enters the magnetic field, measures the deposit of the larger particles. These particles typically range from 2 up to 10 microns. The light which passes up through the tube is blocked by the presence of the opaque metal wear particles. The fractional area of the light beam which is blocked by the particles determines the precentage change of light intensity which is measured by one of the sensing photo resistors in the photo resistor bank.

The sensing photo resistors are connected to integrated operational amplifiers located in the wall-mounted Control/Indicator. The circuits are designed to generate a voltage linearly proportional to the percent area of the light beam covered by the particles. For medium to low densities, the particles are deposited in a single layer and, therefore, the output voltage is linearly porportional to the area of the particles in the field of view. A third light beam is located where smaller particles, on the order of 0.5 microns are deposited.

At the start of an operating cycle, the pump is energized to circulate oil from the engine through the oil passages of the Ferrograph, including a small reservoir of approximately 10cc volume. During this time, an automatic zero circuit adjusts each of the readout circuits to read zero as indicated on the digital displays. At the end of the flushing cycle, which lasts approximately one minute as determined by an internal timing circuit, the pump turns off, the vent line drains, and the oil in the 10cc reservoir begins to run down through the precipitation tube. The speed with which the oil flows through the tube is determined by a restrictor and by the viscosity of the oil. If the oil viscosity is high, the particles migrate through the oil slowly under the influence of the magnetic field, but the oil flows through the restrictor slowly in exactly the same ratio so that the trajectory of the particles is nearly constant and independent of temperature. As the oil heats up, the viscosity decreases so that the oil flows more rapidly. However, the particles also move faster so that the trajectory of the particles remains constant. Therefore, the particles are precipitated in approximately the same location on the precipitation tube independent of temperature.

When all of the oil in the reservoir runs out, air passes the reference poistion causing a sudden increase in the amount of light sensed by the reference photo resistor. This serves as a signal to turn the flushing pump on and the system then automatically recycles itself. At normal operating oil temperatures of 121°C (250°F), the system will recycle approximately once every 10 minutes. At lower temperatures the time increases in proportion to the viscosity.

The percent area covered by the particles at the end of each cycle is proportional to the density of particles having a selected size. During the flushing cycle the particles which have been precipitated are returned to the engine's oil tank from which they came.

The ability of the engine mountable Ferrograph to detect bearing and gear failures was evaluated by rig testing. Ten bearing tests were conducted. Bearing failures were generated by loading the bearings such as to achieve failures in (1) contact fatigue spalling; (2) wear leading to contact fatigue spalling; and (3) excessive wear. Tests were also conducted to simulate various levels of rubbing wear experienced in gear tooth contact using a test rig called the Geared Roller Test Machine (GRTM). Data analysis indicated that the Ferrograph is capable of detecting abnormal wear in each case tested.

After rig testing, the unit was mounted on the TF34 engine to evaluate its ability to function in a test cell environment. Certain deficiencies in the unit were revealed, the major ones relating to false readings obtained as a result of oil aeration and engine vibrations. Trans-Sonics made fixes to the unit to correct these deficiencies. Further testing on the TF34 was aborted because an engine oil leak caused oil seepage into the unit and impaired its ability to make accurate readings. As a result, no reliable data was taken during the engine test.

3. Vibrating Cylinder Pressure Tranducer

a. Description

The vibrating cylinder pressure transducer (VCPT) is a relatively new type of transducer having some inherent advantages over other types (reference 6). This diaphragmless pneumatic pressure transducer utilizes natural vibration modes of a metal cylinder to generate a frequency output as a function of applied pneumatic pressure. Its natural frequency-modulated output makes it immune to noise and drift to which amplitude based transducers are susceptible.

The operating principles can be seen from Figure 3, where a simplified sketch of the VCPT is shown. The vibrating cylinder is energized by the driving coil electromagnet. The driving coil, in turn, is driven by the electronic amplifier. The amplifier has a positive feedback loop, causing it to be inherently unstable and oscillatory. When the VCPT amplifier is first turned on, electronic noise in the amplifier is amplified and sent to the drive coil, causing minute, random excitation of the vibrating cylinder. The vibrating cylinder will, in turn, oscillate at its natural frequency. This oscillation is picked-up by the sensing coil and transmitted to the amplifier, where further amplification occurs. Thus, the osciallation amplitude rapidly builds up until the limiting value (set by amplifier electronics) is reached. The output of the amplifier can be passed through a pulse shaping circuit and monitored on a counter. The natural frequency of the vibrating cylinder is a function of its wall tension. As the applied pressure changes, the wall tension varies, causing the natural frequency to change. In this way, the frequency output of the transducer is a function of applied pressure.

Two other factors also contribute to the wall tension of the cylinder; the temperature and the gaseous composition of the applied pressure (reference 7). Temperature variations change the elastic modulus and linear dimensions of the metal cylinder, causing a change in cylinder frequency. The effects of temperature can be minimized by using low temperature coefficient type metal alloys. In addition, this effect can be eliminated by monitoring the temperature of the cylinder via suitable sensing elements imbedded inside the transducer to provide proper compensation to output data. The effect of gas composition is due to the molecular weight of the gas species. As the cylinder vibrates near its natural frequency, the gas molecules will move with the cylinder wall, thereby adding mass to the cylinder. This effect will vary with different gas species, being more significant with heavier molecules. This effect can be minimized by making the cylinder wall thick. However, this necessitates a design compromise as the increased thickness adversely affects the sensitivity of the transducer (reference 7).

Unlike conventional transducers, the frequency output of the VCPT is a non-linear fuction of applied pneumatic pressure. The exact form of

the function is a polynomial curve. The coefficients of the polynomial are determined for each transducer through individual calibrations and applying computer curve fitting techniques to the new calibration data. The temperature effect can be compensated by varying the calibration temperature and obtaining a family of temperature correction curves.

b. Test Results: A model PT-050S-1D transducer, manufactured by Hamilton Standard was evaluated at NAPTC during TEDD Phase III. This transducer is an absolute pressure unit with a factory calibrated range of 0-350,000 newtons/m^2 (0-50 psia). All pressures were calculated by a polynomial equation and temperature correction curve supplied by the manufacturer. The VCPT was first checked against a laboratory pressure standard ($\pm$0.07% of reading). After calibration, the transducer was mounted on a J-52 engine for endurance evaluations. The VCPT was mounted on the compressor section of the engine and measured turbine discharge pressure through an in-line air filter. During more than 200 hours of engine testing, the VCPT output was monitored and checked against other standard engine instrumentation measuring the same pressure station. Finally, after the engine tests, the VCPT was again calibrated against the same laboratory standard to determine any observable shifts in transducer characteristics. Throughout the entire test program, no adjustments were made on the VCPT.

During laboratory calibration checks before (pre-cal) and after (post-cal) the engine test, the transducer accuracy was determined to be better than 0.2% full scale. Shown in Figure 4 is a plot of percent full scale difference between the laboratory standard and the VCPT, versus pressure. Referring to the Figure, it can be seen that the VCPT accuracy based on manufacturer supplied coefficients is within that of the laboratory standard for pressures up to approximately 240,000 newtons/m^2 (35 psia). Although the VCPT readings were consistently lower, the lower reading of the VCPT is probably due to the differences in gas composition between the manufacturer's calibration air supply and that of NAPTC. This effect becomes more significant at higher pressures because more gas molecules fill-up the cylinder volume, thereby adding significant "effective" mass to the cylinder wall. However, it should be noted from Figure 4 that the repeatability of the transducer, even after more than 200 hours of endurance testing, was well within the uncertainty limit of the laboratory standard ($\pm$0.07% of reading). Thus, if polynomial coefficients were used for the calibration gas, an accuracy of better than $\pm$ 0.07% would be obtained.

During engine tests, the VCPT output was checked against an engine control room gage ($\pm$1% full scale) and the NAPTC computer data acquisition system ($\pm$0.3% full scale). All (calculated) VCPT pressures agreed to well within the accuracy limit of the two instrumentation systems.

In summary, the following advantages and possible drawbacks relative to conventional diaphragm-type transducers can be concluded from NAPTC evaluations. First the advantages:

(1) Ease of operation: There were no calibration adjustments necessary throughout the engine test program.

(2) Accuracy and stability: Throughout the test, the (calculated) pressure data from the VCPT agreed to well within the accuracy range of the standard engine instrumentation system. The transducer performed equally well at the end of the program as in the beginning. Its evaluated accuracy was better than 0.2% full scale and is capable of better than 0.07% of reading if gas composition differences are eliminated or compensated.

(3) Repeatability: The repeatability of the transducer was within the uncertainties of the laboratory standard.

Possible drawbacks are as follows:

(1) Data reduction complexity: The need for polynomial evaluations and temperature compensation required the use of a computer for real-time pressure readouts. However, linearization and temperature compensation circuits have already been manufactured to provide direct read-out pressure; this should remove this drawback of the transducer.

(2) Response Time: The finite "fill" time necessary for the cylinder volume in the transducer inherently limits its response time. For example, for the 350,000 newton/m^2 (50 psia) VCPT evaluated, the manufacturer has quoted a rise time of approximately 10 milliseconds.

(3) Sensitivity to gas composition: For extreme accuracy applications claimed possible with the VCPT (better than 0.015% of full scale), the gas composition of the unknown pressure must be similar to the calibration pressure source. For example, for an aircraft flying from sea level to high altitude at 25°C (77°F) and measuring a pressure of 350,000 newton/m^2 (50 psia), the accuracy of the VCPT could vary by as much as 0.037%, using the same calibration. This is due to the difference in relative humidity between sea level and high altitude.

4. Oil Debris Monitor

As previously discussed, the progression of oil system component (gears and bearings) failures generate large metal particles in the oil. In some diagnostic system applications it will be most cost effective to utilize a relatively small, lightweight, simplified real-time airborne oil system monitor. The K West Model 0252 debris monitor is a candidate for this type of application.

This monitor utilizes a sensing grid woven in a unique pattern. Transparent polyester filaments which serve as insulators are interwoven with stainless steel conductor. These elements are locked together with a third small diameter, stainless steel wire which greatly improves

the contact surface when debris is impinged on the grid by the oil flow. A properietary method of interconnecting each conductive strand of the screen allows the detection of conductive debris as it shorts out adjacent wire pairs. A solid cone at the downstream end of the screen deflects oil through the screen. As debris collects along the surface of the screen, the flow will gradually divert itself to the remaining open area and thus, randomly distribute the debris over the entire area of the sensor. Any debris that is electrically conductive (both ferrous and non-ferrous) will be detected. The effective reduction of electrical resistance as buildup occurs is read out on the data system. Figure 5 shows the equivalent circuit.

This unit has been installed on three TF30-P-408 engine tests, TEDD Phases I and II, and on a TF30-P-412A engine undergoing afterburner lighting tests. The unit was installed in the scavenge oil line for main bearings no. 4, 4 1/2, 5 and 6 on the TF30-P-412A engine for a total of 65 hours test time. There was no change in the output reading during the test. Analysis of material found on the screen after completion of the test showed only a minute quantity of debris (2.0 milligrams) (7×10^{-5} ounces), consisting mostly of fine grit clay with a few carbon particles and one long magnetic particle. Thus, no unsatisfactory operation has been noted with the K West unit during any of the TEDD phases, but it has not been subjected to an engine problem situation where its effectiveness could be evaluated.

5. Hot Section Analyzer

An important element in any diagnostic system is the detection of operational limit exceedances, especially overtemperatures and overspeeds. When those parameters necessary to check these limit exceedances are available, additional information about hot section component status is available. When engine maintenance is to be performed "on-condition" rather than at fixed time intervals, it is necessary to utilize this information to determine the need for hot section inspection or parts replacement. Howell Instruments has developed a Computer Recorder which attempts to interpret this information and provide maintenance guidance.

A Howell Instrument H158A-15 Computer Recorder (Figure 6) was installed on a TF30-P-412A engine which was undergoing a 150 hour accelerated cyclic endurance test at NAPTC. This unit, also referred to as a Time Temperature Recorder and Integrator (TTRI), has inputs of turbine inlet temperature (indirectly measured) and high rotor speed, and provides a cumulative Hot Section Factor Count based on the integrated time-temperature exposure and the hot section metallurgical characteristics of the engine. It also displays Hot Section Factor Time (1015°C (1900°F) and above), time above 1177°C (2150°F), total engine time, and maximum temperature, and has three overtemperature flags and one overspeed flag.

The TF30-P-412A engine, with 113.1 hours since new, was received from the Naval Air Rework Facility, Norfolk, Virginia (NARF NORVA) following a complete engine repair. The total engine test time at NAPTC was 218.5 hours, of which 150 hours were cyclic endurance running. Five different cycles were used during the endurance test. Test cycle profiles were based on the modified Qualification test of an F401-PW-400 engine. To add to the severity of the test, the turbine inlet temperature was adjusted to obtain the maximum allowable value of 1177°C (2150°F). To determine the amount of distress in the engine hot section, three periodic hot section inspections were made, and at the end of the test, a complete engine teardown and analytical inspection was performed at NARF NORVA. This test program was reported on by reference (8).

The Howell unit was installed after the first 10.9 hours of testing and remained in use for the duration of the test. Readings were recorded periodically and the instrument was zeroed out after each reading, except for engine time, which has no external zero adjustment. At the conclusion of the test, the following total readings were recorded:

Maximum Temperature	1231°C (2248°F)
Engine Hours	234.1
Hot Section Factor Count	241,704 units
Hot Section Factor Time	77.5 hours
Time Over 1177°C (2150°F)	21.4 hours

Overtemperature Flag A (1177°C, 10 second delay) had been tripped on 41 of the 53 readings taken.

Overtemperature Flag B (1215°C, 10 second delay), Overtemperature Flag C (1250°C, 10 second delay), and the Overspeed Flag (103.7 % N2) were not tripped.

It is seen that there was a very large amount of overtemperature operation, mostly due to the high engine trim setting, but there were no events extreme enough to trip the B Flag.

The total engine time recorded (234.1 hours) was higher than the actual engine operating time, during which the unit was installed (207.6 hours). This problem was unique to this installation and test program. The Howell unit counts engine time when the temperature reaches a predetermined level, in this case 200°C (392°F) turbine inlet temperature, provided power is on to the unit. During the test, the TF30-P-412A turbine inlet temperature was still between 290°C (555°F) and 315°C (600°F) after completion of rundown, and power remained on. Since there

were approximately 500 starts and shutdowns made, the extra time amounted to a significant amount. This is not a problem in the field, where there is no power to the unit when the engine is shut down, nor did this invalidate any of the other data obtained during this test.

Figure 7 shows a plot of the Hot Section Factor (HSF) count versus engine time (from Howell Unit). The relative temperature exposure severity of different phases of the test can be seen from the different rates of increase in HSF count. The times of hot section inspections are indicated, along with the parts replaced. Reference 8 provides more details on engine inspection and teardown results. The significance of a HSF count must be determined by correlating it with the need for maintenance action. This is done by comparing the count level with actual engine hot section condition over a large enough sample of engines. This has not been established for the TF30-P-412A engine.

In addition to being an indicator of hot section condition, this type of unit has been found to provide other maintenance benefits when used on the F-8/J57, revealing the existence of bad trim boxes, incorrect trim procedure, short throttle rods, incorrectly wired thermocouple harnesses, etc., and documenting overtemperature experiences (reference 9).

Whatever the overall maintenance benefits of this type of unit, it is necessarily limited, since it is a single parameter system. Future hot section diagnostics should take more factors into account, such as low cycle fatigue, thermal shock, and performance degradation. It is noted that Howell has developed a more sophisticated system, called, Jet Engine Monitor (JEM), but this has not been fully evaluated yet.

6. Vibration Analyzer

Vibration analysis is an asset to a diagnostic system. A vibration analyzer coupled with well placed vibration transducers can provide an indication of mechanical health not available from other sources as well as provide second source information to confirm other analysis. The vibration analyzer used in the TEDD program is capable of examining all areas of an engine, from the gearbox to the main rotor bearings.

During the running of Phase I and Phase II of the Turbine Engine Diagnostic Development program, the General Electric engine vibration analyzer was used and found to give unsatisfactory readings for gear-gross experiments (reference 2). To determine the reason for these erroneous readings, the data from the TEDD program was rerun and a detailed analysis was performed on the vibration analyzer in Phase III.

The technique used to do gear-gross analysis is shown in the block diagram of Figure 8. The tachometer signal is conditioned by multi-

plier-dividers to provide a clock signal for the digital comb filter and the synchronous detector. The digital comb filter, a 256 section real time enhancement filter, extracts the gear mesh frequency of interest and its associated harmonics. If there are gross gear defects, such as a worn shaft or bearings or unbalance, the gear mesh frequency will be amplitude modulated by the once per revolution frequency of the gear. In real time, this signal will appear as shown in Figure 8b. The synchronous detector is used to extract the modulating frequency. In the synchronous detector, the gear mesh frequency or carrier frequency is removed and only the modulation is left. The amplitude of the modulation is an indication of gross defects.

Initially, the problem with gear-gross results was thought to be an unstable tachometer signal caused by instantaneous speed changes in the gear train due to backlash and play in the gear mesh.

This torsional play results in a frequency modulated tachometer signal that creates a problem in the analyzer by causing rapid phase shifts through the multiplier-divider circuits. These circuits have a transient response sufficient to track an accelerating engine; however, they require a finite amount of time to settle to a phase locked condition. In order to do gear-gross analysis, five multiplier phase-locked loops are used to condition the tachometer, and it was thought that the rapid phase shifts were propagated through the multipliers, causing the detection circuit to saturate.

To analyze the synchronous detector circuit, a signal from a function generator was used for both tachometer and sensor inputs to insure that the signal was stable. The multiplier circuits were set to one over one ratio and the signal was traced through the various stages of conditioning. It was found that the detector showed modulation on the signal, while there was none on the input. It was found, at this point, that there were some switching incongruities from the digital comb filter that were being amplified by the automatic gain control used in the synchronous detector.

The nature of the digital comb filter is such that the switching spikes are evident in the output but can be smoothed out with proper filtering. The digital comb filter switches the input signal to a series of capacitors in sequence and at a rate determined by the multiplier-divider settings. A simplified diagram is shown in Figure 9a and the resultant output in Figure 9b. The transitions between capacitors is the noise that was being passed to the synchronous filters, generating erroneous gear-gross readings.

When this noise was filtered out just before the automatic gain control, this produced satisfactory results on the synthetic signal. The taped data from the TEDD program was then played into the analyzer. The results are presented in Table I, along with the original readings from the Phase II engine test. The first set of readings were taken

at lower engine speed (Idle) with good correlation obtained for gear local and much better results for gear-gross experiments. At the higher engine speed (Intermediate), however, gear-gross experiments were mostly over limits. This problem is the result of much more frequency modulation on the tachometer signal, and/or poor communication between the object being analyzed and the accelerometer.

In addition to the speed signal changing phase, the gear passage frequencies will also be frequency modulated and perhaps add to the problems encountered in the gear gross defects experiments. This situation can be analyzed only with an unmodulated tachometer signal. Additional vibration analyzer analysis should be done with data that has a tachometer signal with less than .8% modulation to resolve the question of frequency modulation versus lack of communication to provide valid gear-gross experiment results.

7. Speed Sensor

In an attempt to improve the performance of the vibration analyzer on overall gear defect experiments, an investigation was done on various speed sensing techniques. It is believed that part of the problem with the gear-gross defects is due to an unsteady tachometer signal caused by torsional effects and gear meshing tolerances. It is also possible that the various loads on the gear box are not steadily applied and may affect the rotation of the tachometer pad. There are several places on an engine where speed data can be collected. These include a gear box pad, the rotor shaft itself in a nose cone pickup, or from a compressor or turbine stage. Below is a presentation of data recorded and evaluated from tach pickups on the gear box, from a gear reduction from the rotor shaft and directly from the shaft. Also presented is the variation of a calibration signal, recorded and reproduced, which can be used as an indication of the error introduced by tape.

	% Modulation
Tach Calibration Signal	.2
Shaft Pickup	.2
N_1 Pickup from TF-30 (Nose cone gear reduction)	
Idle	.4
Intermediate	.6
N_2 Pickup from TF-30 (Gearbox)	
Idle	.8
Intermediate	2.0

It can be seen that there is approximately 2% jitter on the gear box pickup at higher rpm. This amount is intolerable for vibration analyzer experiments. It was noted that variations to approximately 1% could be tolerated by the vibration analyzer.

Blade passage data was not analyzed quantitatively; however, it is modulated less than that seen on data from the gear reduction in the front cone of the TF-30, and would prove to be satisfactory for the analyzer.

It is recommended that for future vibration analyzer use, a blade passage pickup be used for the high speed rotor and gear box experiments.

8. Radiation Pyrometer

The Solar radiation pyrometers used on TEDD Phase II produced results that required further analysis. The readings from the pyrometers for peak and average peak showed higher values than calculated gas temperature. An oscilloscope was used to look at the analog signal from the pyrometer, and it was noted that, in addition to the blade passage signal, spurious spikes were seen by the pyrometer. Aside from the noise problems, the aperture probe showed a decreasing blade temperature versus time for comparable engine settings, indicating a possible sooting condition. When the pyrometer was removed, a post calibration was run and a degradation was noted. Attempts to clean the probe improved its sensitivity to some extent. Upon shipment to Solar, it was found to be inoperative. Solar disassembled the probe and found that the fiber optics had broken. There was also an oily deposit in the purge air tube that indicated that possibly the purge had been dirty. This did not seem to be a problem with the lens probe. These problems, particularly the noise in the analog output signal, are the ones investigated during this phase of TEDD.

In discussing pyrometry with other manufacturers (at first primarily with Detroit Diesel Allison, Division of General Motors, since they had one of the early probes developed by Solar), it was found that others had seen the type of signal output observed during the TEDD program. In investigations at other facilities, using different installation locations, it was found that the noise could be reduced, or eliminated, by shielding the probe from the flame. This has been done by looking at the back side of the blade or radially to the blade and choosing angles such that the probe cannot view the flame, either directly or through reflections. This approach has resulted in the best reduction of spurious noise, particularly on engines running at current turbine inlet temperatures.

Another approach to measuring the average and peak average blade temperature was to enhance the signal through techniques used for vibration analysis. Data was obtained from Allison that looked very

similar to that seen in the TEDD program. It was played into the vibration analyzer and processed through the digital comb filter to extract the spurious signals. Figure 10 shows scope traces of both the unconditioned signal and the conditioned signal. It can be seen that, in general, the digital comb filter does a reasonably good job of extracting the blade passage frequency. There are some cases, however, where the input electronics were saturated and at these points, there is no blade passage frequency to extract.

The data analyzed by the vibration analyzer was not calibrated to provide temperature information, and it was coupled through the analyzer such that an overall temperature could not be recovered. However, some of the analyzer's detection circuits could be used to automatically flag hot blades. The impact index, the ratio of peak to average signal level, could be used to detect blades, or a blade that was significantly hotter than the average. Separate circuitry would be required to provide the overall average blade temperature level.

A second technique that is being developed by Solar and Allison is to detect the incomming spikes and reject them above a prefixed level, usually a not-to-exceed gas temperature. This seems to work fairly well, but was not analyzed at NAPTC. The disadvantage of this system is that during high temperature running, the signal could conceivably be rejected more often than it would be measured.

9. Internal Accelerometer

In order to monitor bearing health more accurately than has been done in the past, it has been recommended that internal accelerometers should be mounted on the bearings (reference 2). There are some common problems associated with this task that have been under design consideration for several years. These problems are the environmental restrictions on the accelerometer, signal lead routes, and bearing housing accessibility, which places restrictions on the design.

Accelerometers are relatively new devices, coming into full development in the last five to ten years; and have been considered delicate transducers. The piezoelectric material used as the transduction element is sensitive to temperature and has an upper limit dependent on the type of material used. The various housing and lead coupling techniques used in accelerometers are not rugged in construction. Due to the characteristic of the piezoelectric material, very low level signals are produced; thus, careful consideration must be given to the manner in which the signal leads are run.

Current state-of-the-art accelerometers are fairly rugged in that they can withstand temperatures to 500°C (932°F), and the leads are integral to the case so that connections on the accelerometer are not required. An accelerometer of this type was used for the internal accelerometer in the TEDD program.

The second problem for internal accelerometer placement is how to get the signal to the outside of the engine. If it is assumed that the engine will be disassembled for repair of other than the accelerometer, the signal lead should not cross engine boundaries that would be separated. In some engine installations it is possible to mount the accelerometer in a cooled location, and then it becomes necessary to trace the leads through extremely hot sections. This is not as serious a problem as is the accelerometer's installation; however, it must be considered.

The problem of limited life for the accelerometer makes it necessary that it be accessible from the engine case. Several designs have been advocated to permit this accessibility. One concept is to place the accelerometer at the bearing through a "dipstick" approach; that is, a rod, with the signal lead integral with it and the accelerometer at its end, is screwed into the mount. This requires a suitable engine design, but places the accelerometer and lead in a position for accessibility.

This approach, though relatively straight forward, runs into problems when the actual bearing design is considered. In dual rotor engines and engines of advanced design, some of the bearings are designed to be soft mounted. Thus, mounting is affected by a cantilevered design that permits the bearing and bearing housing to float in the engine. The soft mounted bearing is not conducive to an accessible accelerometer installation.

This type of bearing mount was used on the TF30-P-408 rear bearing (TEDD Phase II). The accelerometer was hard mounted to the bearing housing and was only accessible by removing the exhaust section and by entry into the sump oil housing.

In general, these problems were the ones considered by Pratt & Whitney when installing internal accelerometers on the F401 engine. The bearings in which they were interested were the #2 and #3 bearings. The #3 bearing is soft mounted and a dipstick approach was used for accelerometer accessibility. It is their assessment that the information obtained was not pertinent to the bearing problems due to lack of communication between bearing and accelerometer and, therefore, it has been recommended that the accelerometer not be used in F401 production engines.

B. Software

1. Data Smoothing Techniques

In order to perform accurate and valid diagnostic logic, the parameters used in the logic must truly represent the state of the engine. Evaluation of the "truthfulness" of a sensed parameter must consider the accuracy, repeatability and time response of the sensed

parameter relative to the actual state of the parameter. Accuracy, repeatability and time response are performance characteristics of a sensor which may become involved in a system effectiveness trade-off; that is, sensors with the best performance may be large, expensive, or delicate such that their usefulness in an airborne diagnostic system is limited. Therefore, it will be necessary at times to sacrifice sensor performance for system suitability. However, it may be possible to "buy back" the sacrificed sensor performance by applying software techniques designed to optimize the performance. It is obvious that nothing can be done to improve the accuracy of a given sensor, but software techniques which perform data validity tests (i.e., identify failed sensors and signal drift) can be used to maintain the highest possible accuracy. Likewise, it is impossible to improve the time response of a given sensor, but software techniques can be used to minimize the time response distortion inherant in some diagnostic logic applications. Improvement in parameter repeatability can be directly addressed by application of data smoothing software techniques, and the following discussion addresses the TEDD Phase III effort on this subject. A thorough, mathematical discussion of this effort is presented in Appendix A.

In order to evaluate the effectiveness of data smoothing techniques, the software performance goals or criteria must be defined. The following criteria were developed and used in this study:

a. Storage Required: This is concerned with how much data storage is required to perform the various smoothing techniques and also how much storage the technique itself will occupy. Obviously, the less storage required the better.

b. Ability to Adjust Rates of Response: The nautre of TEDD data is such that it is not known whether the next data sample will have a similar magnitude as the last, or represent a radical change. This characteristic dictates that the techniques must be able to assign weights to the data depending on certain engine parameter rates of change. How well the techniques can do this is an important criteria.

c. Simplicity of Computation: Since the ultimate application of TEDD programming is a real time situation in which the computations are repeated with each new data scan, and since applied smoothing will be essentially an iterative processs, the amount of time spent smoothing is critical. Those techniques that employ fewer mathematical steps and can work effectively on less data will be of high interest. Not only will less memory be used, but they will also be faster.

d. Response: This criteria applies mainly to transient conditions. Due to mode detection techniques, little distortion of rates of change of certain key parameters can be tolerated. The tradeoff here is to get the true rate of change of the parameter by smoothing out noise but not to the extent of distorting the true event.

e. Accuracy and Noise Reduction: This criteria is used to compare how well the smoothed data compares to the model of the true event. Standard deviation defined as the measure of how much the data varies from the mean of the sample, will be used to judge this criteria.

Two techniques of data smoothing were evaluated in this study, namely moving average and exponential averaging. The moving average technique is one of the methods chosen for evaluation since it was used previously during TEDD Phase II and, although it had some drawbacks, was fairly successful and accurate enough to warrant further investigation. Simply stated, the moving average technique calculates the average of the last N values of a given parameter. It minimizes the sum of the squares of the differences between the N most recent observations and the best guess for that average. The simplicity of computation for this method is an obvious plus in a TEDD operating environment. The value that is picked for N, the number of data points to be included in each average, will not be the same for all data. A small value of N is useful for eliminating small variations in the data, but is relatively ineffective for large variations. Conversely, if too large a value of N is selected, there is the problem of excessive smoothing, thereby ignoring some of the true event.

An inherent problem in applying this method is the lack of data for initial conditions since there are no previous data points to use in computing the initial average. Extra weight will be given to the initial data points until N readings are obtained.

Exponential smoothing is a method of estimating each new data point in a time series by letting the new smoothed value be equal to a fraction $(1 - \alpha)$ of the previous smoothed value, plus a fraction (α) of the new data point. α is defined as the weight given to the new data point. This method of smoothing is simple to compute and has the advantage of small amounts of data storage. Only two words of storage are required for each parameter instead of the N words required by the moving average technique. Another advantage is its flexibility because only α needs to be varied to change the rate response. When α is small, the method gives little weight to the new data, which is good for smoothing random noise in a steady stage condition. A large α will weight the new data heavily so it responds to rapid changes in the time series, which is necessary for tracking transients.

The data used in this study was stored on magnetic tape during TEDD Phase II TF30-P-408 engine testing. TF30-P-412 data from a NAPTC Fleet Service Test Program was also used. The parameters which were used in the study are power lever angle (PLA), high pressure spool rotor speed (N_2) and burner pressure (P_b). The values of N for the moving average technique were 1, 2, 3, ... 10, and for α in the exponential averaging technique, the values were .1, .2, .3, ...9. The detailed, mathematical results of the study appear in Appendix A. The following summarizes the results.

When comparing the two methods of smoothing with the criteria developed earlier, it is obvious the exponential smoothing technique is better suited to TEDD applications than the moving average. The following chart shows the comparison.

Criteria	Moving Average	Exponential Smoothing
Storage Required	N x (# of parameters)	2 words for each parameter
Ability to adjust rate of response	Programming more complicated	easy to implement
Simplicity of computation	More instructions to implement	Fewer instructions; therefore faster
Response	O.K. for proper N	Always better for tested range
Accuracy and noise reduction	O.K. for proper N	Always better for tested range

To apply the exponential smoothing to TEDD data, it is necessary to have pre-defined separate α's for steady state and transients, depending on response and accuracy desired for each parameter. Upon deciding which mode is current, the appropriate α is applied to the data. Programming details such as initial conditions cannot be overlooked when switching α during a transient.

2. Multiple Fault Gas Path Analysis

In a diagnostic system the gas path analysis element (GPA) is the portion of the logic which addresses the aerothermal performance of the engine components. GPA quantitatively determine changes in some or all of the following: Compressor and turbine efficiencies, changes in turbine and exhaust nozzle areas, bleed and power extractions, and changes in compressor pumping capacity. When one of the goals of a diagnostic system is to improve maintenance through the use of "on-condition" maintenance rather than maintenance at fixed time intervals, GPA provides the "condition" of the engine components which is information not available through visual or other inspection techniques.

A number of GPA techniques exist covering a wide range of capability and complexity. Once a GPA technique has been verified to perform as intended, it is possible to evaluate the technique in terms of capability and complexity. The capability of a technique includes its flexibility, qualitative performance and quantitative performance. Flexibility addresses the ability of the technique to detect the types of gas path faults that the particular engine to be diagnosed exhibits. Flexibility also

considers the measured parameter requirements (are they measurable?) as well as the ability of the technique to detect erroneous input parameters and to function (fully or partially) without that parameter. Qualitative performance addresses the GPA technique's ability to identify the physical fault (dirty compressor, eroded turbine, etc.) responsible for the detected change in gas path performance. An important consideration is the technique's ability to identify multiple simultaneous as well as single faults. Quantitative performance is the GPA technique's ability to calculate the level of component deterioration and the precision of that calculation. The complexity of a GPA technique involves at least three elements; background or development requirements, computational requirements, and computor storage requirements. The background or development requirements effect the lead time requirements for system development and/or modification as well as costs. Computational complexity considers the type and number of calculations required by the technique. Minimizing the computational requirements optimizes the speed of the technique, which is particularly critical when GPA is to be performed airborne. Computer storage requirements addresses the technique's input parameter storage, storage of the computation coding, storage of constants and coefficients associated with the technique, and output data storage. For an airborne application, the computer storage requirements are likely to be a limiting factor.

In TEDD Phase II and III, two approaches to GPA have been examined. In Phase II, an in-house GPA technique was developed using a fault signature recognition approach, described in Reference 2. In Phase III, a GPA technique developed by Hamilton Standard Division of United Technologies Corporation known as Parameter Interrelationships was evaluated using Phase II TF30-P-408 data. The final report by Hamilton Standard (Reference 10) completely describes the Parameter Interrelationships methodology and the results using TEDD Phase II data. Appendix B of this report summarizes the methodology and results. The following chart compares the two methods.

CRITERIA	TEDD PHASE II METHOD	PARAMETER INTERRELATIONSHIPS
A. Capability		
(1) Flexibility	Fault selection limited only by the flexibility of the cycle deck used. Requires only normal measurable parameters. Detect instrumentation failure, system inoperative.	Fault selection limited by parameter selection-involves tradeoff. Instrumentation failure not addressed in this phase.
(2) Qualitative Performance	Single fault only. Provides ranking of probable faults.	Multiple fault capability.
(3) Quantitative Performance	Computes single fault level and Confidence Factor.	Computes a fault level for each possible fault.
B. Complexity		
(1) Background	Extensive cycle deck exercise followed by lengthy data manipulation.	First time development extensive. Completed and reusable.
(2) Computation	Multiple matrix operations. Extensive calculations.	One matrix multiplication.
(3) Storage	Thousands of words of coefficient storage - lengthy program coding.	Less than a thousand words - storage and programming combined.

Whatever form it may take, any engine diagnostic system must rely on discernable changes in observable parameters in order to detect physical faults. Physical faults in an engine are in general some combination of problems such as erosion, corrosion, foreign object damage (F.O.D.), worn seals, etc. Although the physical faults result in changes in observable parameters such as rotational speeds, temperatures, pressures, etc., it is more fundamental to consider the physical faults as causing changes in engine component performance parameters such as component efficiencies, turbine and exhaust nozzle areas, compressor pumping capacities, etc., and that these changes, in turn, result in discernible changes in the measurable engine parameters. If proper equations can be established relating the dependent engine variables (measurable quantities) to the generally nonmeasurable independent component performance variables, then an inverted set of relationships can be obtained relating the independent variables to the dependent variables. This could then form the basis of an engine diagnostic system which would have the capability of detecting multiple faults as well as the magnitude and direction of the fault.

This is the basic technique employed by Hamilton Standard in their engine diagnostic system. The major obstacle in employing such a diagnostic scheme is in establishing the proper relationships that exist between the dependent and independent engine variables. Two different approaches were used to establish these relationships. Before discussing these approaches, it is appropriate, at this time, to define two terms which will be used frequently. The first term is "delta" (Δ). In everything that follows, the term "delta" will be taken to mean the percent of point difference in a particular variable relative to its nominal or baseline value. All Δ's are dimensionless quantities whose value for any variable does not depend on the units used to measure the variable. The second term is "fault coefficient". This is just the percent change in a dependent variable per unit percent change in an independent variable. Note that since the deltas are dimensionless, the fault coefficient is also dimensionless.

Two methods were used in this study to calculate the required fault coefficients. The first method used an elaborate gas path analysis of the engine developed by Hamilton Standard and is primarily theoretical in nature. The second method is empirical and used available baseline test data as well as engine test data obtained with known changes made to the baseline configuration.

As shown in reference 11 a general influence coefficient matrix can be derived for any particular gas turbine cycle. This matrix represents a set of linearized equations which interrelates the various dependent and independent engine performance parameters. Since the book was written, extensive refinements and modifications were made to improve the precision of the coefficients and to extend the approach to twin spool turbofan and other type engines. Each of the coefficients is derived by proper mani-

pulation of the differential forms of the basic thermodynamic equations for each engine type. Factors such as component efficiency variations; specific shapes of the component performance maps; engine power balance; conservation of mass, energy, and momentum; variable specific heat effects; nozzle unchoking effects, etc., are taken into account. For the actual TF30-P-408 engine used in the test, such details as component efficiency variations, specific shapes of component performance maps, etc., were not available. Judgement numbers based on experience and the model specification for this engine were used to obtain the theoretical fault coefficients.

An alternate approach using actual engine data supplied by NAPTC is available for calculating the fault coefficients. This method is empirical and makes use of nominal baseline engine data as well as steady state engine data with deliberate perturbations of known amounts introduced individually. From test data where all independent variables are held fixed except one, the resulting delta of any measurable dependent variable is a result of the one known perturbation. In empirically determining the fault coefficients, it has been tacitly assumed that independent component performance parameters such as component efficiencies, turbine nozzle area, etc., did not independently change during the test. In other words, the only perturbations were exhaust nozzle area changes and varying the three compressor bleeds. It follows, therefore, that only the fault coefficients with respect to these four disturbances can be computed empirically.

Once the numerical values for the fault coefficients have been determined, applying them to engine diagnostics is relatively straightforward. In general, if n faults are to be computed, (n + 1) measurements are required. One measurement serves as the abscissa against which n deviations from baseline values are obtained. If the column vector $\underline{x}$ represents the set of n sought after deltas (such as changes in component efficiencies, bleed flows, geometries, etc.) and the column vector m_i is the set of n delta measurements, then they are related by an nxn matrix of fault coefficients F_i as:

$$\text{Eq. 1} \qquad \underline{m_i} = F_i \underline{x}$$

A subscript i is attached to $\underline{m}$ and F to emphasize that, in general, there may be more than one set of sensor measurements which can be used to diagnose a given set of faults. If the measurement deltas bear a meaningful relationship to the sought after deltas, then F_i in Eq. 1 will have an inverse and we can solve Eq. 1 for $\underline{x}$ to obtain:

$$\text{Eq. 2} \qquad \underline{x} = (F_i - 1)\, \underline{m_i} = F_i^{-1}\, \underline{m_i}$$

The evaluation of Parameter Interrelationships approach using the Phase II data shows that the approach is capable of identifying the presence of faults, singly and multiply. The computed fault levels generally agree quite well with the known implanted fault level. Complete results appear in Appendix B.

3. Diagnostics on Variable Geometry Engines

The need for the capability to simulate the performance of a gas turbine engine with variable geometry arose from the consideration of gas path analysis as one element of a diagnostic package for a 1980-85 aircraft. During the period from January 1974 through March 1975, a variable geometry engine cycle deck was developed at NAPTC. The specific gas turbine cycle simulated by this deck is a two-spool, T-fan[2], mixed-flow turbofan with afterburning. In addition, this cycle deck allows for variable area high and low pressure turbine (HPT and LPT) nozzles and variable exhaust nozzle (A8) area.

Basically, this cycle deck consists of the thermodynamic equations of a two-spool, mixed-flow turbofan. These equations account for flow continuity, energy balance, speed matching, and pressure balance. In addition, the program is required to satisfy the requested HPT, LPT, and A-8 areas. The thermodynamic properties of air are obtained from GASTAB, which is a computerized gas table.

This cycle deck has been written as a design or Parametric deck, so that any engine in the two-spool, T-fan, mixed-flow turbofan catagory can be simulated. To simulate a particular engine, the engine design point information must be provided to the program, operating in the Design Mode.

Operating in its Normal Mode, the program accepts inputs, such as altitude and Mach number, horsepower and bleed air extraction, changes in component performance, changes in HPT, LPT, and exhaust nozzle areas, and rating code (ZRC), which is the power level input. The program can be operated to generate a single data point or to generate a "power series" at the given input conditions.

The data generated by this cycle deck is output to the line printer and/or magnetic tape. Several output formats are available to provide flexibility.

Some of the features of this program which make it flexible are as follows. Each compressor and turbine is individually represented by performance maps. The compressor maps are; (a) referred speed as a function of pressure ratio and referred flow and, (b) efficiency as a function of pressure ratio and referred flow. The turbine maps are: (a) flow parameter as a function of pressure ratio and referred speed and, (b) efficiency as a function of velocity ratio and corrected work. These are stored as percentages of design so that the same maps can be used for many engines. Pressure drops are not considered to be constant. The fan duct, burner, diffuser, mixer, and afterburner friction pressure drops are

---

[2]T-fan implies fan and low pressure compressor on low spool

computed as a function of the referred flow and the design value of the pressure drop, providing more realistic calculations. Also, the afterburner momentum pressure loss is computed as a function of afterburner Mach number and temperature rise. Wherever possible, the program coding was organized into building blocks, that is a subroutine for a compressor, a burner, a turbine vane, a turbine blade, etc. This has been done to facilitate construction of other engine cycles without duplicate effort. Another option within this program involves the number of turbine stages. Both the high and low pressure turbines have the option of being single or two-stage components independently.

Once data has been written on magnetic tape, there are a number of ways to retrieve desired information. One option is to list all runs on tape. It is also possible to output a chosen run or set of runs in any of the data output formats.

Another tape feature which is available is called Tape Edit. This allows output of up to eight stored values (inputs and/or outputs) for all or any selected group of runs. The "editing" is accomplished by disqualifying runs which do not satisfy the editing criteria, and any stored value may be used as an editing criteria. Each editing criteria must be assigned a minium and maximum value.

The building block approach to the coding of this deck allows for the creation of other gas turbine cycles with a minimum effort. All of the programming required for input/output and program control will remain essentially unchanged. The peripheral capabilities are independent of the cycle and are therefore, available for use on any cycle.

The cycles which are planned to be developed in the immediate future are the (a) two-spool, unmixed turbofan with duct burning and/or afterburning, (b) two-spool, mixed turbofan with afterburning, (c) two-spool, regenerative turboshaft with a free power turbine and, (d) high bypass ratio turbofan.

Variable geometry data from this cycle deck was supplied to Hamilton Standard Division, United Technologies Corporation for study using the parameter interrelationships method of gas path analysis.

This data represents an engine whose geometry schedules are designed for 9,144 meters (30,000 ft.), Mach 0.8 Cruise condition because the cruise condition is an appropriate choice for steady state gas path analysis. The geometry schedules were selected to provide <u>installed</u> performance gains. This is accomplished by maintaining the inlet design airflow while reducing thrust (thereby reducing or eliminating spillage drag) and by opening the exhaust nozzle to reduce boattail losses (aft end losses). Additionally, maintaining overall compression ratio tends to minimize uninstalled TSFC. A complete description of this data and a more thorough discussion of the cycle deck itself appears as Appendix C.

4. TEDD Sensitivity Study

In developing an engine diagnostic system, sensitivity studies are necessary to determine which engine parameters are most responsive to changes in engine condition caused by various faults; and therefore, should be used in the diagnosis of these faults. In addition, the measurement accuracy of these parameters, required to detect given minimum fault levels, must be determined. Sensitivity studies can take various forms and the results expressed in different ways. They are needed to establish monitoring parameter requirements for engine thermodynamic performance analysis, but are also done on various engine subsystems. Some examples of sensitivity studies are given in Reference 12 which describes the development of a methodology to identify thermodynamic performance monitoring parameters and their sensitivities, and also gives the results of two computer studies run on engine lube system models to determine the relative sensitivity of lube system parameters to failure/deterioration of various lube system components. The Hamilton Standard approach to multiple fault diagnostics also provides a direct measure of system sensitivity (Appendix A of Reference 11).

When the TEDD Phase II steady-stage performance analysis program was developed, the relative sensitivity of each of 23 elements (pairs of corrected performance parameters) was identified, and this information was used in setting up the Directional Analysis and Quantitative Analysis (calculated fault level and Confidence Factor) parts of the program (Reference 2). During TEDD Phase III, a system sensitivity study was conducted on the TEDD program to determine the effects of parameter errors on the diagnostic capabilities of the system and to get an indication of the measurement accuracies required. The results of this study are presented in Appendix D.

Vibration Experiments Listing and Results

Note: All readings under 50 percent are considered valid.

Experiment Class: Gear/Pump/Accessory Drive - Local Defects
Function SW - Local

Experiment No.	Component	Sensor No.	Reading Percent Idle Eng	Idle Tape	Intermediate Eng	Intermediate Tape
1	Tower Shaft Gears (9), (20)	1	13	8	10	20
2	Gears (21), (22)	1	16	6	18	20
3	Gears (27A), (27B), (35)	1	17	6	20	20
4	UHP Drive Gear (37)	1	21	8	22	20
5	CSD Drive Gear (23)	2	20	10	22	20
6	CSD 35 Tooth	2	20	10	26	18
7	Starter Drive (28)	1	15	8	21	20
8	Gears (24A), (24B), (24C)	2	21	8	17	25
9	De-air Drive Gear (25)	2	21	10	19	24
10	Fuel Pump Drive (29)	1	19	10	19	20
11	Fuel Pump (41)	1	21	6	20	20
12	Fuel Pump (42)	1	16	8	25	20
13	Gears (30A), (30B)	1	17	8	16	20
14	Main Oil Pump Drive (31)	1	22	6	23	20
15	N_2 Tach Drive (32)	1	21	6	20	20
16	Fuel Boost Drive (26)	2	19	10	19	19
17 - 24	Unassigned					

Experiment Class: Gear/Pump/Support Bearing - Overall Defects
Function SW - Gross

25	Shaft A - G (9) and SB	1	99	22	99	24
26	Shaft A - G (20) and SB	1	52	20	77	24
27	Shaft B - G (21) and SB	1	34	20	90	24
28	Shaft B - G (22) and SB	1	31	40	33	65
29	Shaft C - G (23) and SB	2	99	40	71	80
30	Shaft C - CSD 37 and SB	2	77	99	44	80
31	Shaft W - CSD 35	2	59	99	99	70
32	Shaft D - G (24A) and SB	2	99	45	99	95
33	Shaft D - G (24B)	2	99	60	65	99
34	Shaft D - G (24C) and SB	2	99	99	99	99
35	Shaft E - G (25) and SB	2	99	20	99	95
36	Shaft G - G (27A) and SB	1	14	40	31	80
37	Shaft H - G (27B)	1	28	65	23	99
38	Shaft H - G (35) and SB	1	65	95	85	99
39	Shaft J - G (37) and SB	1	99	90	99	99
40	Shaft J, K - UHP, LPH	1	98	99	99	99
41	Shaft L - G (28) and SB	1	22	30	50	80
42	Shaft M - G (29) and SB	1	77	40	99	99
43	Shaft M - FPG (40)	1	89	90	84	99
44	Shaft M_1 - FPG (40)	1	99	99	90	99
45	Shaft P - FPB (41)	1	99	99	99	99
46	Shaft Q - FPG (42)	1	99	99	84	99
47	Shaft R - G (30A)	1	32	40	19	99

FIGURE 1: TURBINE INLET TEMPERATURE SENSOR

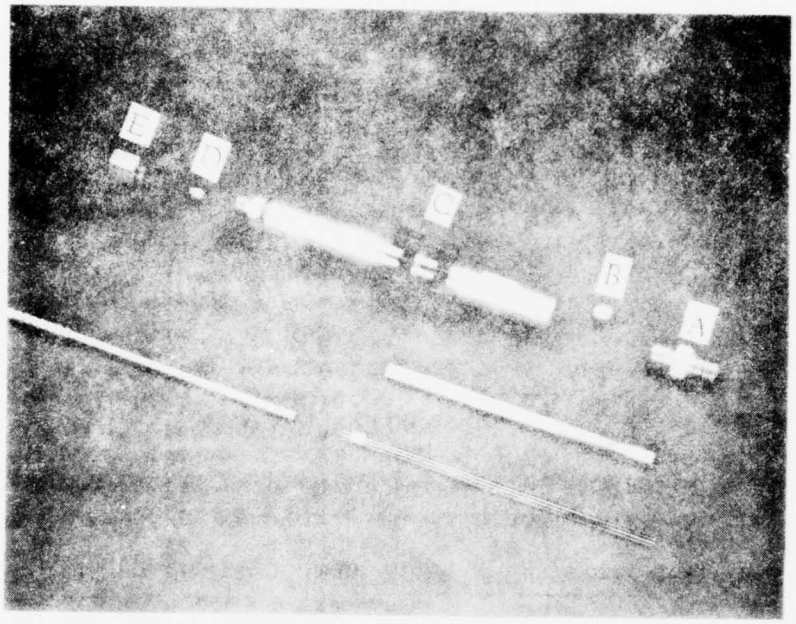

PROBE PIECES

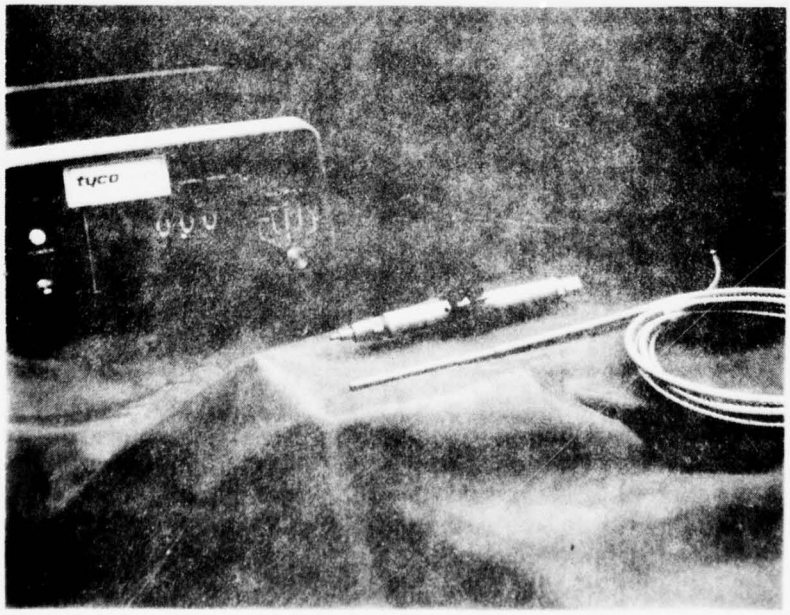

ASSEMBLED SYSTEM

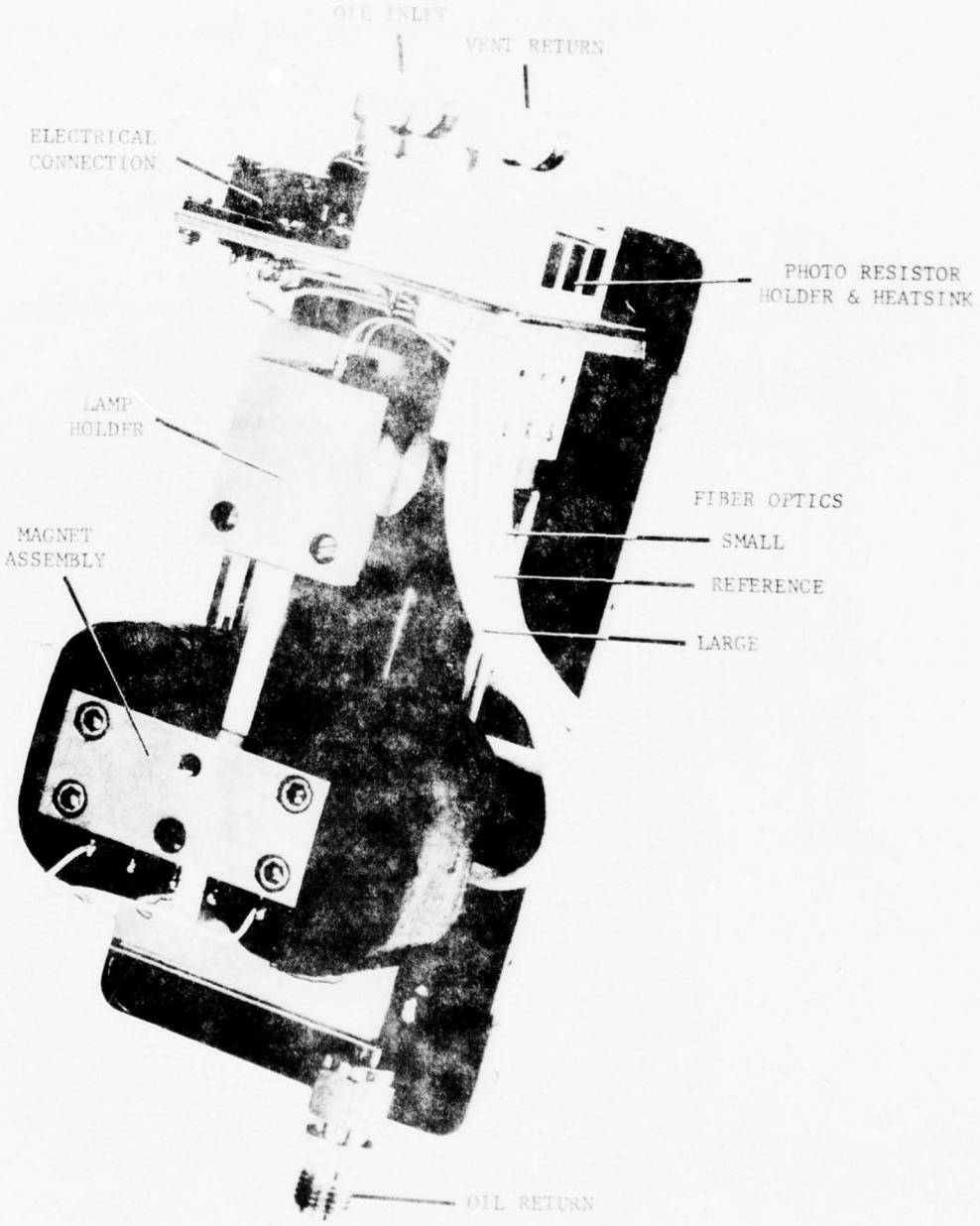

FIGURE 2. RT FERROGRAPH TYPE 7081 (with cover removed)

(3/4 Actual Size)

FIGURE 3: VIBRATING CYLINDER PRESSURE TRANSDUCER SCHEMATIC

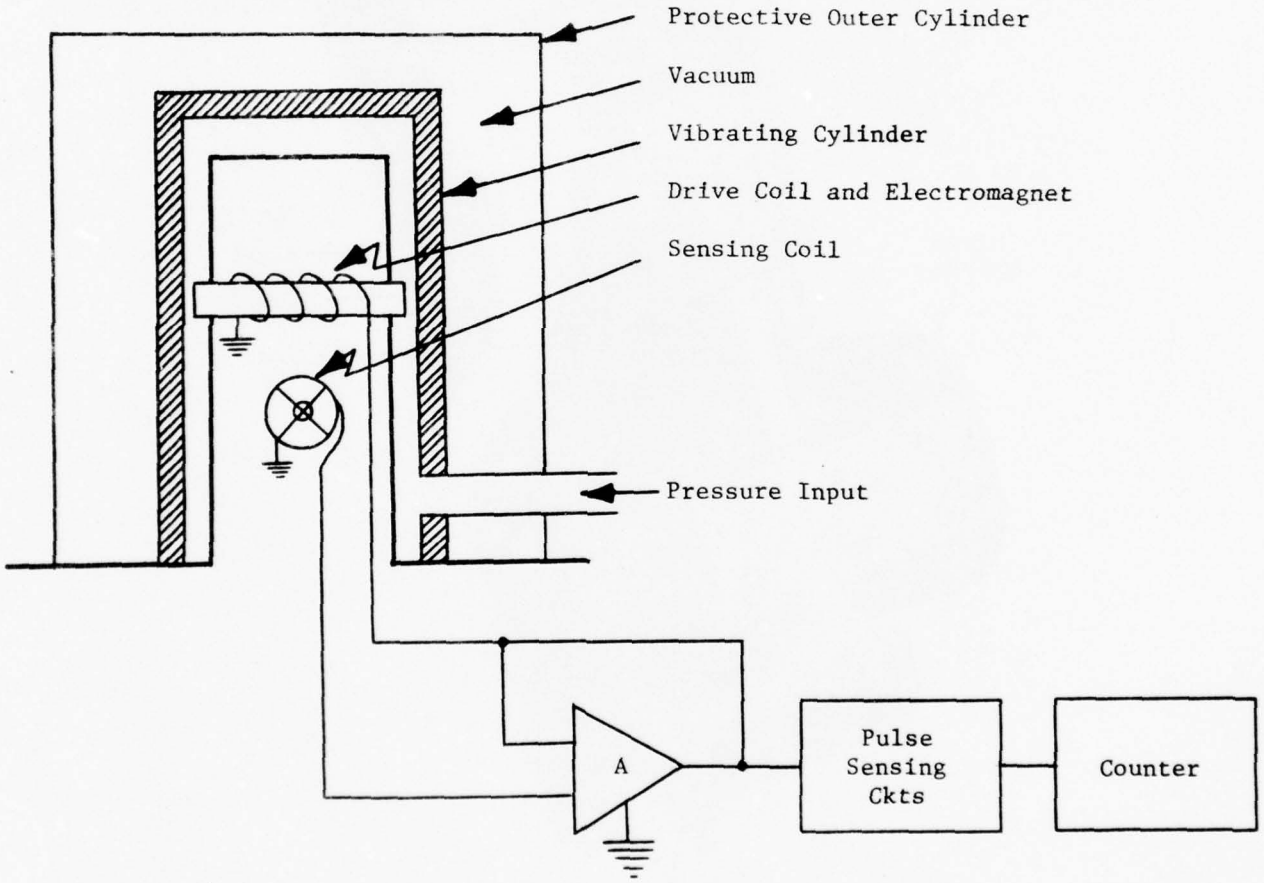

FIGURE 4: PLOT OF PERCENT FULL SCALE DIFFERENCE BETWEEN THE VCPT AND THE LABORATORY STANDARD

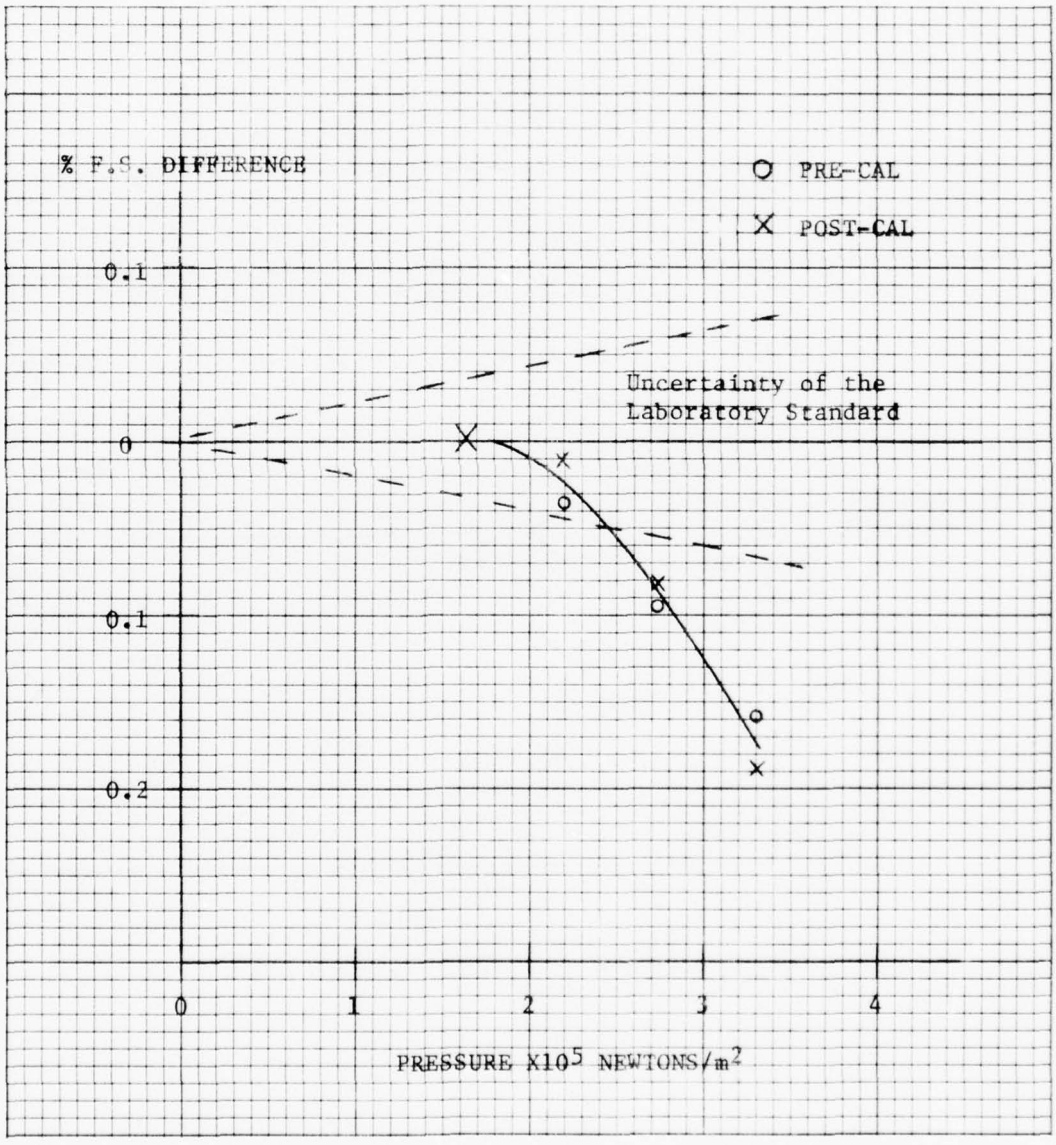

FIGURE 5: K WEST DEBRIS MONITOR EQUIVALENT CIRCUIT

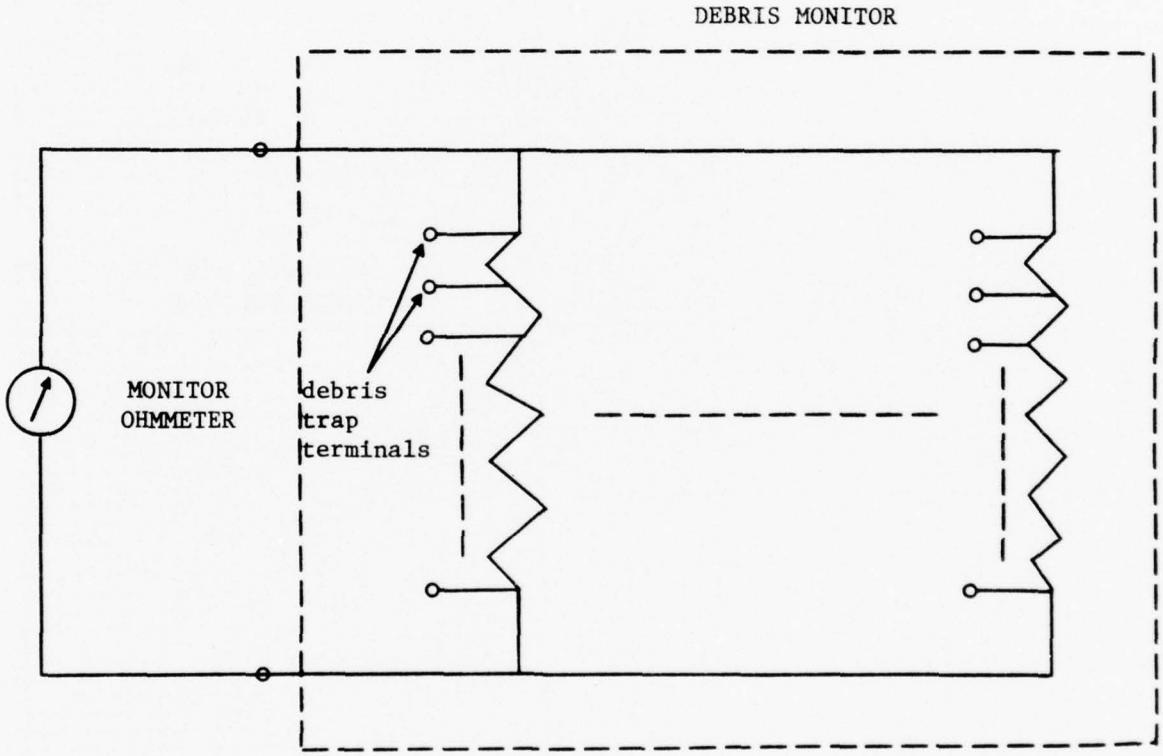

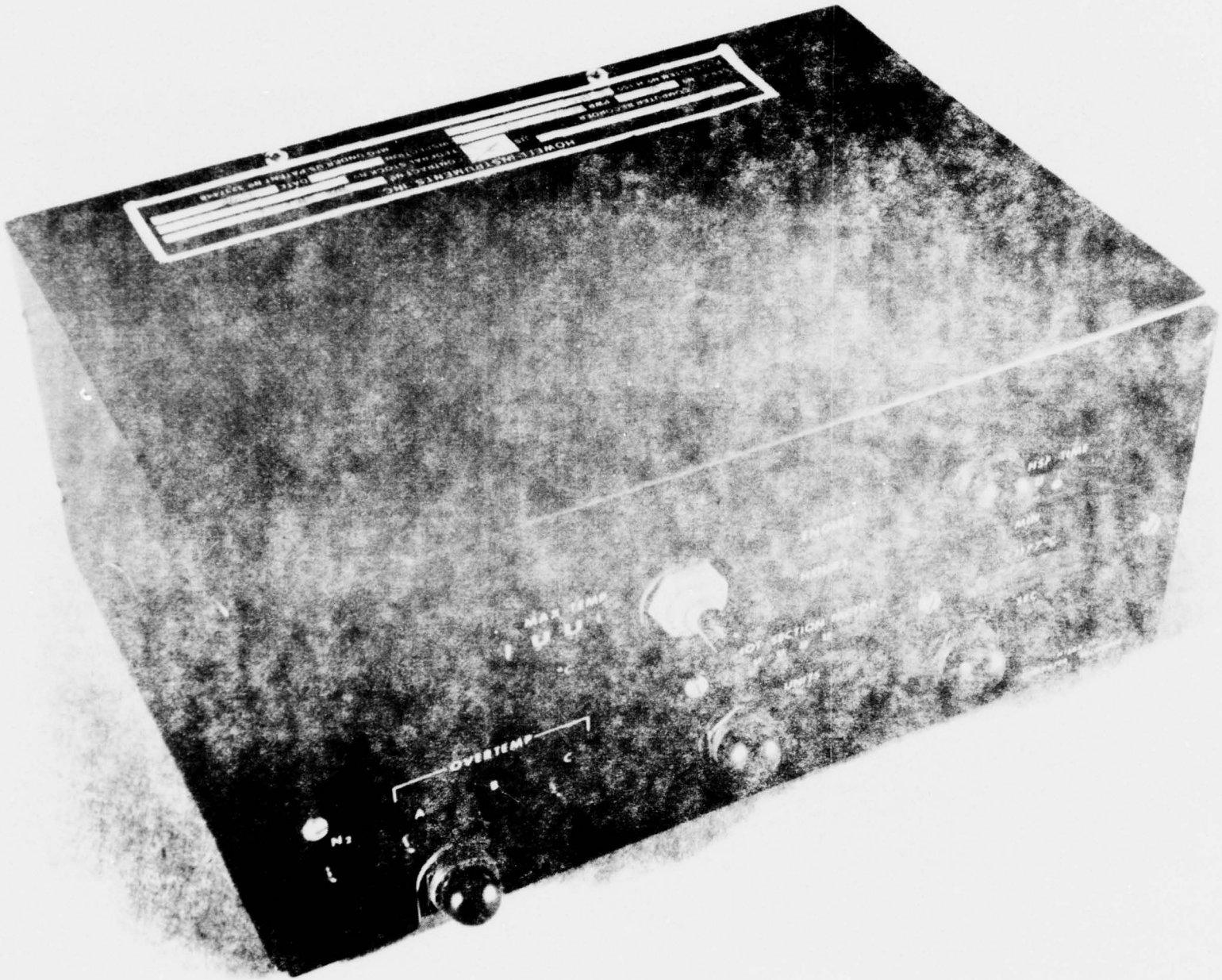

FIGURE 6 : HOWELL COMPUTER RECORDER MODEL 81583-13

FIGURE 7: CUMULATIVE HOT SECTION FACTOR COUNT VERSUS ENGINE HOURS

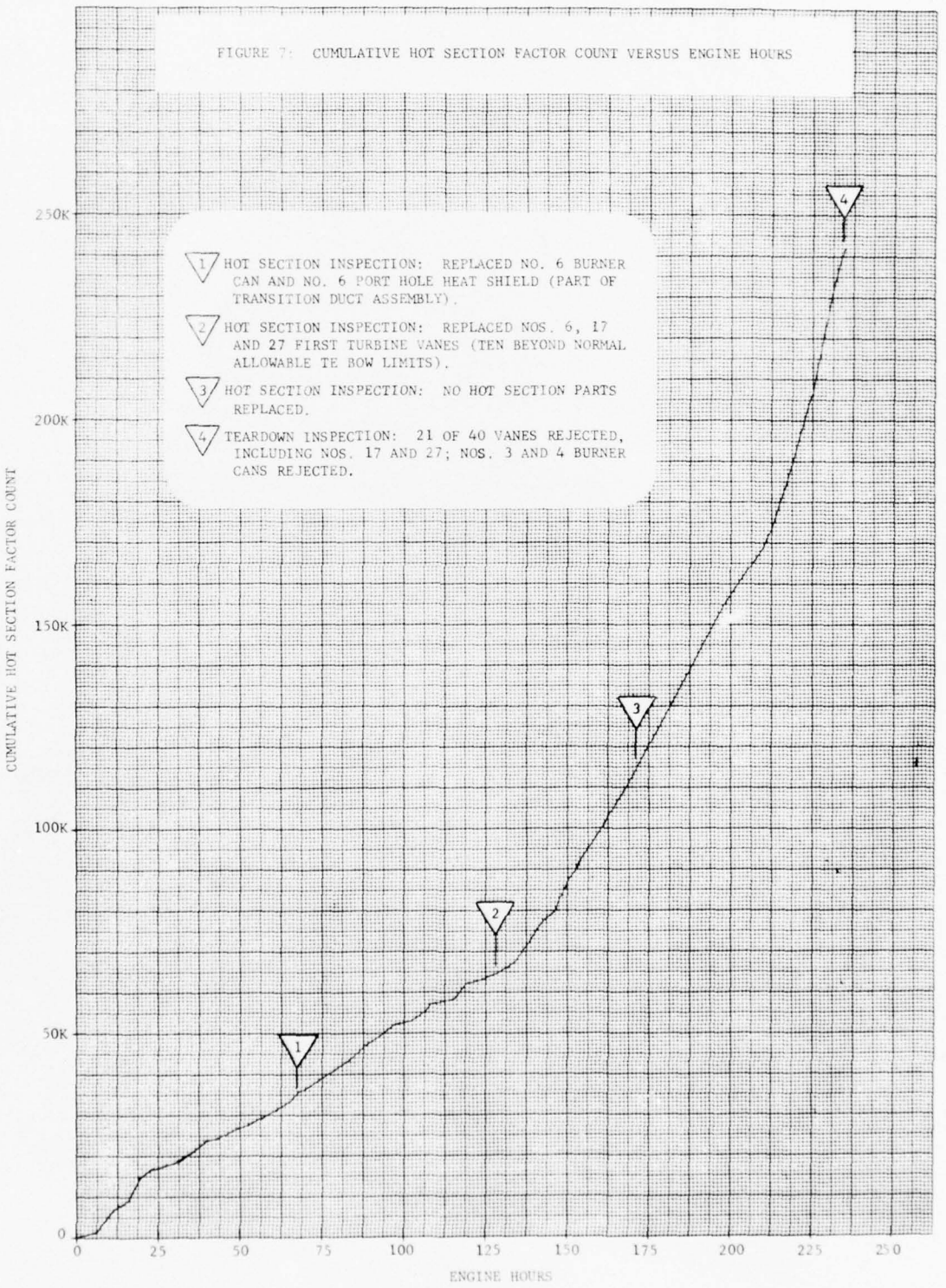

FIGURE 8: OVERALL GEAR DEFECT ANALYSIS

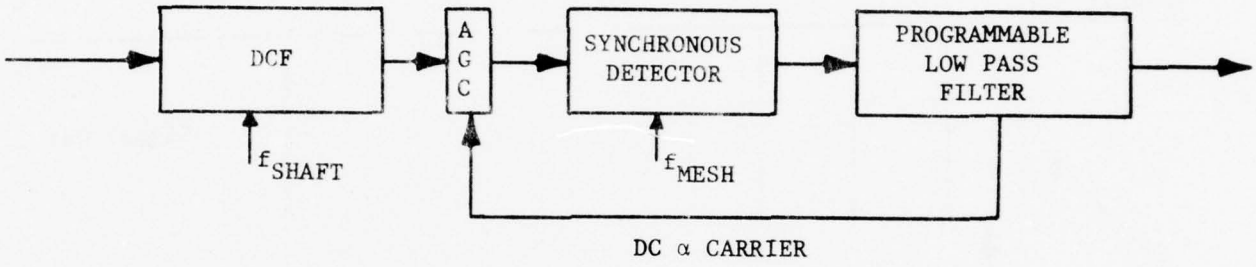

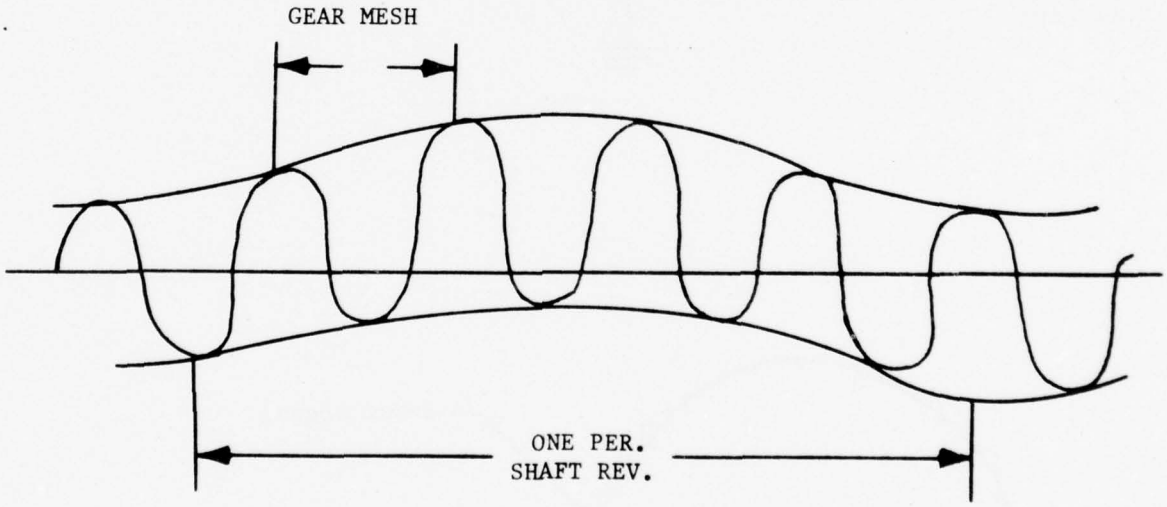

FIGURE 9: DIGITAL COMB FILTER

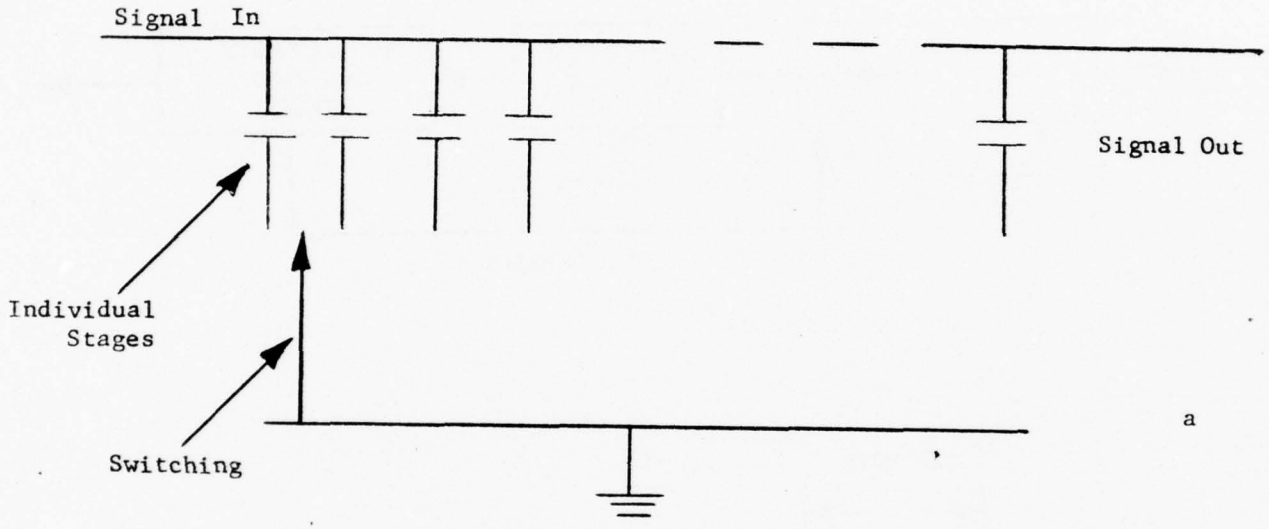

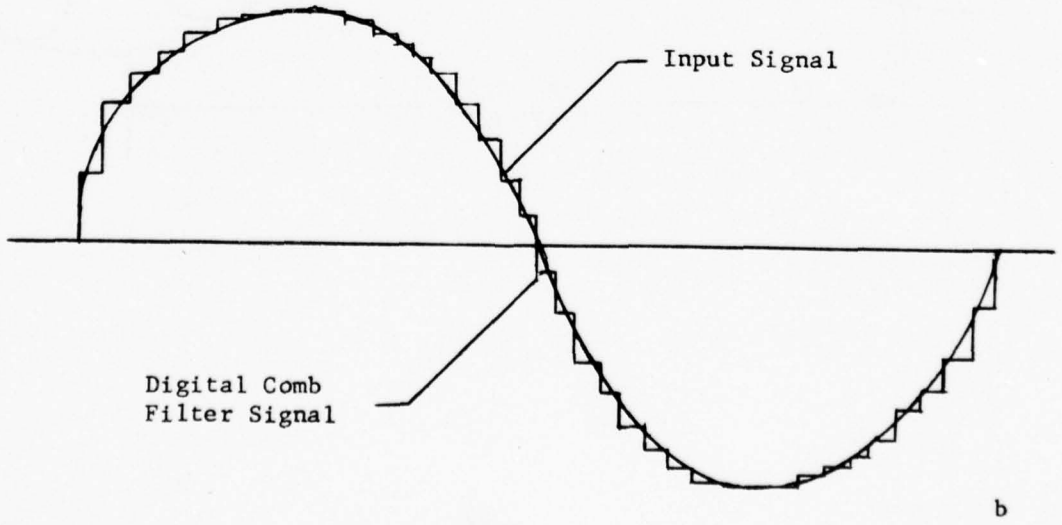

FIGURE 10: COMPARISON OF PYROMETER SIGNAL IN TO DIGITAL COMB FILTER OUT

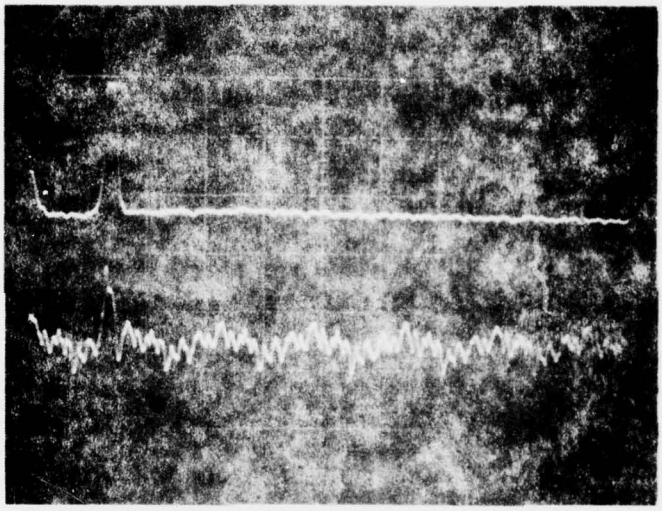

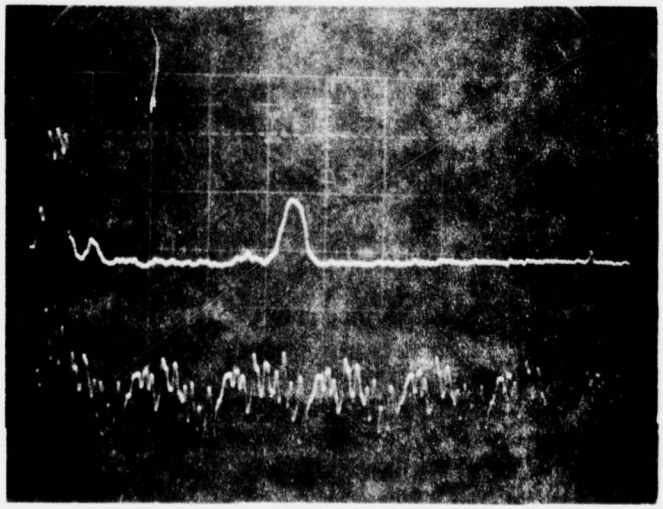

REFERENCES

1. AUTHORIZATION - AIRTASK No. A3305360/218B/2F00433301, Naval Air Systems Command (AIR-330C), of 13 July 1971.

2. REPORT - van Gelder, F.M., "Turbine Engine Diagnostic Development Phase II Report", Naval Air Propulsion Test Center, NAPTC-PE-29 of March 1974

3. AUTHORIZATION - AIRTASK No. A3303300/052B/4F41000000, Naval Air Systems Command (AIR-330C), of 10 August 1973

4. REPORT - Entine, G., "Turbine Inlet Temperature Sensors", Tyco Laboratories, Inc., Contract No. N00140-73-C-1065 Final Report of August 1974

5. REPORT - Westcott, V.C., and Wright, R.W., "Real Time Ferrograph for Application on Jet Engines In A Test Cell Environment", Trans-Sonics, Inc., Contract No. N00140-73-C-1065 Final Report of July 1974

6. TECHNICAL PAPER - Meyer, R.C., "A New Digital Pressure Transducer", Proceedings of the 27th Annual Conference and Exhibit of the ISA, Paper No. 72-601 of October 1972.

7. REPORT - Moffatt, E.M., "High-Pressure Vibrating Pressure Transducer", U.S. Army Air Mobility Research and Development Laboratory, USAAMRDL Technical Report 72-42 of November 1972

8. REPORT - Mihalek, E.W., "Reliability Testing of the Pratt and Whitney Aircraft TF30-P-412A Afterburning Turbofan Engine", Naval Air Propulsion Test Center

9. REPORT - Lutes, J.E., and Mileto, L.A., "Configuration Development Test and Evaluation Of The Time Temperature Recorder and Integrater For The F-8J/J57-P-420 Engine", Naval Air Test Center, ST-187R-71 of 9 September 1971

10. BOOK - Urban, L.A., "Gas Turbine Parameter Interrelationships, Second Edition, United Aircraft Corporation, 1969

11. REPORT - Kos, J.M., "Multiple Fault Gas Path Analysis Applied to TF30-P-408 Engine Data", Hamilton Standard Division of United Technologies Corporation, HSER 6587 of June 1974

12. REPORT - Skovholt, R.L., et al., "Integrated Engine Instrument System (U)", General Electric Co., Contract No. N00019-70-C-0619, Final Report DF71AEE170 of August 1971

APPENDIX A

TEDD Data Smoothing Study

A. Introduction

The purpose of this study was to analyze data smoothing techniques in order to improve on the smoothing calculations used in TEDD Phase II software, particularly in the logic of the mode-detect section of the program.

During Phase II a limited moving average technique was employed. It was limited because of core size restrictions, and was only partially successful for the following reasons: (1) lack of sufficient data to define high rate of change engine events, and (2) inflexibility to change the number of points included in the moving average during real time processing.

Specifically, one severe problem was encountered in the mode detection logic. Due to noise fluctuations, the speed derivatives taken with respect to time were unstable. To have good mode detection, it was therefore necessary to use derivatives that were taken over a longer time span. However, because of these longer derivative response times, the mode detection logic could not properly recognize rapid transients, such as Bodies, that have two rapid changes in slope polarity.

The data used for this analysis was stored on magnetic tape during TEDD Phase II TF30-P-408 engine testing. TF30-P-412 data from a NAPTC Fleet Service Test Program was also used.

This report describes the data used and the different techniques used to smooth it. Criteria are developed that judge these techniques, and some viable methods of smoothing applicable to diagnostic data are presented.

B. TRANSIENT DATA - GENERAL DISCUSSION

TEDD transient data, especially that used for mode detection, have characteristics that make any fixed degree of smoothing difficult to apply. During Phase II of TEDD, short time duration Bodies (rapid deceleration followed immediately by a rapid acceleration) were encountered which occurred in less than three seconds. The high rates of change in the speed parameters, combined with a sample rate of about 5 samples per second, eliminated the possibility of smoothing these parameters, because any attempt to smooth the noise would distort the rates of change so vital for transient mode detection. The other extremes encountered were slow transients and steady state conditions where there were very little changes in parameter magnitudes. In such

cases, data was sampled about every 0.5 to 2.5 seconds and a high degree of smoothing could be done without any concern about distorting the rates of change. However, other criteria such as accuracy entered into consideration.

In this report, moving averages and exponential smoothing techniques are applied to the data. Due to the uniqueness of the application of TEDD data, criteria to judge the results of data smoothing must be developed.

C. CRITERIA

1. Storage Required

This is concerned with how much data storage is required to perform the various smoothing techniques and also how much storage the technique itself will occupy. Obviously, the less storage required the better.

2. Ability to Adjust Rates of Response

The nature of TEDD data is such that it is not known whether the next data sample will have a similar magnitude as the last, or represent a radical change. This characteristic dictates that the techniques must be able to assign weights to the data depending on certain engine parameter rates of change. How well the techniques can do this is an important criteria.

3. Simplicity of Computation

Since the ultimate application of TEDD programming is a real time situation in which the computations are repeated with each new data scan, and since applied smoothing will be essentially an iterative process, the amount of time spent smoothing is critical. Those techniques that employ fewer mathematical steps and can work effectively on less data will be of high interest. Not only will less memory be used, but they will also be faster.

4. Response

This criteria applies mainly to transient conditions. Due to mode detection techniques, little distortion of rates of change of certain key parameters can be tolerated. The tradeoff here is to get the true rate of change of the parameter by smoothing out noise but not to the extent of distorting the true event.

5. Accuracy and Noise Reduction

This criteria is used to compare how well the smoothed data compares to the model of the true event. Standard deviation defined

as the measure of how much the data varies from the mean of the sample, will be used to judge this criteria.

D. TECHNIQUES APPLIED

1. Moving Average Techniques

This is one of the methods chosen for evaluation since it was used previously during TEDD Phase II and, although it had some drawbacks, was fairly successful and accurate enough to warrant further investigation. It minimizes the sum of the squares of the differences between the most recent N observations and the best guess for that average. The simplicity of computation for this method is an obvious plus in a TEDD operating environment.

The moving average technique operates on a time series by computing a series of averages, based on a given number of points in the original series. For example, if Xi is the ith data point in a time series of data points, and N is the number of discrete points to be averaged, the corresponding point in the average series would be computed as shown below:

$$\frac{\sum_{j=i-N+1}^{j=i} X_j}{N}$$

In the same way the following point X_{i+1} would be:

$$\frac{\sum_{j=i-N+2}^{j=i+1} X_j}{N}$$

The value that is picked for N, the number of data points to be included in each average, will not be the same for all data. A small value of N is useful for eliminating small variations in the data, but is relatively ineffective for large variations. Conversely, if too large a value of N is selected, there is the problem of excessive smoothing, thereby ignoring some of the true event.

An inherent problem in applying this method is the lack of data for initial conditions since there are no previous data points to use in computing the initial average. Extra weight will be given to the initial data points until N readings are obtained.

2. Exponential Averaging Technique

Exponential smoothing is a method of estimating each new data point in a time series by letting the new smoothed value be equal to a fraction of the previous smoothed value, plus a fraction of the new data point. This can be written as:

$$S_t(x) = \alpha X_t + (1-\alpha)S_{t-1}(x)$$

$S_t(x)$ = new smoothed data point

α = smoothing constant; the weight given to the new data point

$S_{t-1}(x)$ = previous smoothed data point

X_t = new data point

This method of smoothing is simple to compute and has the advantage of small amounts of data storage. Only two words of storage are required for each parameter instead of the N words required by the moving average technique. Another advantage is its flexibility because only α needs to be varied to change the rate of response. When α is small, the method gives little weight to the new data, which is good for smoothing random noise in a steady stage condition.. A large α will weight the new data heavily so it responds to rapid changes in the time series, which is necessary for tracking transients.

To illustrate the weighting of data in both the moving average and exponential smoothing techniques, see Figure A-1 where N = 4 for the moving average and $\alpha = 0.6$. In the exponential smoothing technique, the weight of data for a given age may be found by substituting for the previous smoothed value the equation that defines in the same terms a still earlier smoothed value (Reference 1). Since $\alpha = 0.6$, the current data point has a weight of 0.6 and the previous data points are weighted 0.24, 0.096, 0.0384, respectively.

$S_t(x) = \alpha X_t + (1-\alpha)S_{t-1}(x)$ substituting for the $S_{t-1}(x)$ term

$S_t(x) = \alpha X_t + (1-\alpha)\ [\alpha X_{t-1} + (1-\alpha)S_{t-2}(x)]$, and continuing to substitute for N earlier values of $S_t(x)$ $S_t(x) = \alpha \sum_{k=0}^{k=t-1} (1-\alpha)^k X_{t-k} + (1-\alpha)^t X_o$

The weight given to the X_{t-k} term with $\alpha = 0.6$; for K = 1, 2, 3 are:

$$.6(1-.6)^1 = .6(.4) = 0.24$$

$$.6(1-.6)^2 = .6(.16) = 0.096$$

$$.6(1-.6)^3 = .6(0.064) = 0.0384$$

When applying the smoothing techniques to transient data it was obvious that no fixed degree of smoothing would satisfy the criteria already discussed. As an example of this in Figure A-2, a moving average with N = 2 is shown along with an exponentially smoothed timed series with $\alpha = 0.2$. It is seen that the moving average follows the real data with almost no change in amplitude, but with a very slight time lag. The exponentially smoothed trace, with little weight given to each new reading, smoothes the steady state interval (from 5.0 to 6.8 seconds) rather well. During the transient, however, there is serious distortion.

If the other extremes (N = 8, $\alpha = 0.8$) are plotted for the same data, it is seen that the smoothing results are almost reversed. Figure A-3 shows that the exponential method tracks the transient almost exactly and does not have as much time lag as did the moving average in Figure A-2. Also, as expected, the moving average smoothed the steady state data well but distorted the transient.

Figures A-2 and A-3 illustrate the "classical" problem of data smoothing for TEDD applications. The main purpose of the TEDD computer program is to diagnose engine problems. Therefore, it is desirable to spend only a small percentage of time reading and smoothing data and to devote a larger percentage to doing actual diagnostics. The conflict arises when trying to get good smoothing results. A high sample rate gives better smoothing, but takes more time to process. A low sample rate takes less time to process, but gives poorer results in smoothing. Figure A-4 states this problem graphically.

E. TECHNIQUES ANALYZED

When analyzing the data, it was convenient to consider the steady state and transient data separately. This is a natural division in that it gives the two extremes of data characteristics to be encountered.

The steady state case will be considered first. Accuracy and how sample rate affects accuracy are the main criteria. Standard deviation will be used as the indicator of accuracy. The standard deviation is defined as the measure of how much the data varies from the mean of a given sample. The expression is given below.

$$\sigma = \left[\frac{\sum_{i=1}^{i=N} (X-\bar{X})^2}{N-1} \right]^{\frac{1}{2}}$$

Where X_i is the ith data point in the sample, $\bar{X}$ is the mean of the sample.

Three parameters (PLA, N2, and PB) will be analyzed. PLA and N2 are key parameters for mode detection and PB is representative of a pressure whose signal noise has to be reckoned with. The data was processed at sample rates of 100, 50, 10 samples/second. Moving averages with N ranging from 2 to 10 were computed. Exponential smoothing was done for $\alpha = 0.9$ to $\alpha = 0.1$. The ranges for N and α were selected to show trends and do not necessarily show the optimum smoothing that is possible. The results of the processing are shown in Tables I, II, and III.

The tables show that each parameter responds to degrees of smoothing in different ways. Not only does the magnitude of the σ's vary from parameter to parameter, but for increasing values of N the standard deviation does not always improve. Because of various frequency components present in the different parameters, higher sampling rates did not always give lower standard deviations. However, the general trends shown in the tables indicate that as N went from 2 to 10 and α from 1.0 to 0.9, the standard deviation of the parameters improved; likewise for increasing sampling rates. It is obvious from the tables that for any degree of smoothing, the smoothed data has a lower standard deviation than the unsmoothed data. For the values of $N = 10$ and $\alpha = 0.1$, the exponential technique was consistently better.

Figure A-5 is a graphic illustration of the effectiveness of exponential smoothing. The unsmoothed data has a σ of 38.665 which is interpreted as the signal varying ±38.665 rpm about the mean of the sample. The smoothed trace has an σ of 6.734. Overall, the percentage of relative error improves from 0.591% to 0.102%.

$$\frac{\Delta Q}{Q} \times 100 = \% \text{ relative error}$$

$$\frac{77.33}{13078} \times 100 = 0.591\%$$

$$\frac{13.468}{13078} \times 100 = 0.102\%$$

TABLE I

EFFECT OF VARYING N, α, AND SAMPLE RATE ON STANDARD DEVIATION OF STEADY STAGE PLA DATA

PLA, DEGREES

N	100 samples/sec σ	50 samples/sec σ	10 samples/sec σ
2	.0737	.0436	.0602
3	.0532	.0311	.0500
4	.0350	.0308	.0413
5	.0245	.0233	.0323
6	.0260	.0278	.0253
7	.0284	.0269	.0199
8	.0274	.0252	.0269
9	.0241	.0285	.0298
10	.0236	.0280	.0359
Unsmoothed data σ	.0947	.0918	.0779
α			
.1	.0138	.0109	.0098
.2	.0226	.0178	.0197
.3	.0316	.0244	.0293
.4	.0140	.0314	.0383
.5	.0507	.0389	.0465
.6	.0604	.0472	.0539
.7	.0698	.0566	.0656
.8	.0788	.0669	.0667
.9	.0870	.0786	.0724

TABLE II

EFFECT OF VARYING N, α, AND SAMPLE RATE ON STANDARD DEVIATION OF STEADY STATE N2 DATA

N2, RPM

N	100 samples/sec σ	50 samples/sec σ	10 samples/sec σ
2	20.666	25.903	21.823
3	14.66	19.959	17.957
4	12.881	17.667	15.454
5	11.643	16.068	19.202
6	11.332	16.370	19.141
7	13.053	16.111	22.219
8	12.888	16.103	22.373
9	13.301	16.302	24.927
10	13.946	16.189	24.777
Unsmoothed data σ	38.665	36.927	30.715
α			
.1	6.734	10.479	9.5036
.2	7.605	12.223	11.469
.3	10.156	14.687	13.358
.4	13.261	17.412	15.573
.5	16.682	20.304	17.894
.6	20.380	23.336	20.264
.7	24.372	26.502	22.677
.8	28.702	29.812	25.177
.9	33.437	33.280	27.833

TABLE III

EFFECT OF VARYING N, α, AND SAMPLE RATE ON STANDARD DEVIATION OF STEADY STATE Pb DATA

Pb, Psia

N	100 samples/sec σ	50 samples/sec σ	10 samples/sec σ
2	.6322	.3610	.5392
3	.4653	.2582	.4926
4	.3127	.2705	.4530
5	.2239	.2224	.3940
6	.2297	.2242	.3436
7	.2454	.2174	.3358
8	.2432	.2179	.3641
9	.2240	.2537	.3976
10	.2034	.2593	.4116
Unsmoothed data σ	.7805	.7656	.6649
α			
.1	.1352	.1059	.1240
.2	.2029	.1474	.1997
.3	.2770	.1989	.2800
.4	.3551	.2561	.3562
.5	.4348	.3192	.4236
.6	.5137	.3892	.4820
.7	.5893	.4673	.5332
.8	.6597	.5550	.5793
.9	.7235	.6538	.6225

In Figure A-5, there is a good illustration of response. The first data point in the time series is 13,400 rpm. With $\alpha = 0.1$ there is little weight given to each new data point. The lag of the smoothed data is slightly less than 0.4 seconds. This lag would have to be taken into account when this technique is applied to data. A higher alpha could be applied until the initial lag time is reached.

The transient data smoothing analysis illustrates the criteria of response and noise reduction. Again, as in the steady state case, PLA, N2 and PB are the parameters to be examined. One criterion for transient data will be time lag, defined as the time in seconds, the smoothed values lag the actual data. Also how smooth the speed and PLA time derivatives are will determine how well the mode detection routine will function. Effects of sample rates will not be analyzed because the minimum sample rate will be dictated by the worst case parameter. In this situation PB was the worst case parameter, having a negative slope of about 56 Psia in 0.08 seconds. It is considered that a minimum of three equally spaced data points is required to define a given slope.

The transient event analyzed was a Bodie combined with a stall. Tables IV through VI show time lags for moving averages with N ranging from 2 to 10 and exponential smoothing with α's ranging from 0.1 to 0.9. The time lags recorded in Tables IV through VI occur at the most abrupt change in slope during the transient. Again, a compromise must be made between response and noise reduction.

The steady state analysis showed that for TEDD application, the exponential smoothing did a better job of noise reduction. For this reason, the moving average technique will not be considered further.

The mode detection routine used in TEDD Phase II looked for a PLA change of one degree in one second to help determine transient and steady state modes. The PLA signal was repeatable to within ± 0.5 degrees. To apply smoothing, it would be desired to smooth the data to be repeatable to within ± 0.1 degrees.

It is estimated that a lag of 0.25 second from the true event to its detection, for current engines, is tolerable. From Table II it is determined that an α of 0.5 will meet the response criteria and in Table I an α of 0.5 has a standard deviation of 0.0465 which is acceptable for repeatability. Figure A-6 shows the results of smoothing with $\alpha = 0.5$ and illustrates that the above criteria can be met.

PB, the parameter that dictates sample rate for transient analysis, has the fastest rate of change of all the parameters examined for diagnostics. In this case, response is the most important criterion and any noise reduction we can get will be acceptable. As mentioned before, during a stall PB dropped as fast as 56 Pisa in 0.08 seconds. To be able to detect this slope before the event is over, a time lag

TABLE IV

EFFECT OF VARYING N AND α ON TIME LAG

OF TRANSIENT PLA DATA

PLA	Samples/sec = 50		
N	Time Lab (sec)	α	Time Lay (sec)
10	.16	.9	.02
9	.14	.8	.02
8	.12	.7	.025
7	.10	.6	.04
6	.07	.5	.06
5	.065	.4	.10
4	.05	.3	.18
3	.03	.2	.31
2	.01	.1	.82

EFFECT OF VARYING N AND α ON TIME LAG OF TRANSIENT N2 DATA

N2 Samples/sec = 50

N	Time Lag (sec)	α	Time Lag (sec)
10	.15	.9	.01
9	.10	.8	.01
8	.10	.7	.01
7	.50	.6	.02
6	.30	.5	.03
5	.04	.4	.05
4	.02	.3	.07
3	.02	.2	.09
2	.01	.1	.15

TABLE VI

EFFECT OF VARYING N AND α ON TIME LAG

OF TRANSIENT P_B DATA

P_B	Samples/sec = 50		
N	Time Lag (sec)	α	Time Lag (sec)
10	.08	.9	.01
9	.06	.8	.01
8	.06	.7	.01
7	.05	.6	.02
6	.04	.5	.03
5	.03	.4	.05
4	.03	.3	.05
3	.02	.2	.05
2	.02	.1	.06

of 0.02 seconds would be acceptable. Table VI shows that an α of 0.6 will give this response. In Figure A-7, the raw data is plotted with the smoothed data and illustrates that the above criterion can be met. With an α of 0.6, standard deviation of steady state before the transient is 0.39.

Another important parameter for mode detection is N2. It was used in the mode detection logic in Phase II to help determine steady state or transient modes, and then further to indicate fast or slow transient. As stated earlier, a change in N2 over a three second period was sought. If the absolute value of the delta was greater than 160 rpm, a transient mode was indicated. Please note this was not the only criterion used to indicate transient or steady state modes. The three second interval was used because of the noise in the N2 trace. It was determined that for the given signal noise level and sample rate, the above was the best criteria. If the sample rate were faster and exponential smoothing methods have been available, the mode detection would have been much improved, especially in the transient section. Again, looking at the Bodie-Stall sequence in Figure A-8, it is seen that the rate of change of N2 to be detected is approximately -625 rpm/sec. To detect this slope and still remain as close in time to the true event as practical, an α of 0.5 is used. The time lag is 0.03 seconds with the results shown in Figure A-8. From Table II, the standard deviation is 20.3. This is a rather large deviation about the mean and probably would not give good slope definition. A standard deviation of 10.479 has very good noise reduction.

F. CONCLUSION

When comparing the two methods of smoothing with the criteria developed earlier, it is obvious the exponential smoothing technique is better suited to TEDD applications than the moving average. Table VII shows the comparison. To apply the exponential smoothing to TEDD data, it is necessary to have pre-defined separate α's for steady state and transients, depending on response and accuracy desired for each parameter. Upon deciding which mode is current, the appropriate α is applied to the data. In Figure A-10, an α of 0.1 is applied to the steady state section and an α of 0.3 is applied to the transient section. Programming details such as initial conditions cannot be overlooked when switching α during a transient.

TABLE VII

CRITERIA	MOVING AVERAGE	EXPONENTIAL SMOOTHING
Storage Required	N x (# of parameters)	2 words for each parameter
Ability of adjust rate of response	Programming more complicated	Easy to implement
Simplicity of computation	More instructions to implement	Fewer instructions; therefore faster
Response	O.K. for proper N	Always better for tested range
Accuracy and nose reduction	O.K. for proper N	Always better for tested range

REFERENCES

Cited

A-1 BOOK - Brown, R. G., "Smoothing, Forecasting and Preduction of Discrete Time Series", Prentice Hall, 1963

Uncited

A-2 BOOK - Elgerd, O., "Control Systems Theory", McGraw-Hill, 1967

A-3 BOOK - Sterling, T. and Pollock, S., "Introduction to Statistical Data Processing", Prentice-Hall, 1968

A-4 BOOK - Kleror, M., and Korn, G. A., "Digital Computer Users Handbook", McGraw-Hill, 1967

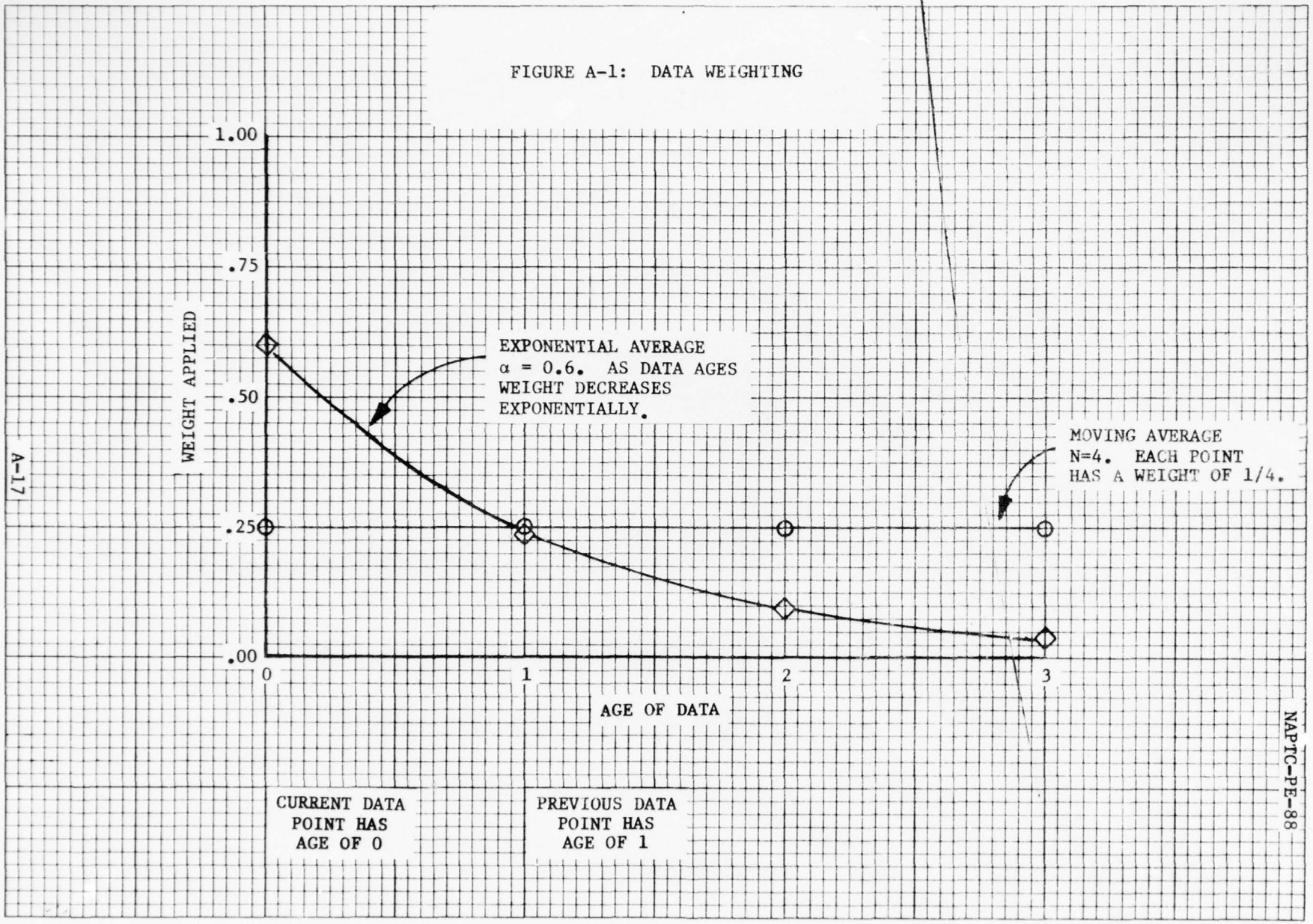
FIGURE A-1: DATA WEIGHTING
1.00
.75
.50
.25
.00
WEIGHT APPLIED
EXPONENTIAL AVERAGE
α = 0.6. AS DATA AGES
WEIGHT DECREASES
EXPONENTIALLY.
MOVING AVERAGE
N=4. EACH POINT
HAS A WEIGHT OF 1/4.
0
1
2
3
AGE OF DATA
CURRENT DATA
POINT HAS
AGE OF 0
PREVIOUS DATA
POINT HAS
AGE OF 1

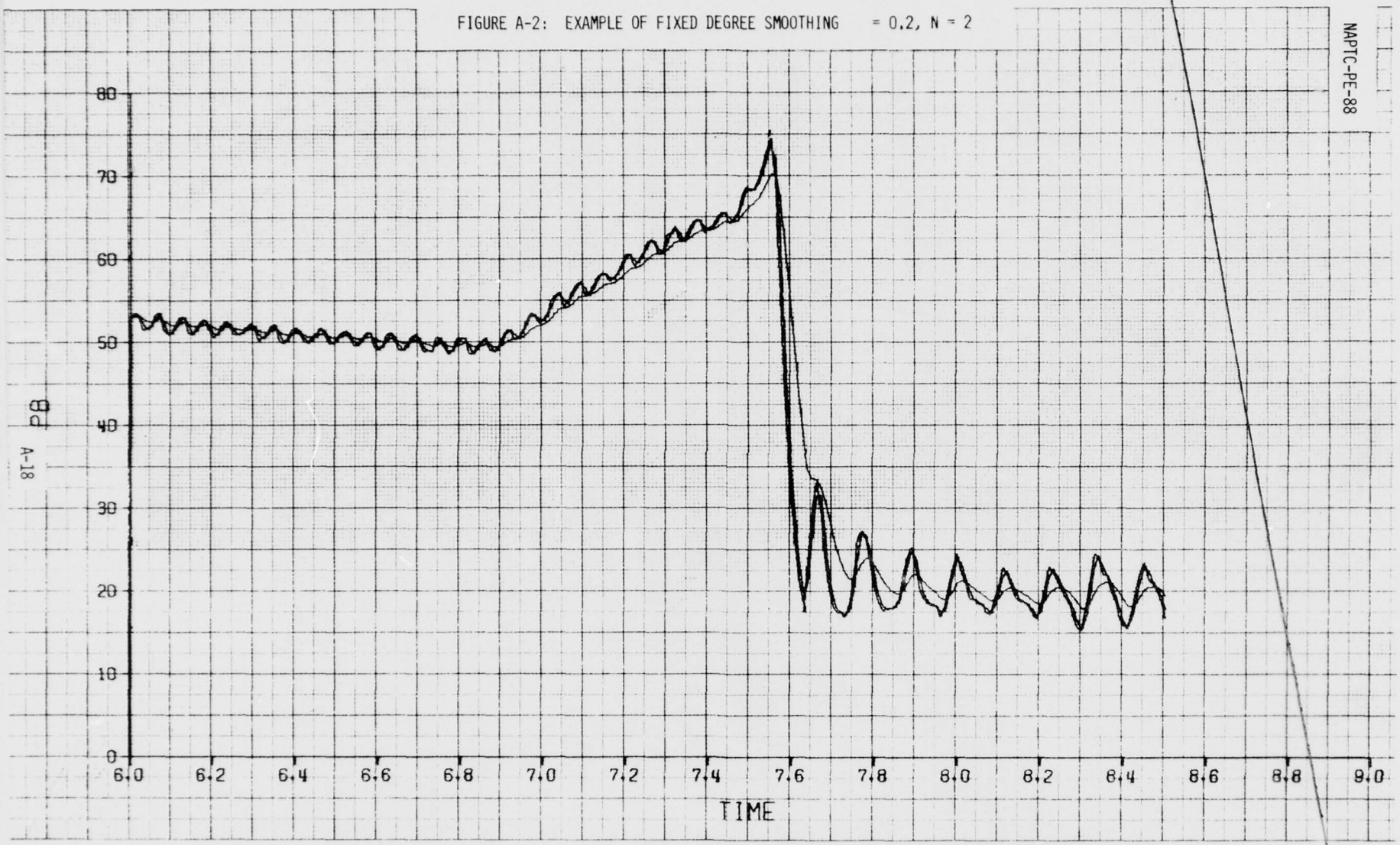
FIGURE A-2: EXAMPLE OF FIXED DEGREE SMOOTHING = 0.2, N = 2
NAPTC-PE-88
dB
80
70
60
50
40
30
20
10
0
6.0
6.2
6.4
6.6
6.8
7.0
7.2
7.4
7.6
7.8
8.0
8.2
8.4
8.6
8.8
9.0
TIME
CALIFORNIA COMPUTER PRODUCTS, INC ANAHEIM CALIFORNIA CHART NO. 02

FIGURE A-3: EXAMPLE OF FIXED DEGREE SMOOTHING = 0.8, N = 8

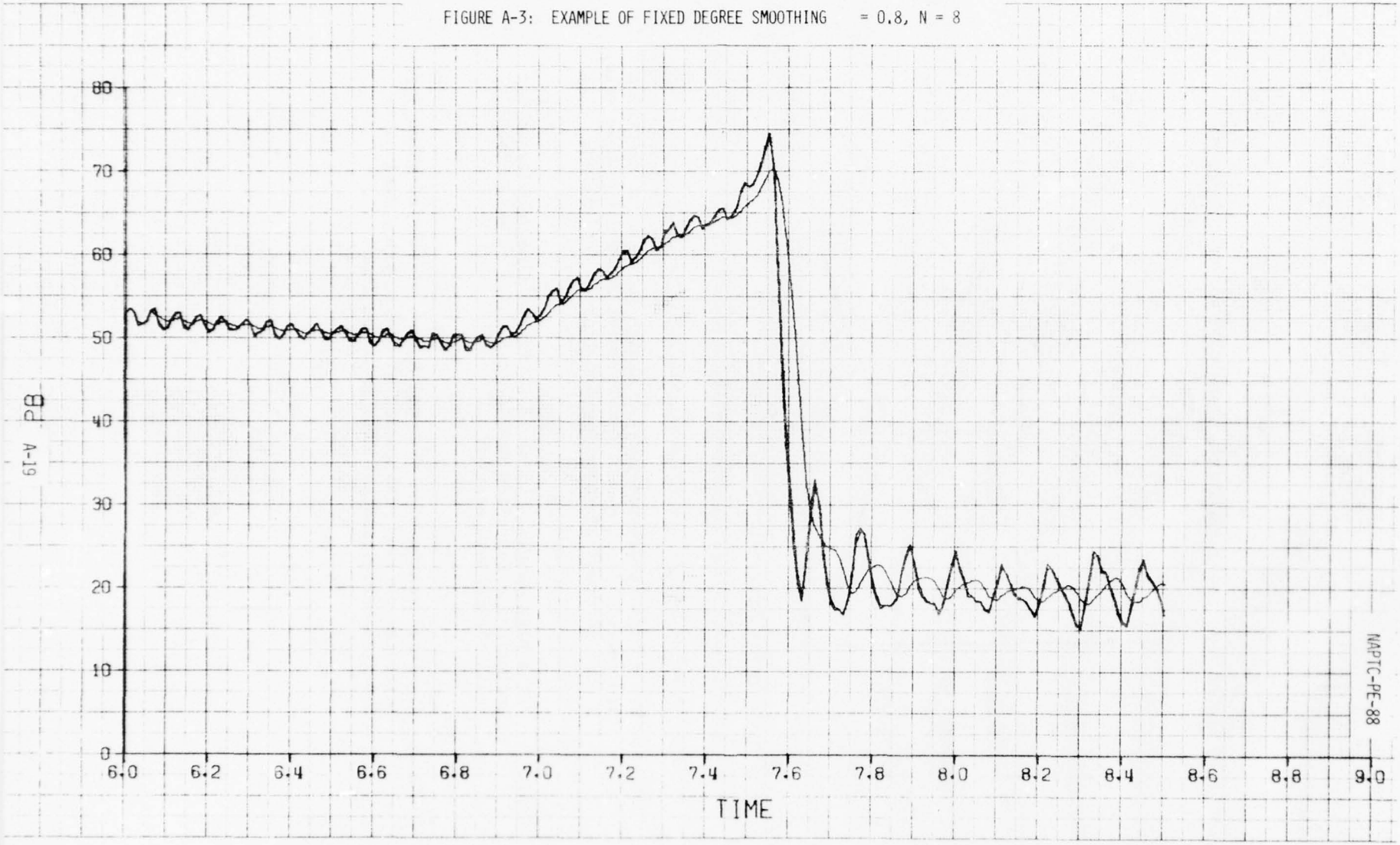

CALIFORNIA COMPUTER PRODUCTS, INC. ANAHEIM, CALIFORNIA CHART NO.

FIGURE A-4: DATA SMOOTHING TRADE-OFFS AND OPTIMIZATION

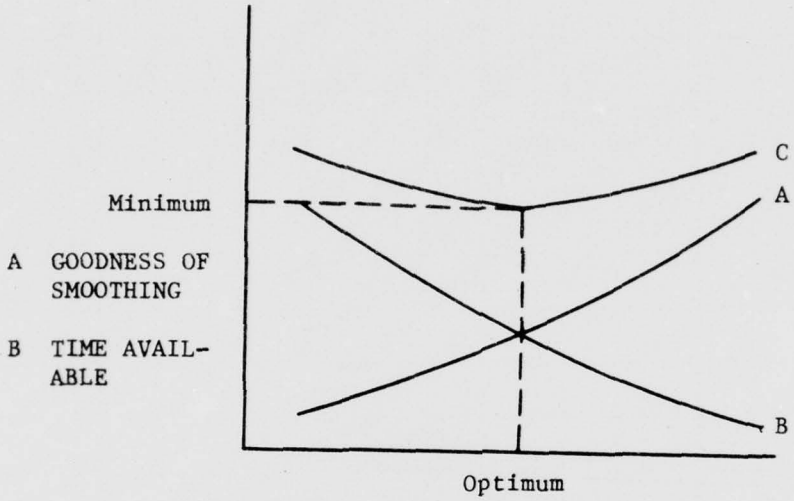

CURVE A: For a high sample rate we get a high goodness of smoothing and definition of event. Conversely, for a low sample rate, a poor goodness of smoothing and lack of definition.

CURVE B: For a high sample rate there is little time for diagnostic analysis and for a low sample rate there is more time available for diagnostics.

CURVE C: Algebraic combination of A and B, the minimum of which indicates the optimum combination of sample rate, diagnostic time available, and goodness of smoothing.

FIGURE A-5: EXPONENTIAL SMOOTHING EFFECTIVENESS

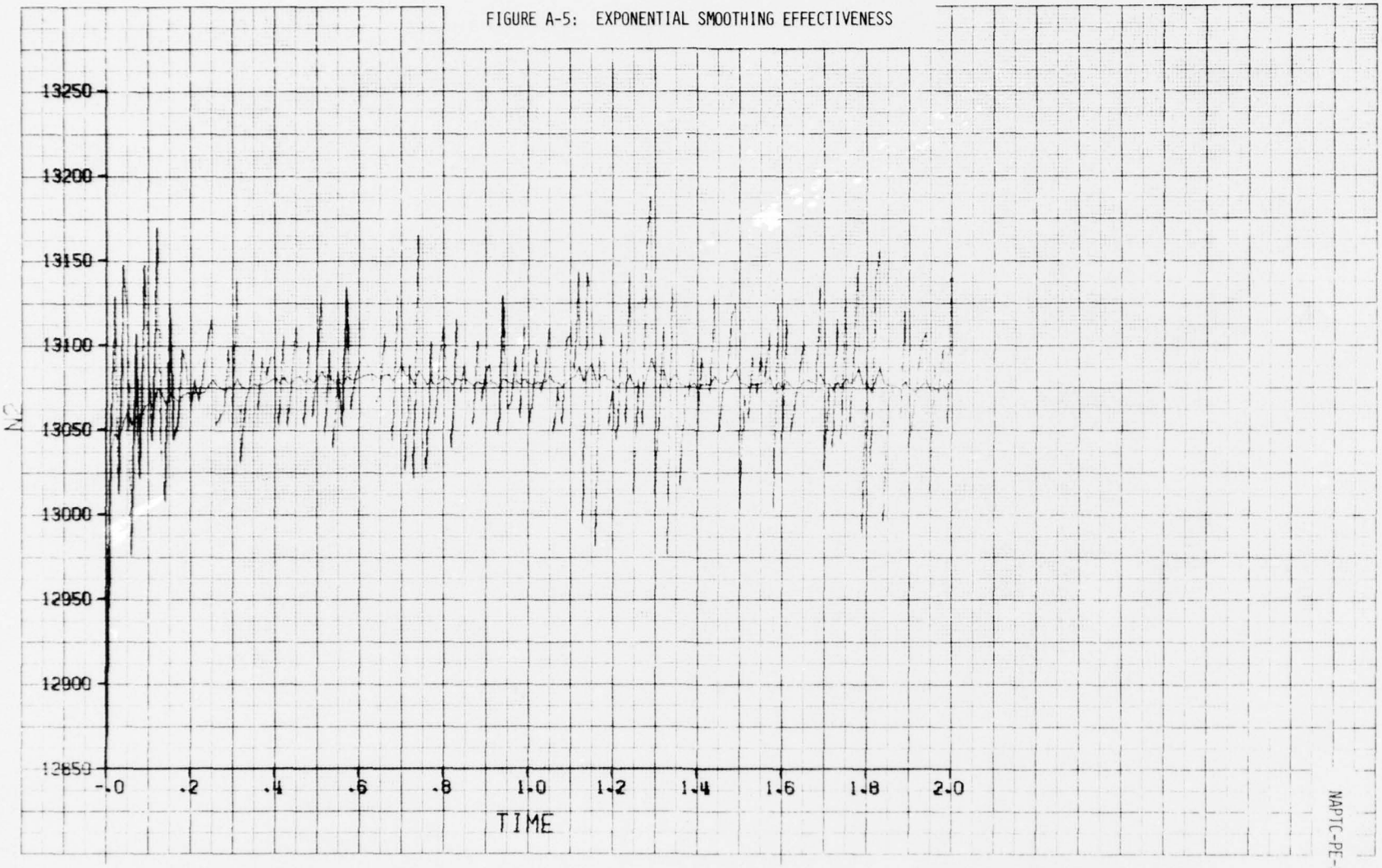

CALIFORNIA COMPUTER PRODUCTS INC. ANAHEIM, CALIFORNIA CHART NO. 026 ↑ 20 DIV. (I) → 20 DIV. (X)

FIGURE A-6: SMOOTHING RESULTS WITH = 0.5

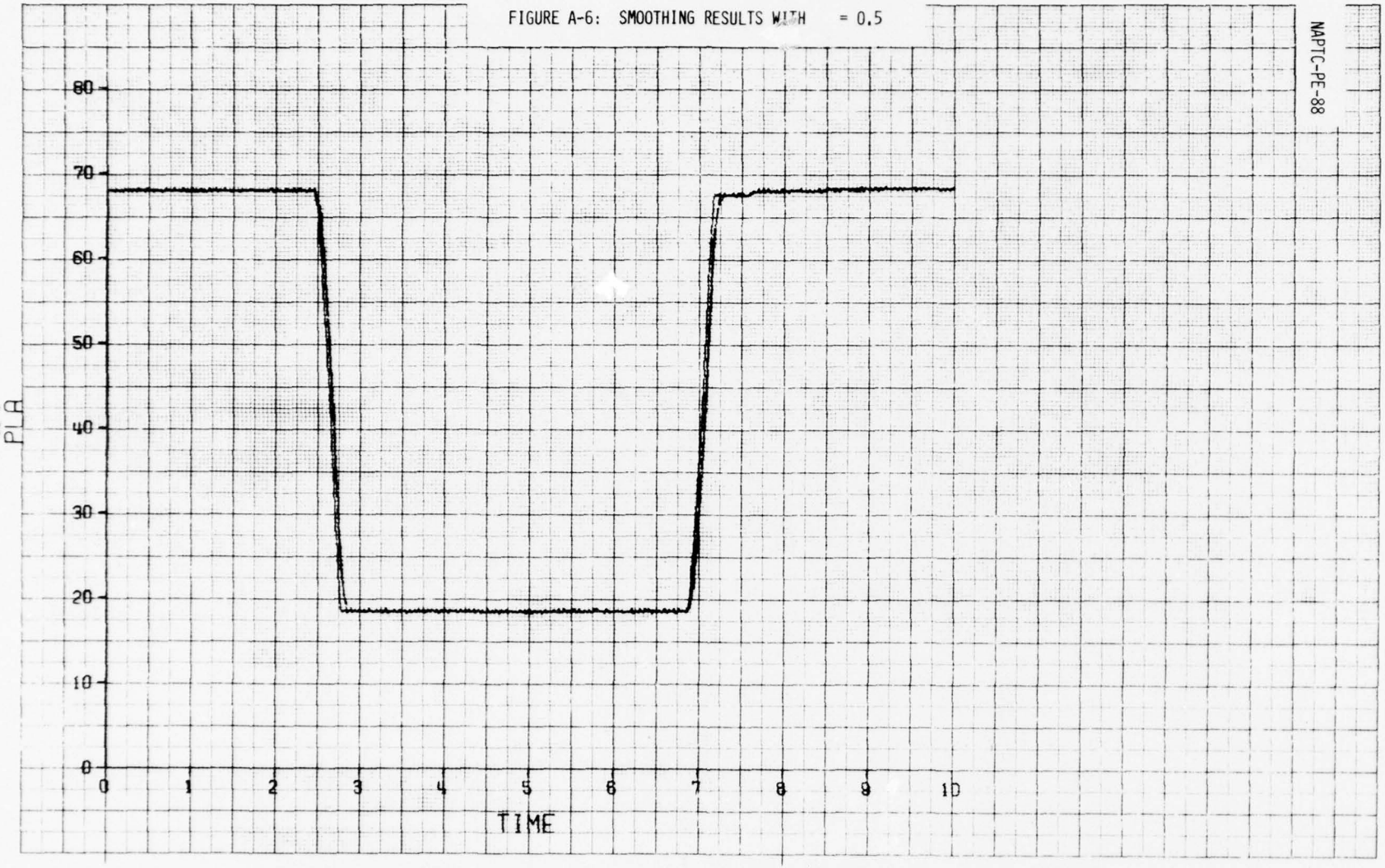

NAPTC-PE-88

CALIFORNIA COMPUTER PRODUCTS, INC. ANAHEIM, CALIFORNIA CHART NO. 028 ↑ 20 DIV. IN → 20 DIV. IN

FIGURE A-7: SMOOTHING RESULTS WITH = 0.6

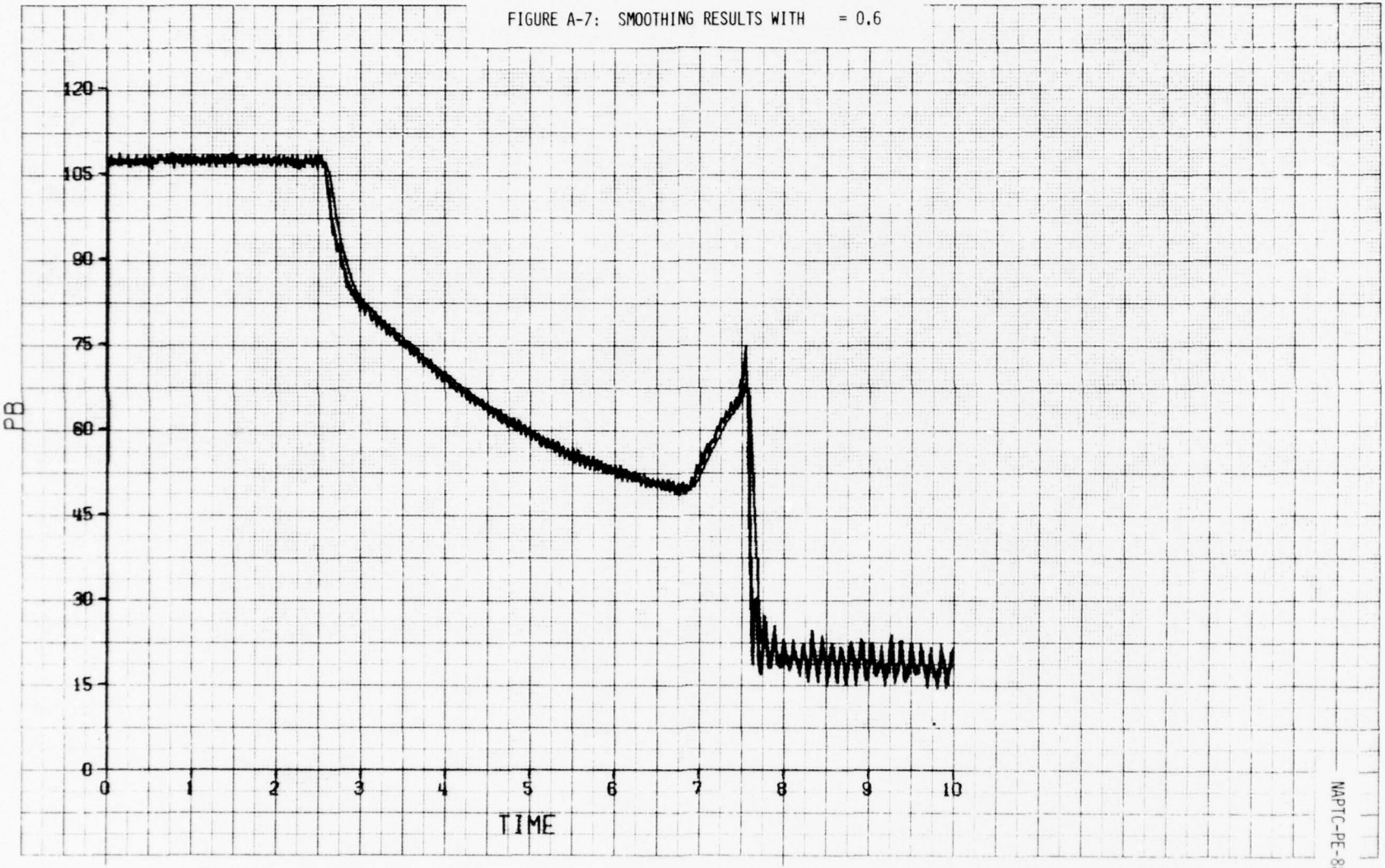

NAPTC-PE-88

FIGURE A-8: SMOOTHING RESULTS WITH = 0.5

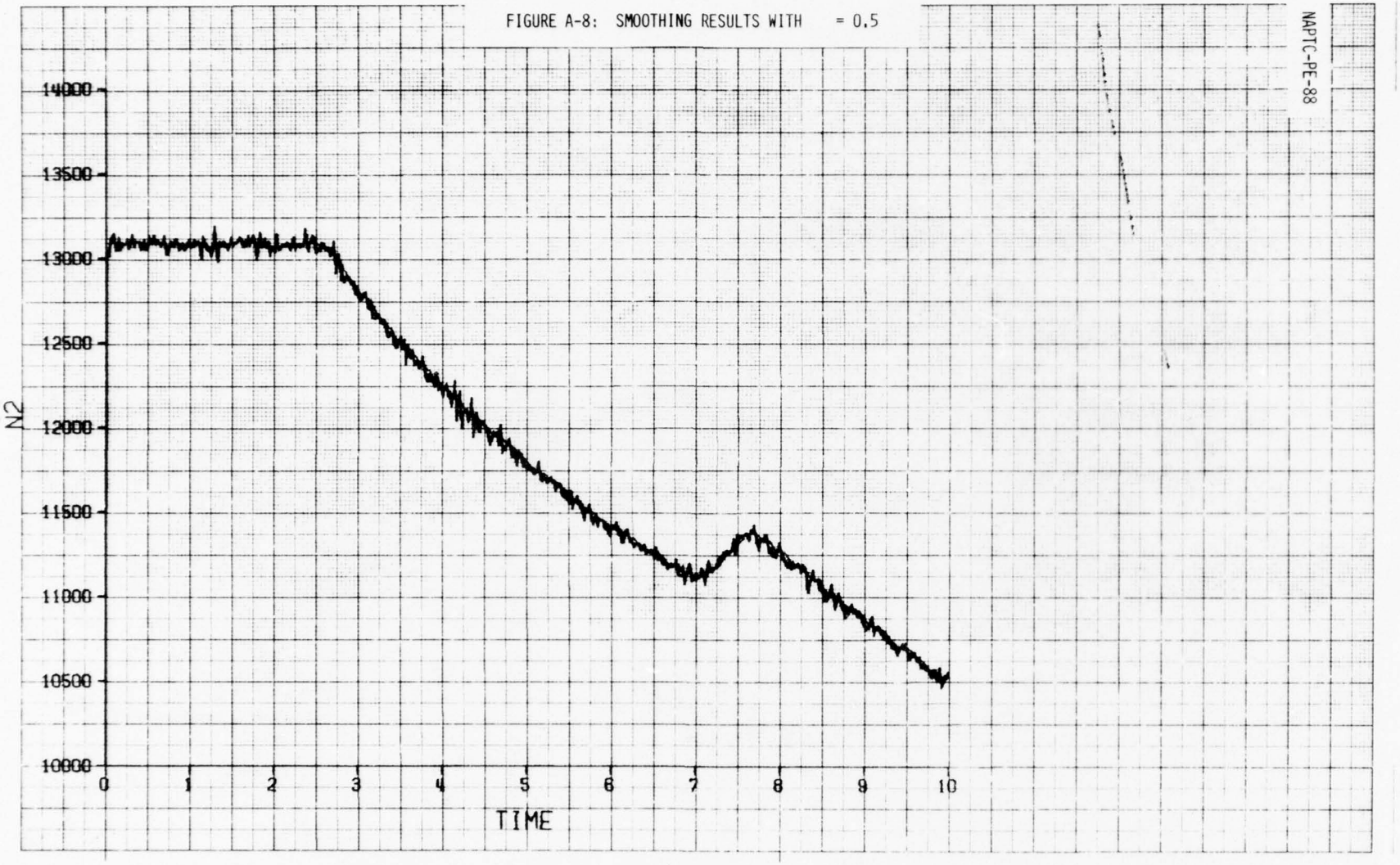

FIGURE A-9: SPEED DERIVATIVES WITH ENGINE MODE CORRELATION = 0.1

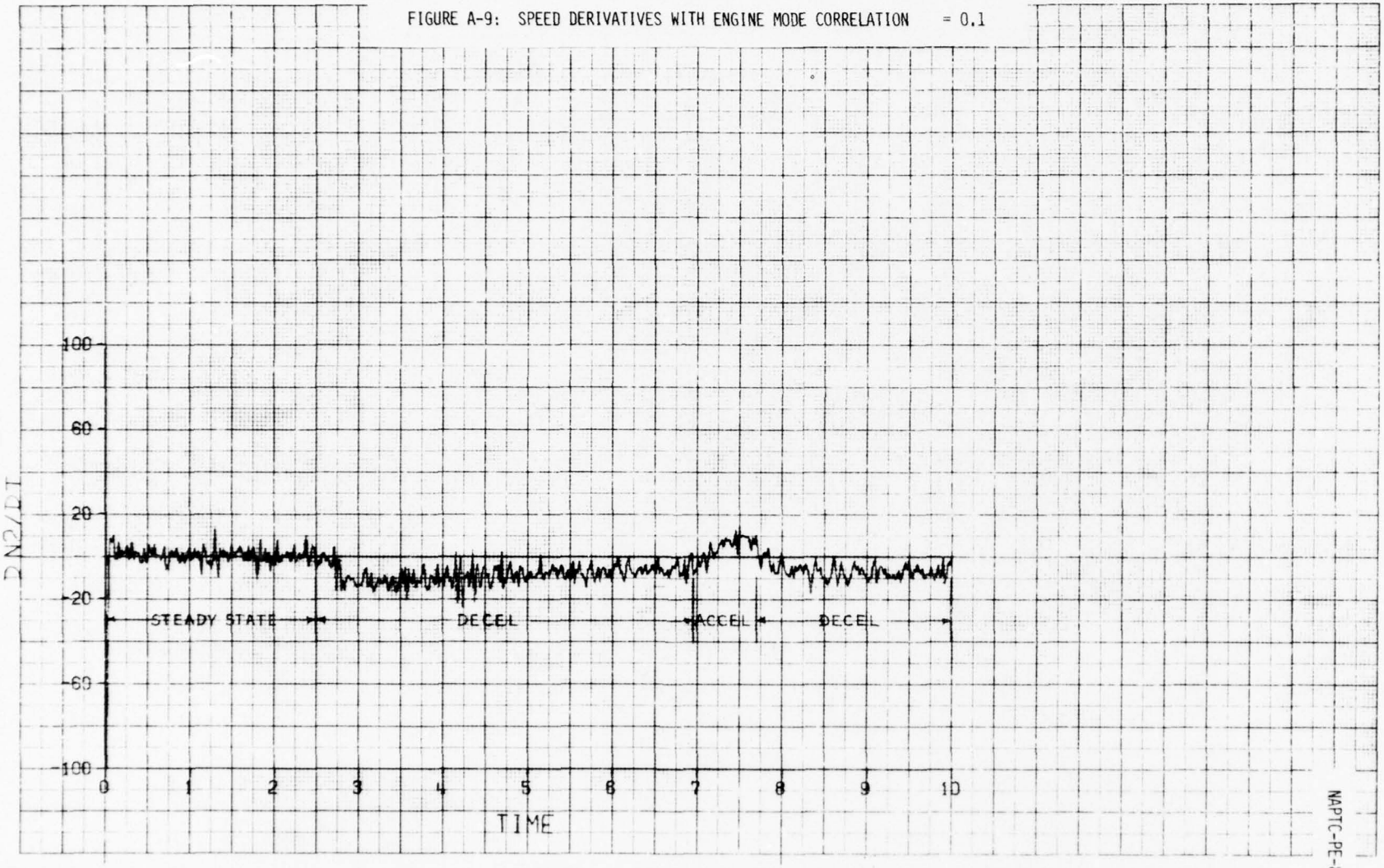

A-25

I.T./CNC

NAPTC-PE-88

CALIFORNIA COMPUTER PRODUCTS, INC. ANAHEIM, CALIFORNIA CHART NO. 028 ↑ 20 DIV. IN → 20 DIV. IN

FIGURE A-10: SMOOTHING WITH MULTIPLE 's

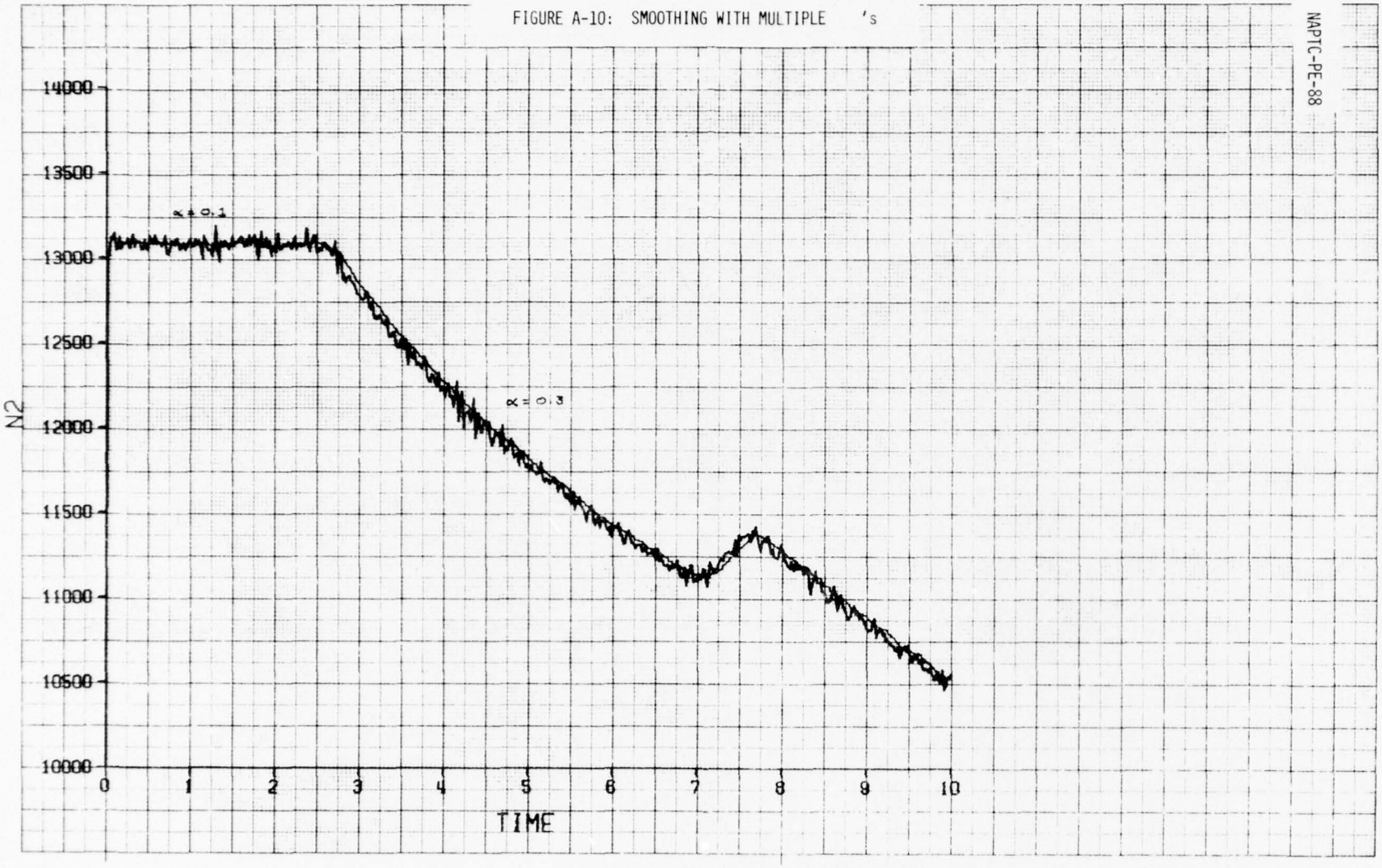

CALIFORNIA COMPUTER PRODUCTS, INC. ANAHEIM, CALIFORNIA CHART NO. 02B ↑ 20 DIV. IN → 20 DIV. IN

APPENDIX B

Multiple Fault Gas Path Analysis

Applied to TF30-P-408 Engine Data

(SUMMARY OF HAMILTON-STANDARD REPORT HSER 6587)

A. INTRODUCTION

Under Phase II of the Turbine Engine Diagnostics Development Program, steady state data from the TF30-P-408 engine was obtained, with and without deliberately introduced faults. This data was supplied to the Hamilton-Standard Division of United Technologies Corporation, under Contract Number N00140-74-C-0582 for the purpose of applying the Parameter Interrelationships method of gas path analysis. The results of this study provide a means for evaluating this approach to multiple fault gas path analysis. This document serves only as a summary of the effort conducted by Hamilton-Standard. A thorough description of the Parameter Interrelationships method, as well as a complete set of results, are contained in Reference B-1.

B. DESCRIPTION OF DATA SUPPLIED

The data supplied to Hamilton-Standard for this study are of three types; steady state engine data with and without known faults, engine base line calibration data, and TF30 cycle deck data at sea level, Mach number >0. Each of the engine parameters was acquired 200 times through the transient data system over a period of six seconds and statistically averaged to a single value. Fifty channels of data comprise a "snapshot" and 97 "snapshots" were provided for analysis. Fifty-three of these "snapshots" are data acquired at sea level static with one or two deliberately introduced faults. The remaining 44 "snapshots" are data acquired at sea level with inlet ram conditions simulating Flight Mach numbers from .25 to .75, with and without introduced faults. Five difference faults were introduced: customer bleed air extraction from the ninth (BL3) and sixteenth (BL4) stage, surge bleed air extraction (BL3.5) and two abnormal exhaust nozzle areas (AJN+)(AJN-). The engine power settings ranged between 1.6 and 2.2 in engine pressure ratio (PT7/PT2).

C. DESCRIPTION OF ANALYTICAL TECHNIQUES

Whatever form it may take, any engine diagnostic system must rely on discernable changes in observable parameters in order to detect physical faults. Physical faults in an engine are in general some combination of problems such as erosion, corrosion, foreign object damage (F.O.D.), worn seals, etc. Although the physical faults result in changes in observable parameters such as rotational speeds, temperatures, pressures, etc., it is more fundamental to consider the physical faults as causing changes in engine component performance parameters such as component efficiencies,

turbine and exhaust nozzle areas, compressor pumping capacities, etc., and that these changes, in turn, result in discernible changes in the measurable engine parameters. If proper equations can be established relating the dependent engine variables (measurable quantities) to the generally nonmeasurable independent component performance variables, then an inverted set of relationships can be obtained relating the independent variables to the dependent variables. This could then form the basis of an engine diagnostic system which would have the capability of detecting multiple faults as well as the magnitude and direction of the fault.

This is the basic technique employed by Hamilton-Standard in their engine diagnostic system. The major obstacle in employing such a diagnostic scheme is in establishing the proper relationships that exist between the dependent and independent engine variables. Two different approaches were used to establish these relationships. Before discussing these approaches, it is appropriate to define two terms. The first term is "delta" (Δ). The term "delta" means the percent of point difference in a particular variable relative to its nominal or base line value. For example, if y_m and x_m are the measured values of two engine parameters y and x, then Δy at x = constant and Δx at y = constant would be calculated as illustrated in Figure B-1. Note that by the above definition, all Δ's are dimensionless quantities whose value for any variable does not depend on the units used to measure the variable. The second term is "fault coefficient." This is just the percent change in a dependent variable per unit percent change in an independent variable. For example, if in Figure B-1, Δy at x = constant was the result of a change in exhaust nozzle area of an amount ΔA_{JN} only, then the fault coefficient of y with respect to A_{JN} at x = constant would be simply $\Delta y/\Delta A_{JN}$. Note that since the deltas are dimensionless, the fault coefficient is also dimensionless. Two methods are used in this study to calculate the required fault coefficients. The first method uses an elaborate gas path analysis of the engine developed by Hamilton-Standard and is primarily theoretical in nature. The second method is empirical and uses available base line test data as well as engine test data obtained with known changes made to the base line configuration.

As shown in Reference B-2, a general influence coefficient matrix can be derived for any particular gas turbine cycle. This matrix represents a set of linearized equations which interrelates the various dependent and independent engine performance parameters. Each of the coefficient is derived by proper manipulation of the differential forms of the basic thermodynamic equations for each engine type. Factors such as component efficiency variations; specific shapes of the component performance maps; engine power balance; conservation of mass, energy and momentum; variable specific heat effects; nozzle unchoking effects, etc., are taken into account. For the actual TF30-P-408 engine used in the test, such details as component efficiency variations, specific shapes of the component performance maps, etc., were not available. Judgment numbers based on experience and the model specification for this engine were used to obtain the theoretical fault coefficients. The theoretical fault coefficients were computed at low, medium and high power conditions at sea level static and a linear least square line was fitted to the data.

An alternate approach using actual engine data is available for calculating the fault coefficients. This method is empirical and makes use of nominal base line engine data as well as steady-state engine data with deliberate perturbations of known amounts introduced individually. From test data where all independent variables are held fixed except one, the resulting delta of any measurable dependent variable is a results of the one known perturbation. In empirically determining the fault coefficients, it has been tacitly assumed that independent component performance parameters such as component efficiencies, turbine nozzle area, etc., did not independently change during the test. In other words, the only perturbations were exhaust nozzle area changes and varying the three compressor bleeds. It follows, therefore, that only the fault coefficients with respect to these four disturbances can be computed empirically.

Once the numerical values for the fault coefficients have been determined, applying them to engine diagnostics is relatively straightforward. In general, if n faults are to be computed, n+1 measurements are required. One measurement serves as the abscissa against which n deviations from base line values are obtained. If the column vector $\underline{x}$ represents the set of n sought after deltas (such as changes in component efficiencies, bleed flows, geometries, etc.) and the column vector $\underline{m_i}$ is the set of n delta measurements, then they are related by an nxn matrix of fault coefficients F_i as:

$$\underline{m_i} = F_i \, \underline{x}$$

A subscript i is attached to $\underline{m}$ and F to emphasize that, in general, there may be more than one set of sensor measurements which can be used to diagnose a given set of faults. If the measurement deltas bear a meaningful relationship to the sought after deltas, then F_i will have an inverse and we can solve the above equation for $\underline{x}$ to obtain:

$$\underline{x} = (F_i)^{-1} \, \underline{m_i}$$

This equation represents the diagnostic routine used in this study. Eleven different diagnostic routines (eleven different sets of sensors and sought for faults) were considered in this study and a comparison was made of their ability to diagnose a known set of changes made to the base engine configuration. Figure B-2 summarizes the eleven systems considered in this study. There eleven systems by no means represent all possible systems. However, these eleven systems are sufficient to demonstrate the validity and versatility of Hamilton-Standard's approach to engine diagnostics.

Referring to Figure B-2 Systems 1 and 2 use two different sets of sensor measurements to look for the same set of faults. The sought for faults for Systems 1 and 2 are precisely those which were varied during the test. Because of the very limited amount of data available with a surge bleed (W_{BL} 3.5) change introduced, the remaining systems replace the ΔW_{BL} 3.5 calculation with one or more additional independent parameter

changes. The magnitudes of these additional parameter changes were assumed to be zero. This assumption is reasonable since the data was taken over a time period too short for the engine components to degrade significantly. It is necessary, of course, to use the theoretically determined fault coefficients to relate the measurement deltas to these additional independent parameter deltas. Systems 3, 4, and 5 have replaced the ΔW_{BL} 3.5 calculation with $\Delta A5$. Systems 6 and 7 have increased the number of measurement deltas (and sought for deltas) by 1. Systems 8-11 have increased the number of measurement deltas by 2. Note that Systems 1 and 4 and Systems 2 and 3 use the same set of measurement deltas to look for different sets of independent parameter deltas.

D. ANALYSIS RESULTS

A Fortran IV Computer Program for use on the IBM 370/155 Digital Computer was written to evaluate the various diagnostic systems indicated in Figure B-2. For any of the systems, the program establishes the matrix of fault coefficients using N1C2 as the abscissa; calculates the set of measurement deltas at N1C2 = constant from the actual snapshot measurements and the base line performance curves; performs the required matrix inversion and calculates the independent parameter deltas. This procedure is repeated using N2C2 and PT7/PT2 as the abscissa. Theoretically, the calculated independent deltas should be the same regardless of which parameter is used as the abscissa. Results were obtained using both the theoretically determined fault coefficients as well as the empirical fault coefficients. Results obtained with the latter are identified by the term "mixed."

1. Sea Level Static

In order to assess the relative merits of the various diagnostic system shown in Figure B-2, several individual snapshots were passed through all eleven systems and a comparison made of their ability to predict the engine configuration.

Figure B-3 shows what the predicted independent deltas would be for each of the eleven systems using the data of Snapshot 114. For Snapshot 114, the engine pressure ratio was approximately 2.0. The actual parameter deltas are indicated by the solid horizontal lines. As shown in Figure B-3, the only change to the base engine configuration was a +5% change in the exhaust nozzle area A_{JN}. Results using both the theoretical as well as the mixed fault coefficients are shown in Figure B-3. Note that for each system, three points are shown. The left most point for each system gives the results using N1C2 as the abscissa in evaluating the fault coefficients and calculating the measurement deltas. The middle point for each system gives the results using N2C2 as the abscissa and the right most point for each system gives the results using PT7/PT2 as the abscissa.

All systems attempt to diagnose the changes in A_{JN}, WBL3 and WBL4. Systems 1-6 do about equally well in predicting ΔA_{JN}. Depending on the

abscissa, they calculate ΔA_{JN} to be 4.4 to 4.6%, which is quite close to the actual value of 5%. System 7 does a little better with a ΔA_{JN} calculation of about 4.7%. Figure B-3 shows that System 8 calculates ΔAJN most accurately. Since the only perturbation deliberately introduced was a +5% change in A_{JN}, the actual levels of the other independent deltas is taken to be zero. Systems 1-7 do a reasonably accurate calculation of the independent deltas. The results obtained using the mixed fault coefficients are somewhat better overall than the results using purely theoretical coefficients. Systems 8-11 show significant differences between the actual and calculated independent parameter changes. Systems 10 and 11 for example predict that the 3.0 bleed was approximately 2.9% and 2%, respectively, even though for this snapshot though for this snapshot the actual bleed was zero. The calculated deltas for WBL3, WBL4, Γ_3 and η_{CH} for System 8 using the mixed fault coefficients showed such a wide variance depending on the abscissa used that these points were not plotted in Figure B-3. Thus, although System 8 does the best job of predicting ΔA_{JN}, it predicts the other deltas so poorly that, based on the results for this single snapshot, it would have to be rejected as an acceptable diagnostic system.

Figure B-4 shows the diagnostic results using the data for Snapshot 115. For this case, two perturbations were introduced simultaneously; a 5% increase, A_{JN} and a 4.0 bleed of approximately 2.2%. Systems 1-7 using the mixed matrices predict these changes quite well. For all systems, the predicted ΔA_{JN} using the theoretical fault coefficients is about 0.5 to 1% lower than the ΔA_{JN} predicted using the mixed matrices. System 8 again stands out as an undesirable diagnostic system.

Figure B-5 shows the diagnostic system results for Snapshot 116. This is a multiple fault condition where the actual change to the base engine configuration was a 5% increase in A_{JN} and a 3.0 bleed of about 2.6%. Systems 1-7 do a good job of predicting these changes. Systems 8 and 9 are judged unacceptable since they have difficulty distinguishing between the 3.0 and 4.0 bleeds. Using the theoretical fault coefficients, Systems 10 and 11 predict the 3.0 bleed significantly higher than the actual value. System 10 predicts a fan efficiency change of -2.6%. System 11 predicts a fan efficiency change of -2%. In both cases, the actual fan efficiency change is assumed to be zero. For these reasons, Systems 10 and 11 are also judged unacceptable as diagnostic systems.

Figures B3-5 show one way of presenting the diagnostic results. These figures show various snapshots passed through all systems. Such an analysis is useful in quickly isolating unacceptable systems. An alternate way of presenting the diagnostic results is to pass all snapshots through a single system. Rather than considering all seven of the remaining acceptable systems, four which were judged best in overall performance were analyzed in this manner. Figure B-6 shows the diagnostic results for all snapshot cases for System 1. The abscissa used in the diagnostic system was engine pressure ratio (PT7/PT2). The actual fault is indicated by the solid lines. To provide greater visibility to the

results, various snapshots were divided into six groups. The first group had just a +5% A_{JN} fault introduced. This group consisted of seven snapshots. The second group has eleven snapshots and are those cases that had just a 3.0 bleed. The third group had just a 4.0 bleed fault. The total number of snapshots in this group is 14. The fourth grouping are those snapshots which have both a 5% A_{JN} increase and a 4.0 bleed. The fifth grouping are those snapshots which have both a 5% A_{JN} increase and a 3.0 bleed. The total number of snapshots in each of the latter two groups is four. The last group are those snapshots for which no fault was indicated. It was assumed that these cases were run with the base engine configuration and therefore all independent deltas were taken to be zero. The total number of snapshots in this last group is seven. Figure B-6 shows Snapshot 97 to be a bad data point. Close examination of the data confirmed the error. Figures B-7, B-8 and B-9 show the diagnostic results for all snapshots for Systems 2, 5 and 7, respectively. These figures also indicate that Snapshot 97 is a bad data point.

A total of 53 snapshots were run at the sea level static condition. Six of the 53 snapshot cases were not included in Figures B-6 through B-9. Two cases were with just a 5% A_{JN} decrease and two cases were with a 5% A_{JN} decrease and bleed. For Systems 1 and 2 which look for the surge bleed change, the calculated deltas for the two surge bleed cases were in very close agreement with the assumed actual values using the empirical coefficients but showd a very wide variance using the theoretical coefficients. The wide variation between the assumed and calculated fault levels was obtained for all the calculated faults. The reason for this is that the surge bleed is such a severe disturbance to the base line configuration and produces such large measurement deltas that the linearization procedure on which the theoretical fault coefficients are based is no longer valid. For those systems which did not look for a surge bleed change, the two surge bleed cases gave totally erroneous results as expected. How an unsought for independent delta affects the calculated deltas is discussed in Reference A.

For the cases where a -5% change in A_{JN} was made, the diagnostics systems calculated the change to be between approximately -8% and -10%. This is caused by the nonlinear nature of the problem. Comparing the dependent parameter deltas for a +5% change in A_{JN} and a -5% change in A_{JN} showed that the resulting deltas were not equal in magnitude and opposite in sign as would be the case if everything were purely linear.

2. Non Zero Mach No. Conditions

In order to establish the proper measurement deltas at the different Mach number conditions, two methods are available. One method uses the static base line to establish a gross delta from which the effect due to Mach number must be subtracted to obtain the net delta for use in the diagnostic routine. Another method is to use a base line customized for the particular Mach number. The latter approach is used in this study. Due to the relatively significant differences between

the empirical and the cycle deck derived Mach effects, only the empirical data was used.

At Mach 0.25, the no fault snapshot cases were sufficiently close to the static base lines to allow the use of the static base line characteristics. At Mach 0.5 and 0.75, however, custom base lines had to be obtained. Using the no fault snapshot cases, various engine parameters were plotted as a function of N1C2, N2C2 and PT7/PT2. A polynomial curve in the least square error sense was fitted to the data. These curves were used to establish the measurement deltas at Mach 0.50 and 0.75.

Eight snapshots were obtained at the simulated Mach = 0.25 condition. Three had just a 5% A_{JN} increase and five had no indicated fault. Figures B-10, B-11, B-12 and B-13 show the diagnostic results for all snapshots for systems 1, 2, 5, and 7, respectively. The static base lines and the mixed fault coefficients were used to obtain the calculated results shown in Figures B-10 through B-13. The abscissa used to establish the measurement deltas and fault coefficients was engine pressure ratio (PT7/PT2). Systems 2 and 7 are somewhat better in their ability to calculate ΔA_{JN}, ΔWBL3 and ΔWBL4 than systems 1 and 5. The calculated deltas for most of the snapshots agree well with the actual deltas.

Using the Mach No. = 0.50 base line characteristics and the mixed fault coefficients, Figures B-14 through B-17 show the diagnostic results for Systems 1, 2, 5 and 7, respectively. Snapshots 175 and 176 were the only non-zero Mach number conditions which had multiple faults introduced. Figures B-14 through B-17 show the calculated deltas to be very close to actual deltas for these cases.

Using the Mach No. = 0.75 base line characteristics and the mixed fault coefficients, Figures B-18 through B-21 show the diagnostic results for Systems 1, 2, 5 and 7 for the simulated Mach = 0.75 snapshots. The calculated deltas for the no fault conditions agree quite well with the actual faults. Only three snapshots were obtained with just 5% area increase. In two out of these three snapshots the calculated change in WBL3 is about +1% compared to the true value of 0.

Of the different diagnostic systems considered, System 7 was chosen as the primary diagnostic system. Although it does not calculate the surge bleed change, it does calculate the changes in A_{JN}, WBL3 and WBL4 quite well. In addition to these three primary perturbations introduced, System 7 also calculates the change in the gas producer turbine effective nozzle area (ΔA5) and also the change in the gas producer turbine efficiency ($\Delta\eta_{TH}$). For most of the 97 snapshots the calculated deltas in A5 and η_{TH} were very close to the assumed values of 0.

System 2 is chosen as an alternate to System 7. This system is simpler in that it only considers the actual perturbations introduced.

This sytem also calculates the changes in A_{JN}, WBL3 and WB14 quite well.

A comment sometimes encountered concerning Hamilton Standard's technique for multiple fault engine diagnostics is that excessive computer storage is required to store and interpolate the fault coefficient matrices and to do the necessary matrix inversion to obtain the required diagnostic matrix. This of course is not the case. It is important to realize that all the matrix inversions necessary to establish the final diagnostic matrix are done offline. Only the final, inverted, diagnostic matrices need be stored. Secondly, it is usually not necessary to store more than one diagnostic matrix. In a practical diagnostic system, the actual diagnostics would be done within a specified power band. How wide this band is depends on the particular application. Usually, a single diagnostic matrix evaluated at the mid power condition within this band is all that is required to do the engine diagnostics.

The required memory increment to include the gas path analysis of System 7 in the computer of a total engine monitoring system would be quite minimal. If we assume all base lines have a common abscissa, then approximately 152 sixteen bit word storage capacity would be required to do the following:

a. To store 5 base lines at three Mach numbers. It is assume that the base lines can be adequately represented by 5 common abscissa values for each base line. Using a 16 bit work to represent two points, 40 words are required.

b. To store the elements of a single 7 x 5 diagnostic matrix D. For precision, 35 sixteen bit words are used.

c. To calculate and store the fault vector $\underline{x}$ by performing the matrix multiplicate $\underline{x} = D\,\underline{m}$, given the measurement vector $\underline{m}$.

Note that, as a kind of bonus, the percentage change in turbine inlet temperature and referred specified fuel consumption measured against the assumed abscissa N2C2 are also computed in this analysis. Since these two parameters are dependent, their changes can be calculated on the basis of the changes in the independent variables. This is an automatic fallout of the gas path analysis technique. The calculated change in T5C2 and SFC will be the change that would be observed if N2C2 were held fixed. This does not imply that N2C2 must be used as an abscissa in establishing the measurement deltas. The assumed abscissa for T5C2 and SFC need not be the same for both, nor do they necessarily have to be the same as the abscissa used in establishing the measured parameter deltas.

It should be noted that WBL3 and WBL4 faults are relatively small (2-3% range). In the sense that bleed is analogous to compressor or turbine degradation in adversely affecting engine performance, the bleed levels detected and diagnosed in this program were equivalent to relatively minor degradation problems elsewhere in the engine.

REFERENCES

B-1 REPORT - Kus, J. M., "Multiple Fault Gas Path Analysis Applied to TF30-P-408 Engine Data", Hamilton Standard Division of United Technologies Corporation, HSER 6587 of June 1974

B-2 HANDBOOK - Urban, L. A., "Gas Turbine Engine Parameter Interrelationships", Hamilton Standard Division of United Technologies Corporation, 1969

FIGURE B-1: GENERAL DEFINITION OF Δ

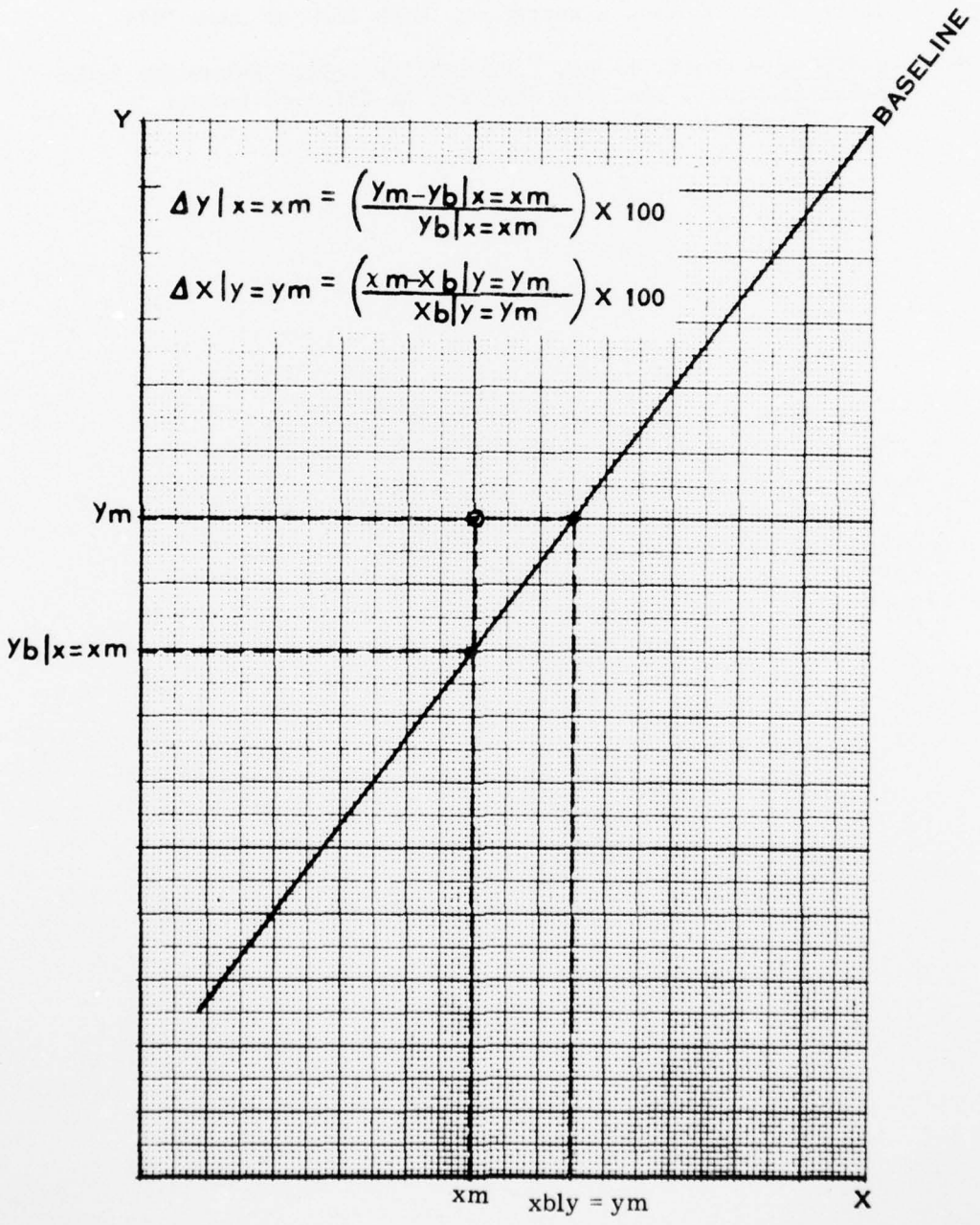

FIGURE B-2: POSSIBLE GAS PATH ANALYSIS SYSTEMS FOR NAPTC TF30-P-408 DATA ANALYSIS

	Measured Parameters	SYSTEM NO. 1	2	3	4	5	6	7	8	9	10	11
1	$N_1/\sqrt{\theta_2}$	X	X	X	X	X	X	X	X	X	X	X
2	T_3/θ_2											X
3	P_3/P_2	X	X	X	X	X	X	X	X	X	X	X
4	$N_2/\sqrt{\theta_2}$	X	X	X	X	X	X	X	X	X	X	X
5	T_4/θ_2								X			
6	P_4/P_2					X	X	X	X	X	X	X
7	$W_f/\delta_2\theta_2^{.62}$	X			X		X			X	X	
8	T_7/θ_2		X	X					X	X		X
9	T_5 CALC$/\theta_2$							X			X	
10	P_7/P_2	X	X	X	X	X	X	X	X	X	X	X

	Calculated Parameters	SYSTEM No. 1	2	3	4	5	6	7	8	9	10	11
1	ΔAJN	X	X	X	X	X	X	X	X	X	X	X
2	ΔWBL 3.0	X	X	X	X	X	X	X	X	X	X	X
3	ΔWBL 3.5	X	X									
4	ΔWBL 4.0	X	X	X	X	X	X	X	X	X	X	X
5	$\Delta\Gamma_{T2}$								X	X	X	X
6	$\Delta\Gamma_3$								X	X	X	X
7	ΔA_5			X	X	X	X	X	X	X	X	X
8	$\Delta\eta$F										X	X
9	$\Delta\eta$CH								X	X		
10	$\Delta\eta$TH						X	X				
11	$\Delta T_5/\theta_2$	X	X	X	X	X	X	X	X	X	X	X
12	ΔSFC$/\sqrt{\theta_2}$	X	X	X	X	X	X	X	X	X	X	X

FIGURE B-3: DIAGNOSTIC SYSTEM PREDICTION RESULTS FOR SNAPSHOT 114

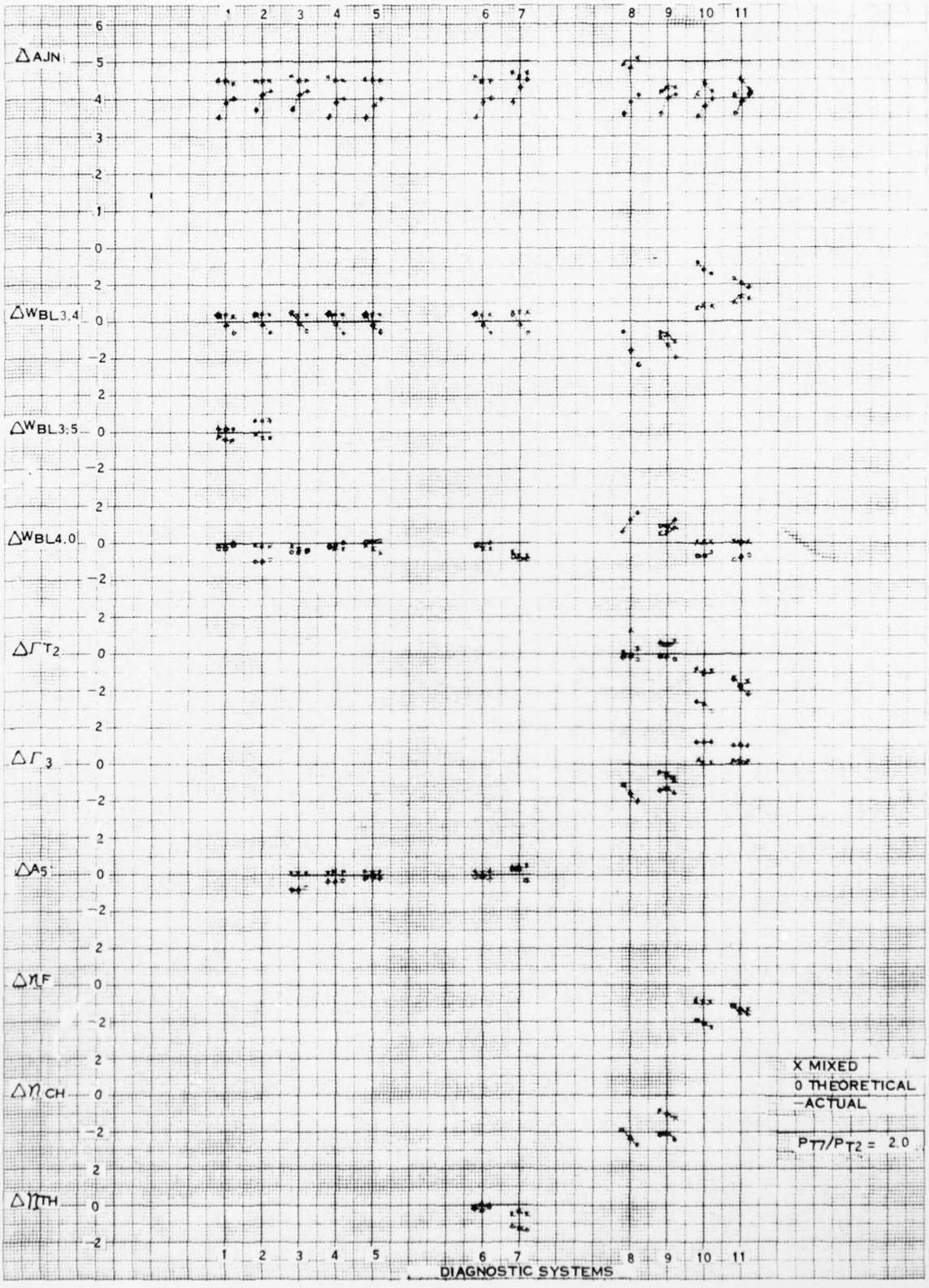

FIGURE B-4: DIAGNOSTIC SYSTEM RESULTS FOR SNAPSHOT 115

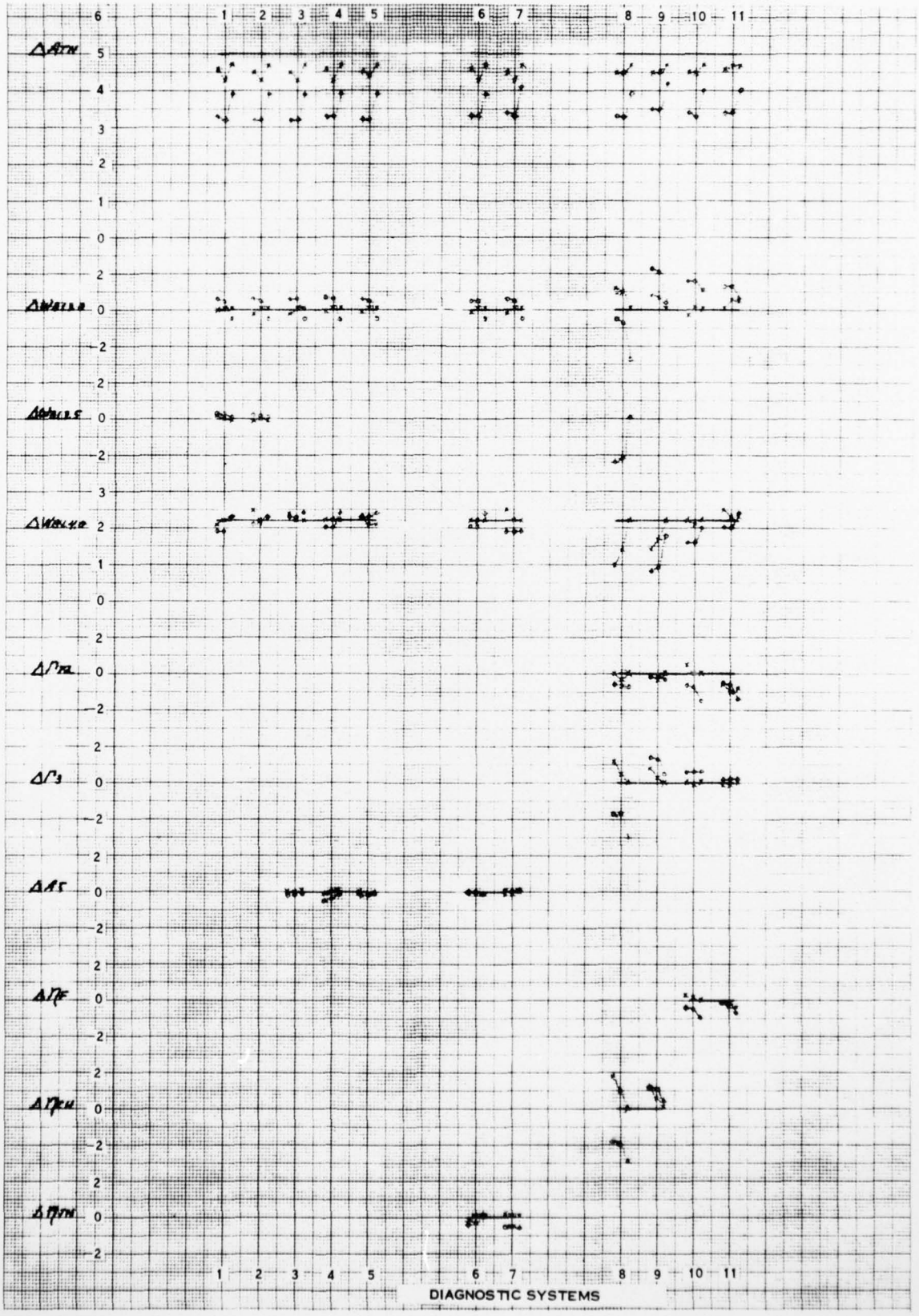

FIGURE B-5: DIAGNOSTIC SYSTEM RESULTS FOR SNAPSHOT 116

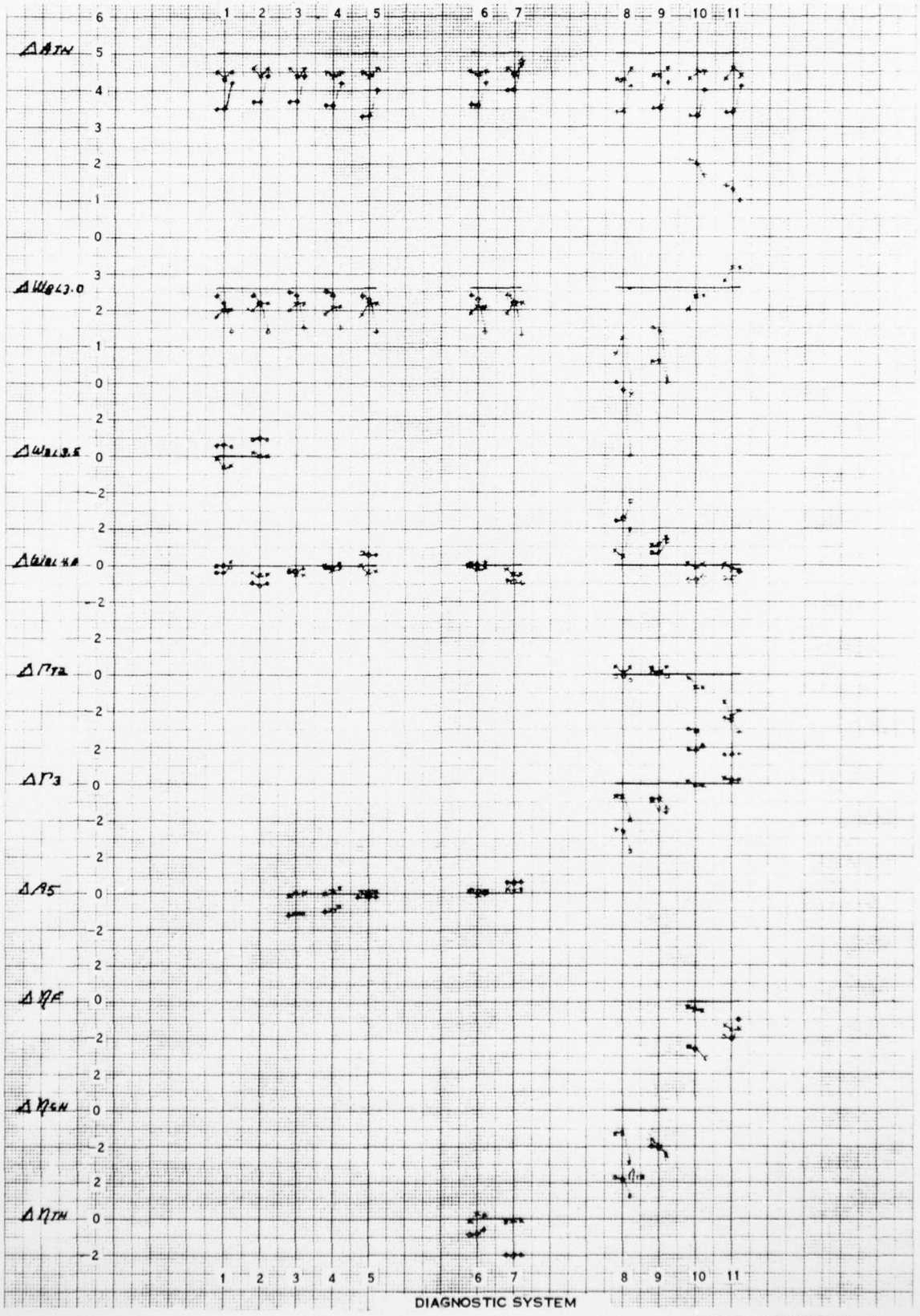

FIGURE B-6: SYSTEM 1 TF30-P-408 MN=0 DIAGNOSTIC RESULTS

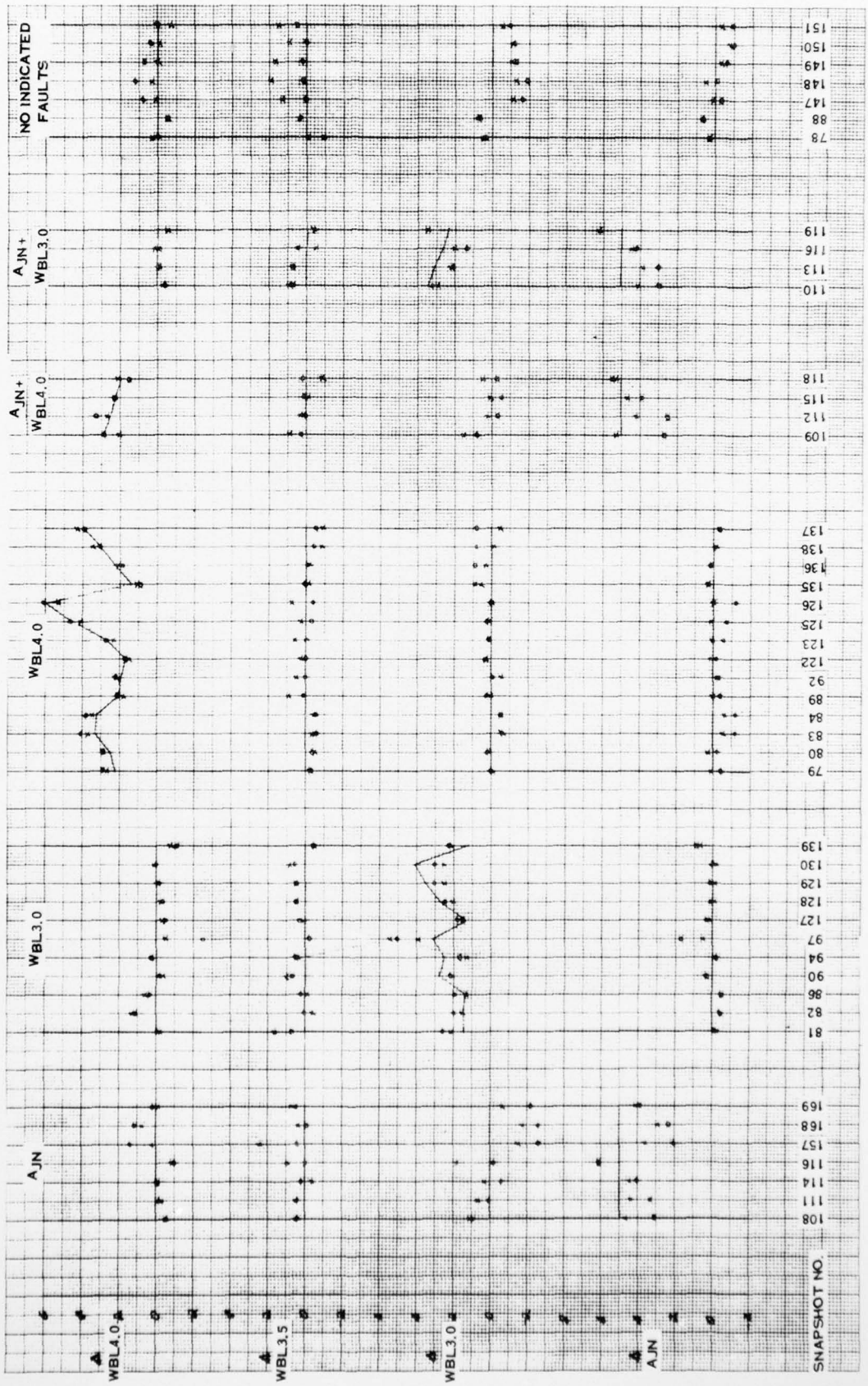

FIGURE B-7: SYSTEM 2 TF30-P-408 MN=0 DIAGNOSTIC RESULTS

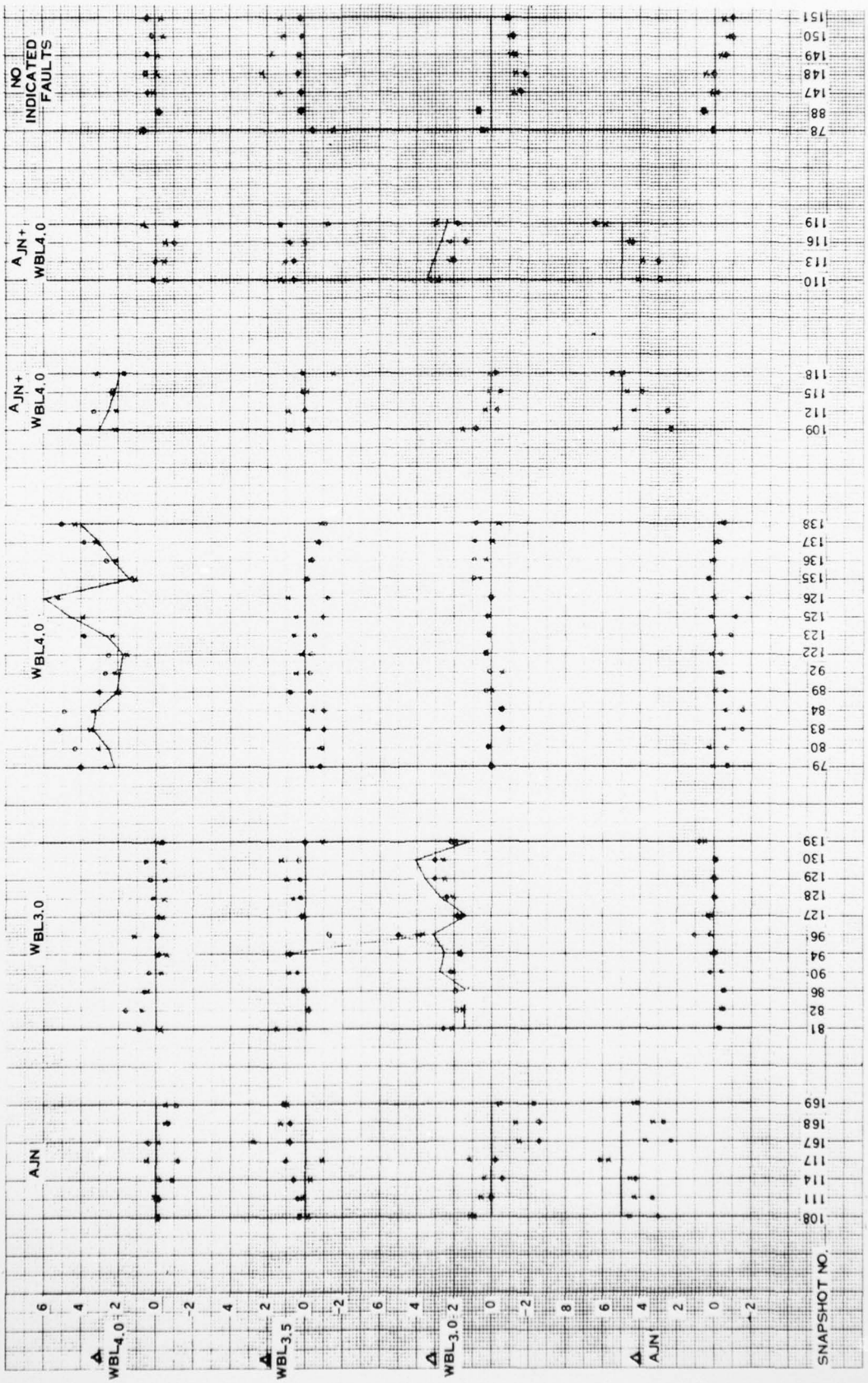

FIGURE B-8: SYSTEM 5 TF30-P-408 MN=0 DIAGNOSTIC RESULTS

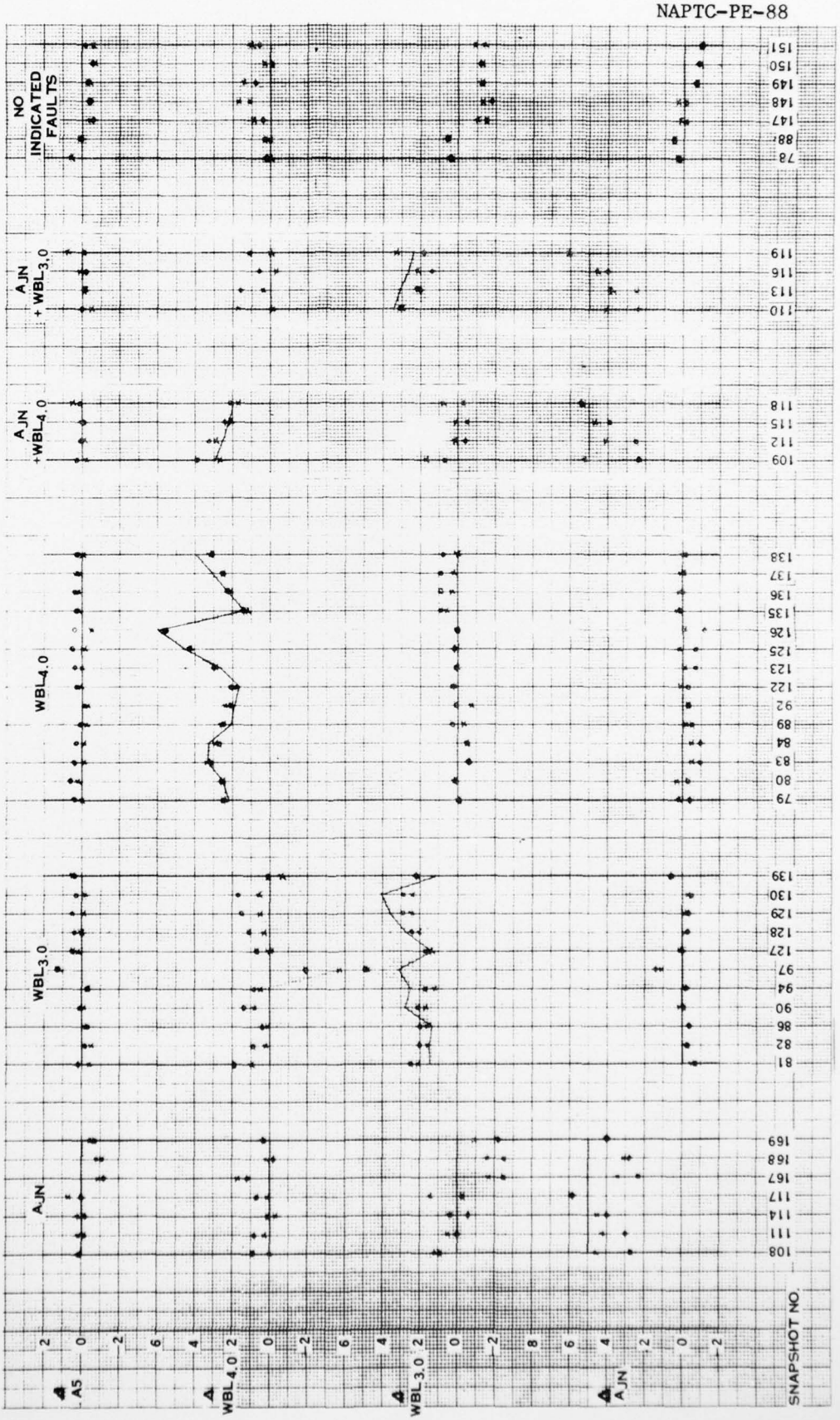

FIGURE B-9: SYSTEM 7 TF30-P-408 MN=0 DIAGNOSTIC RESULTS

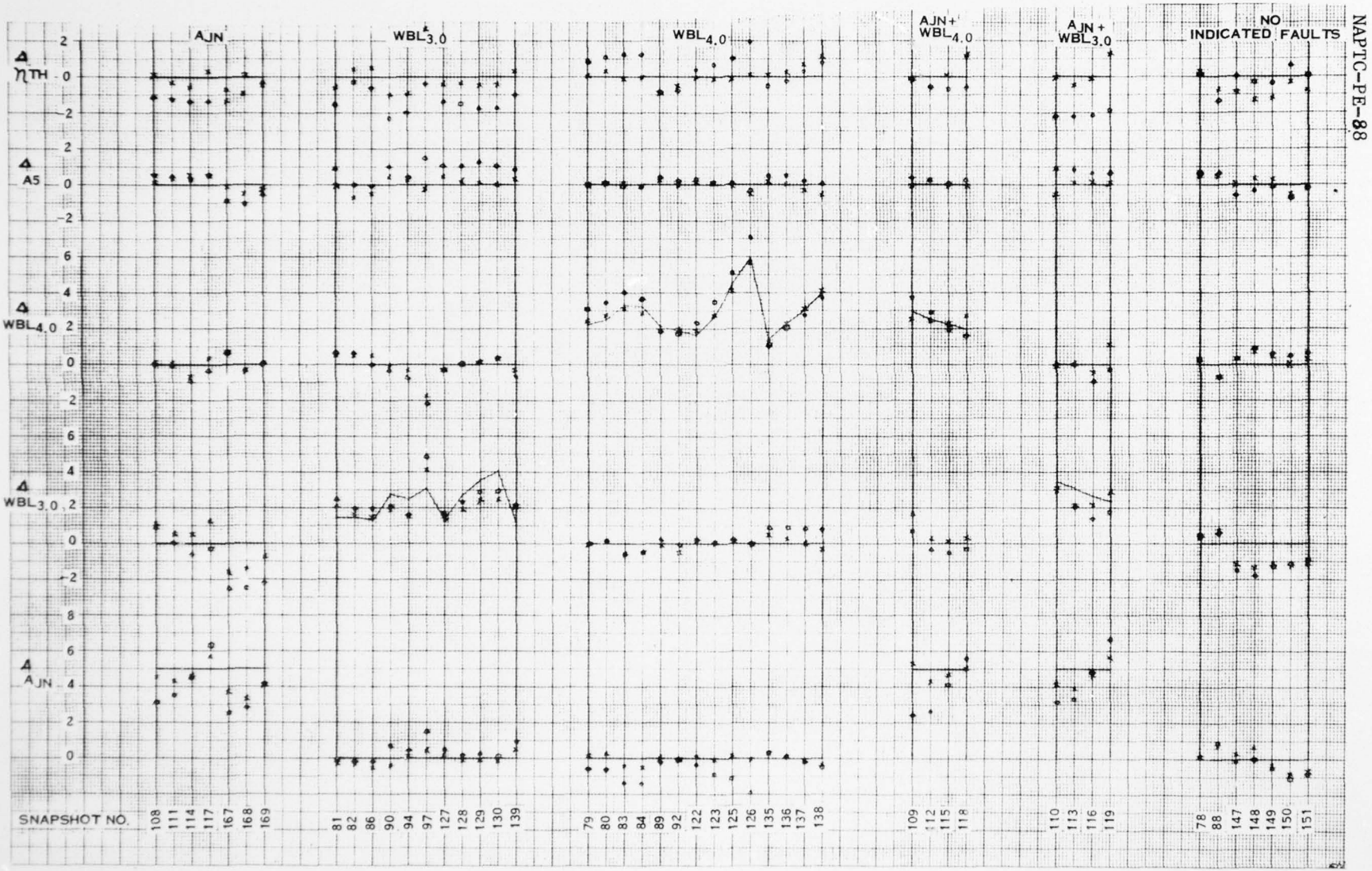

NAPTC-PE-88

AD-A044 471 NAVAL AIR PROPULSION TEST CENTER TRENTON N J PROPULS--ETC F/G 21/5
TURBINE ENGINE DIAGNOSTICS DEVELOPMENT PHASE III REPORT.(U)
JAN 77 R T LAZARICK, P WOROBEI, J E ZOOG

UNCLASSIFIED NAPTC-PE-88 NL

2 OF 2
AD A044471

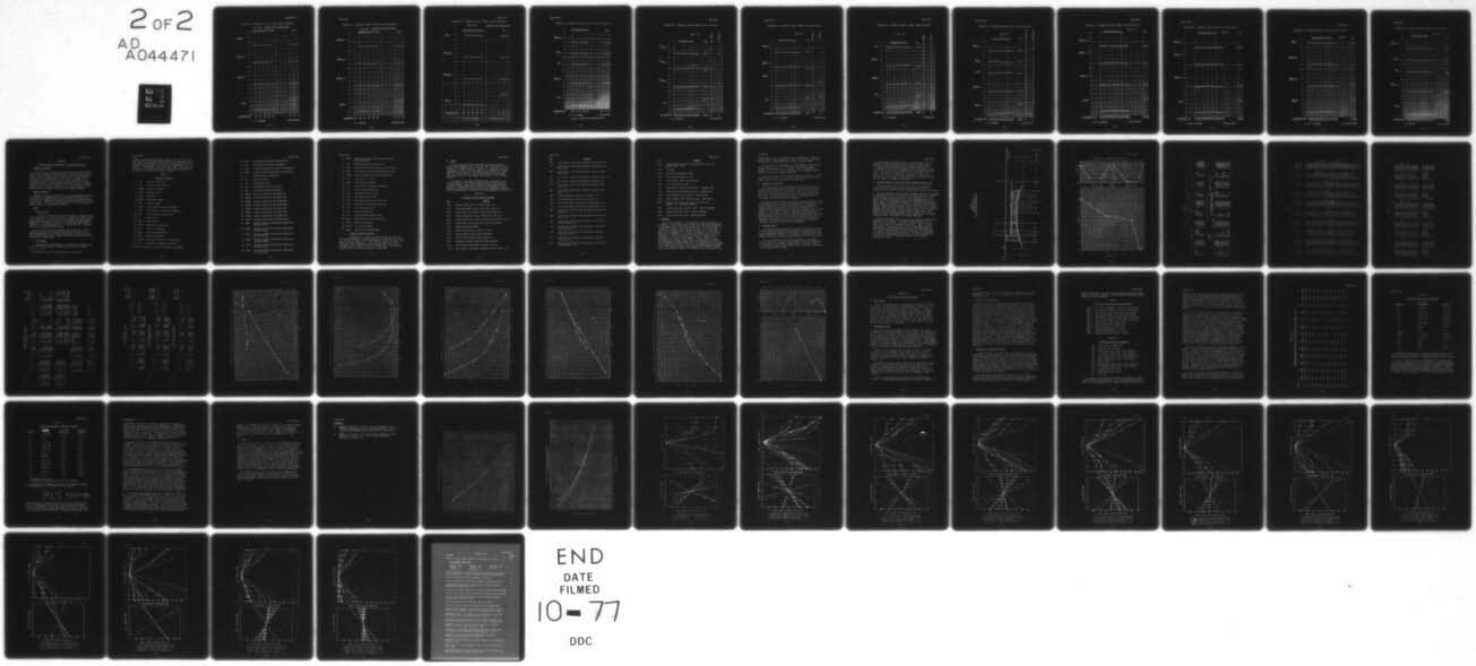

END
DATE FILMED
10-77
DDC

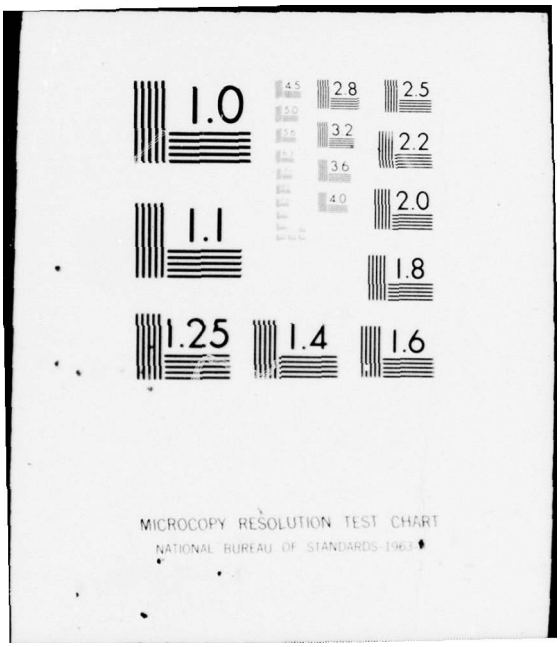
1.0
1.1
1.25
1.4
1.6
1.8
2.0
2.2
2.5
2.8
3.2
3.6
4.0
4.5
5.0
5.6
MICROCOPY RESOLUTION TEST CHART
NATIONAL BUREAU OF STANDARDS-1963-A

FIGURE B-10: DIAGNOSTIC RESULTS SYSTEM 1 TF30-P-408 MN=0.25

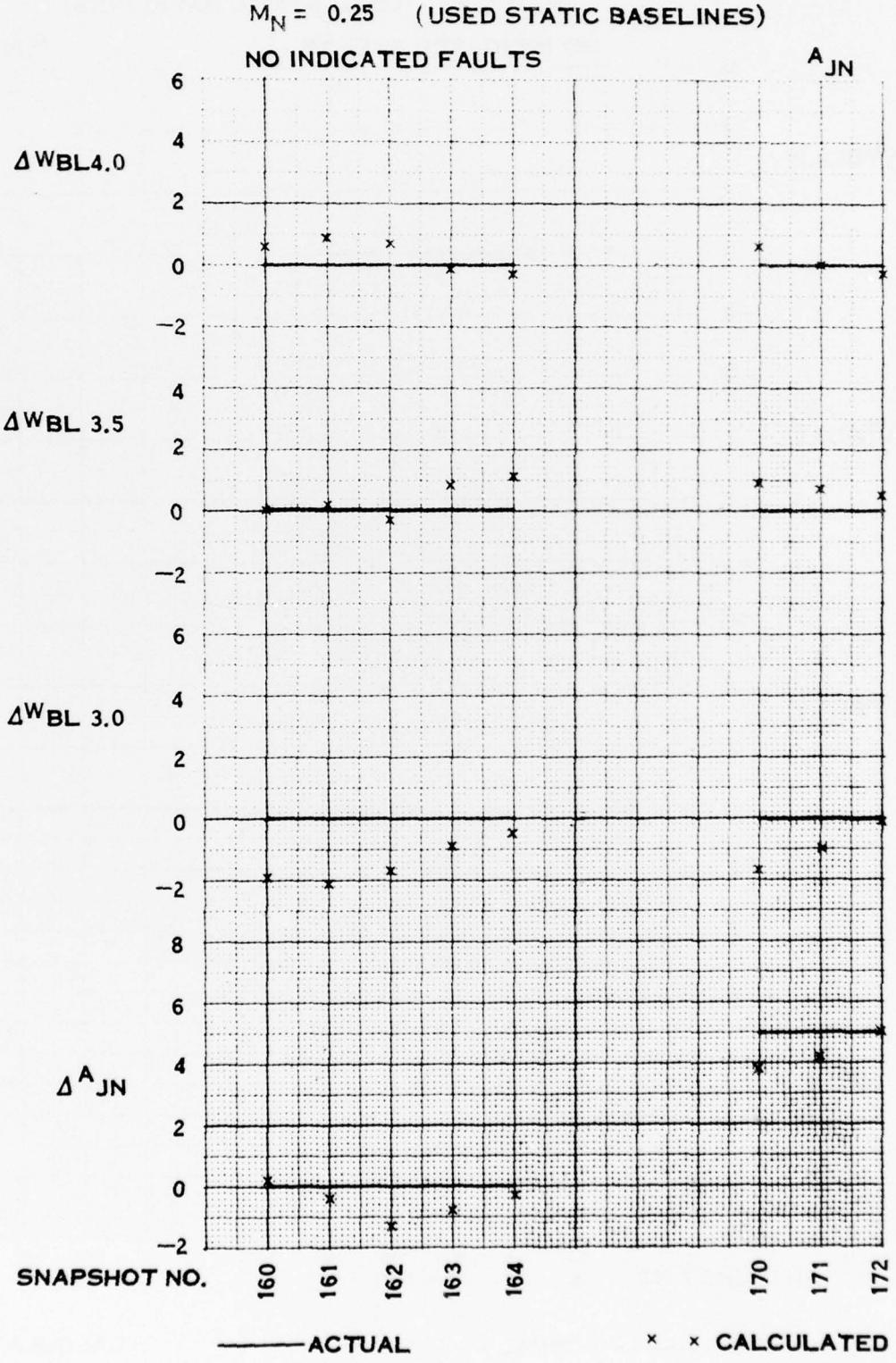

FIGURE B-11: DIAGNOSTIC RESULTS SYSTEM 2 TF30-P-408 MN=0.25

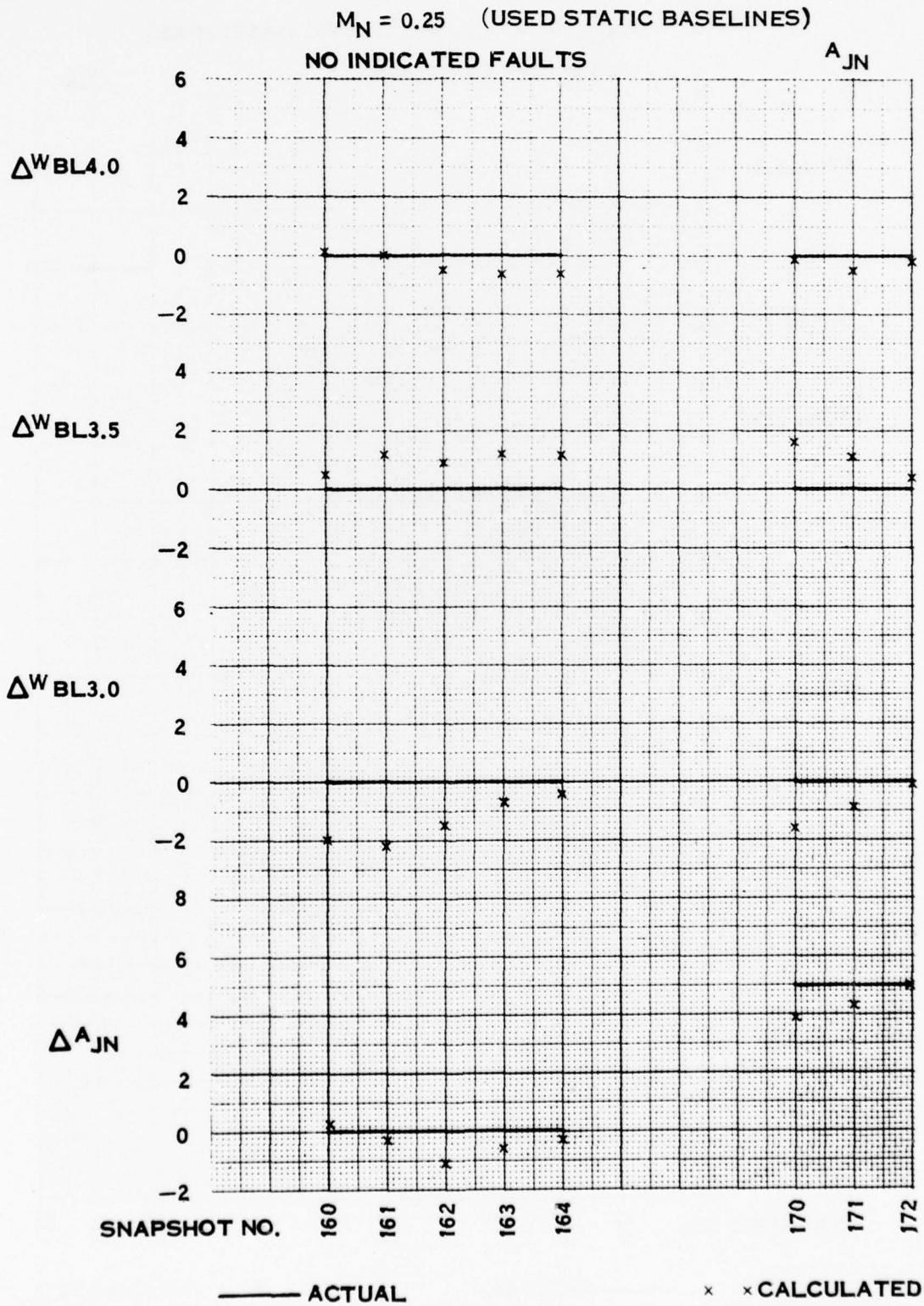

FIGURE B-12: DIAGNOSTIC RESULTS SYSTEM 5 TF30-P-408 MN=0.25

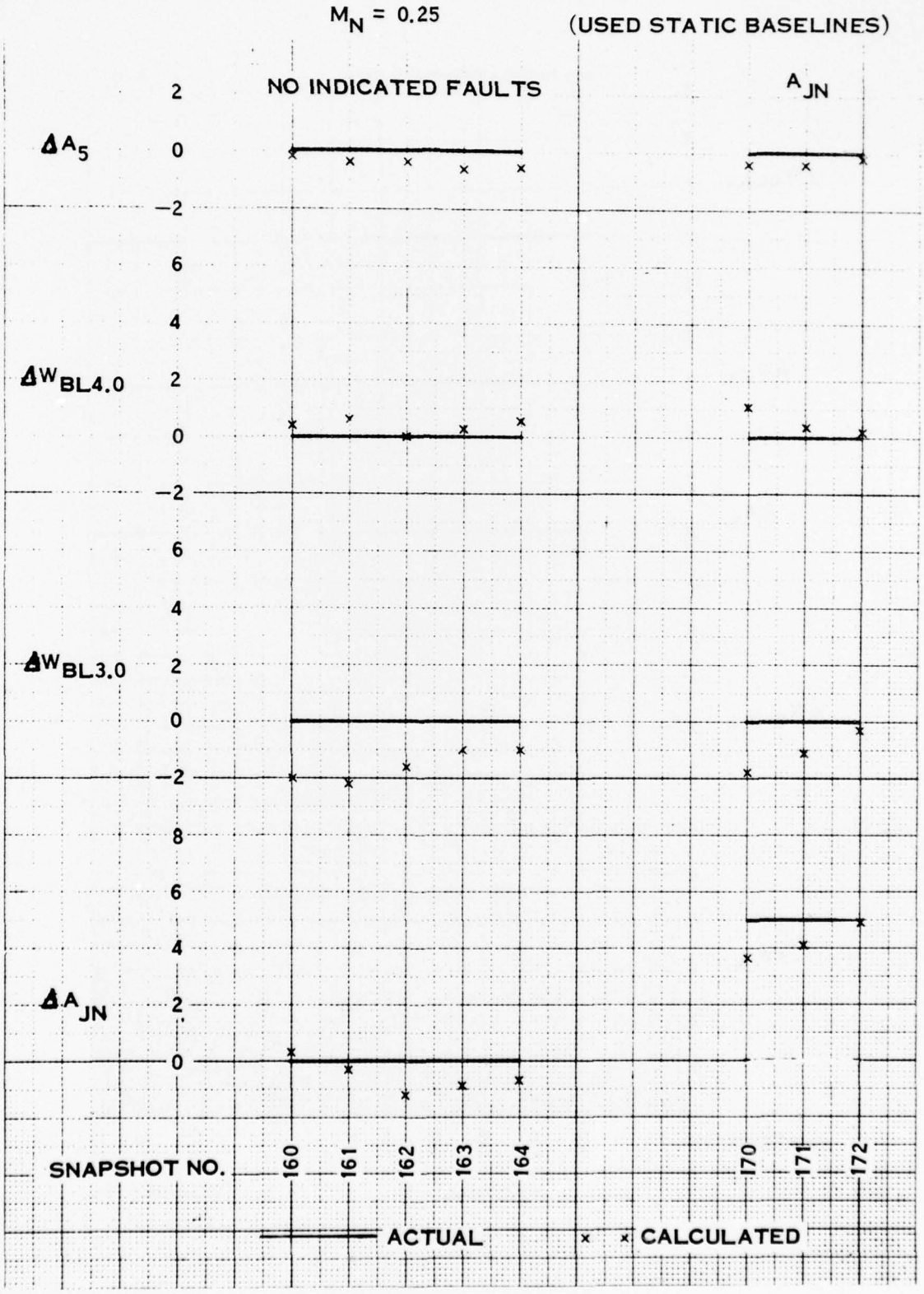

FIGURE B-13: DIAGNOSTIC RESULTS SYSTEM 7 TF30-P-408 MN=0.25

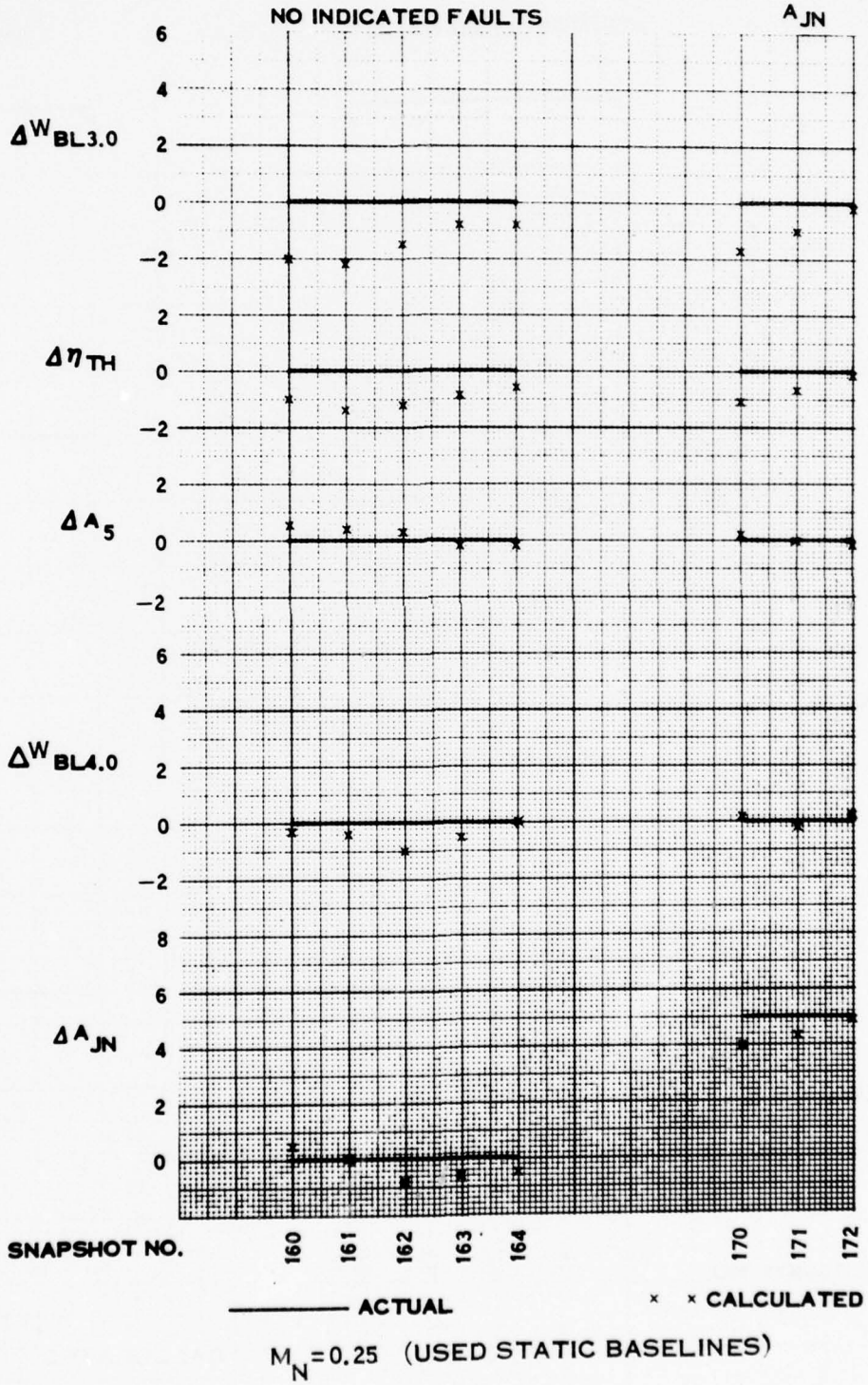

FIGURE B-14: DIAGNOSTIC RESULTS SYSTEM 1 TF30-P-408 MN=0.5

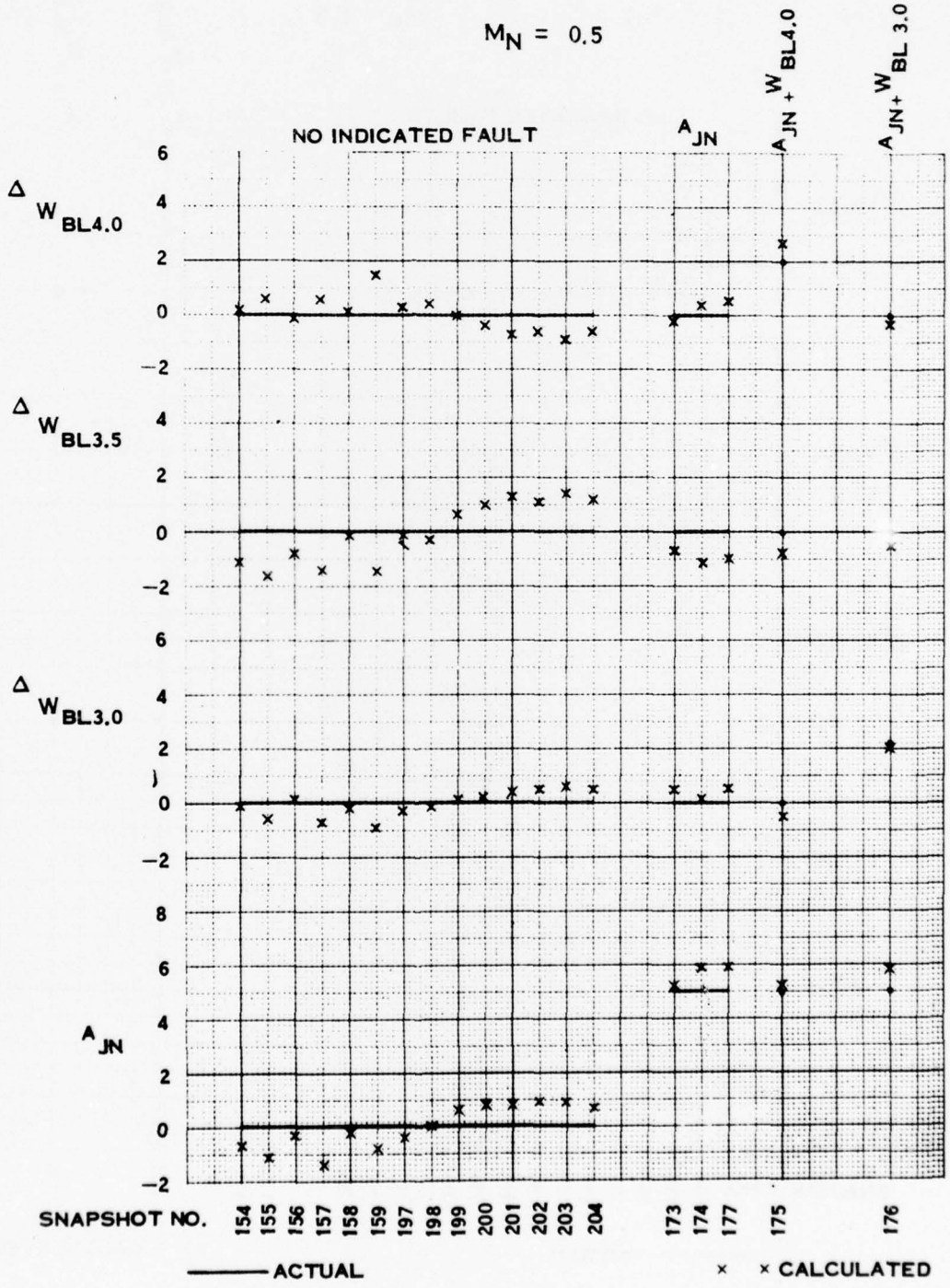

FIGURE B-15: DIAGNOSTIC RESULTS SYSTEM 2 TF30-P-408 MN=0.5

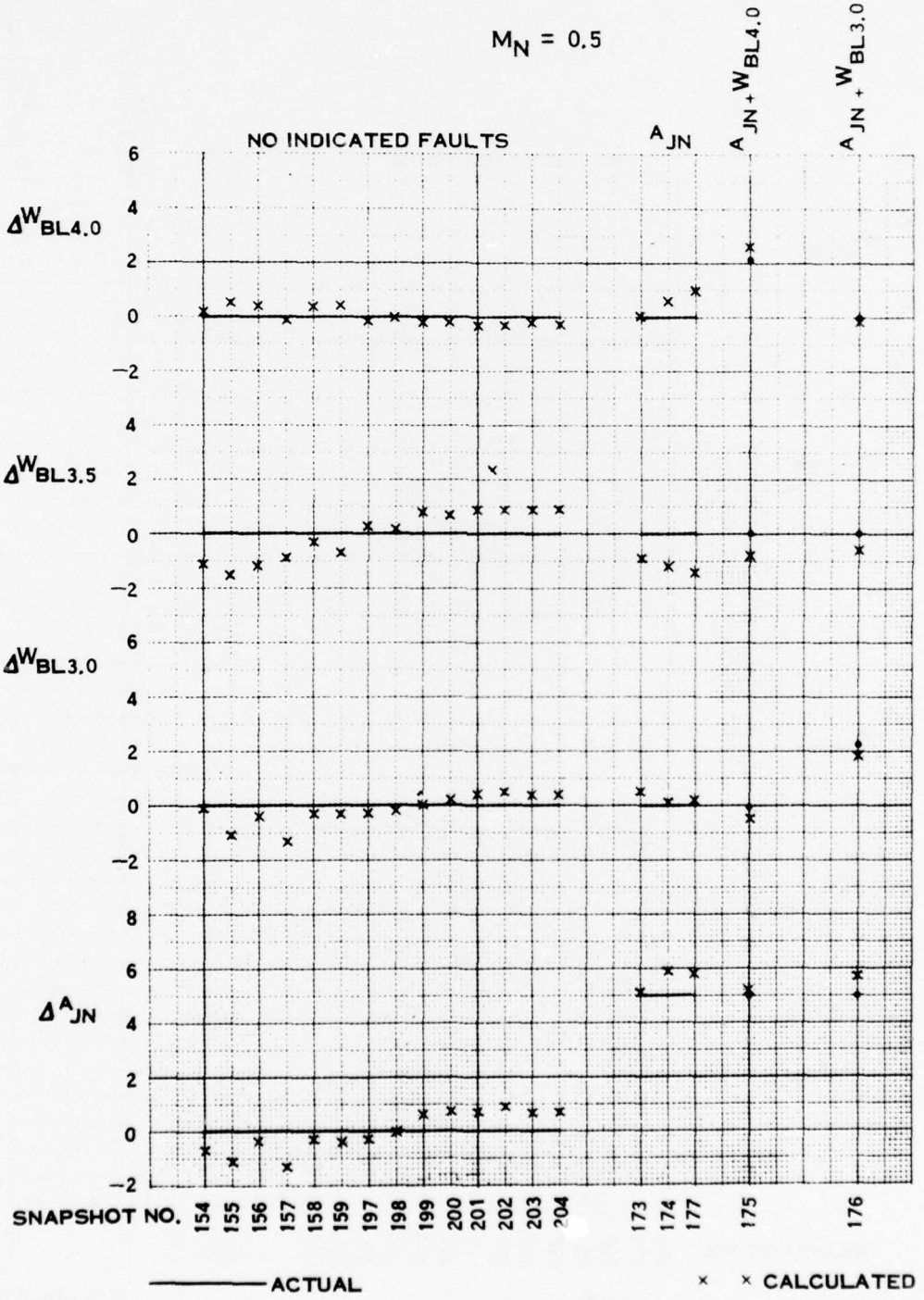

FIGURE B-16: DIAGNOSTIC RESULTS SYSTEM 5 TF30-P-408 MN=0.5

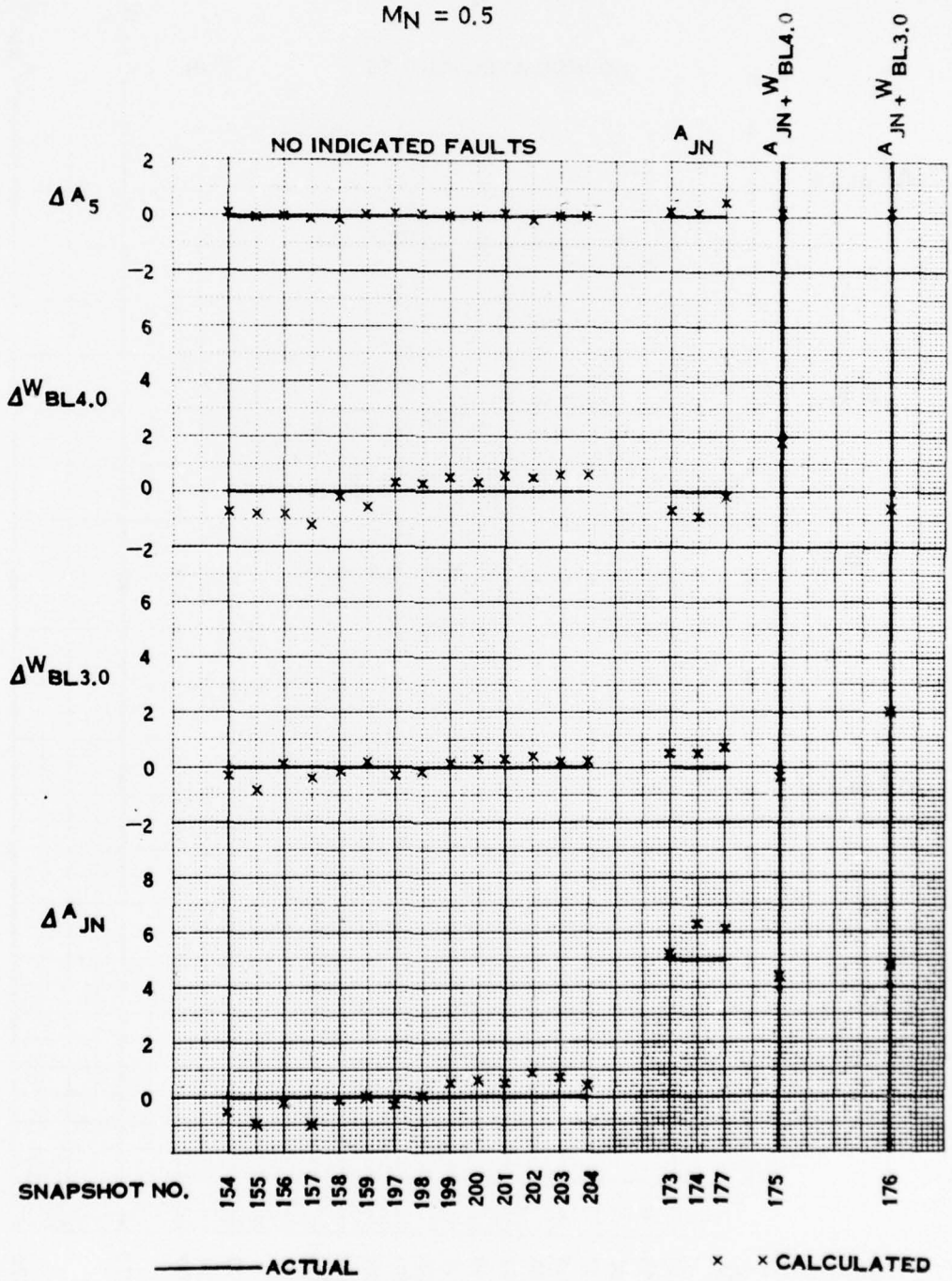

FIGURE B-17: DIAGNOSTIC RESULTS SYSTEM 7 TF30-P-408 MN=0.5

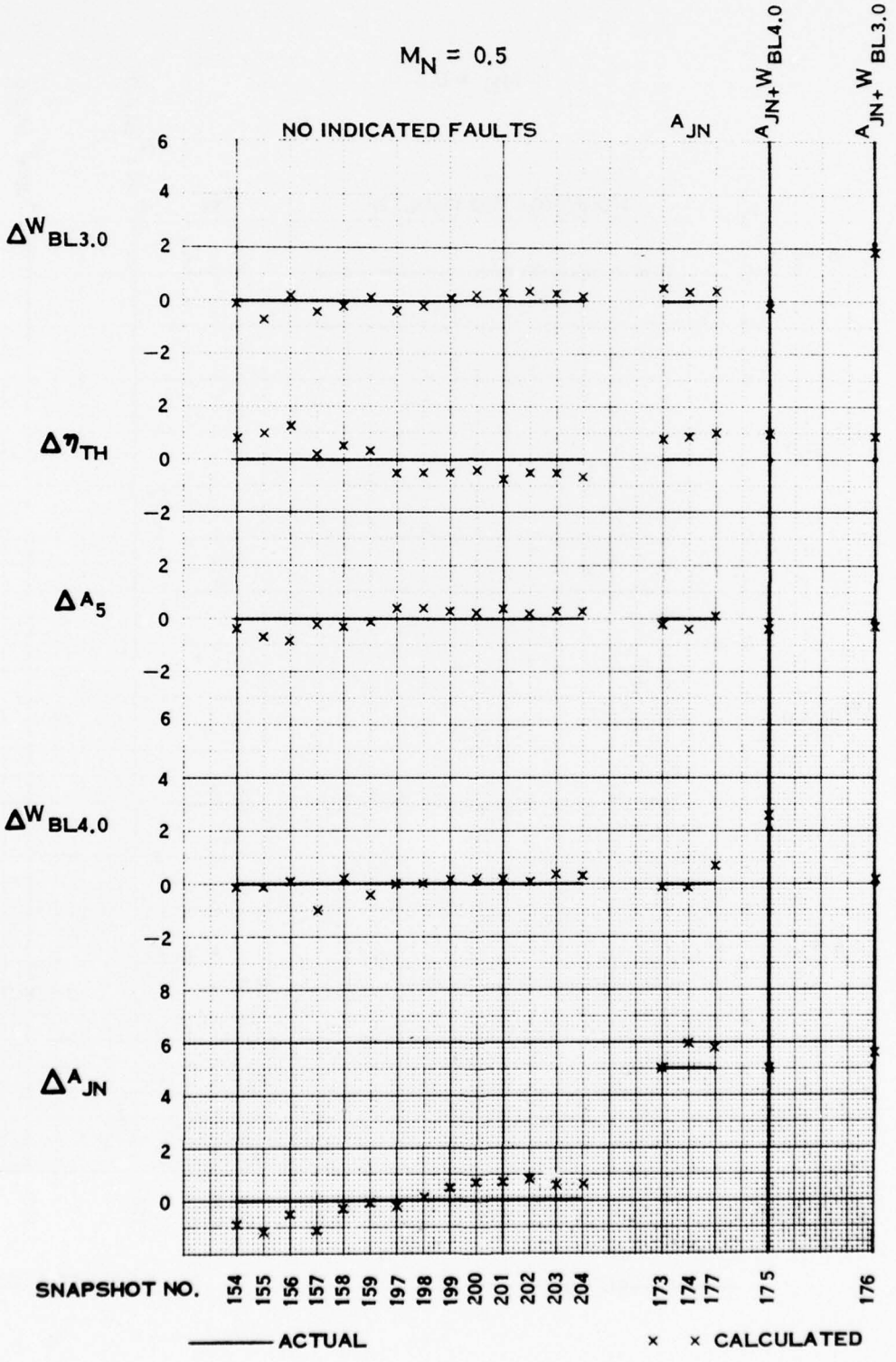

FIGURE B-18: DIAGNOSTIC RESULTS SYSTEM 1 TF30-P-408 MN=.075

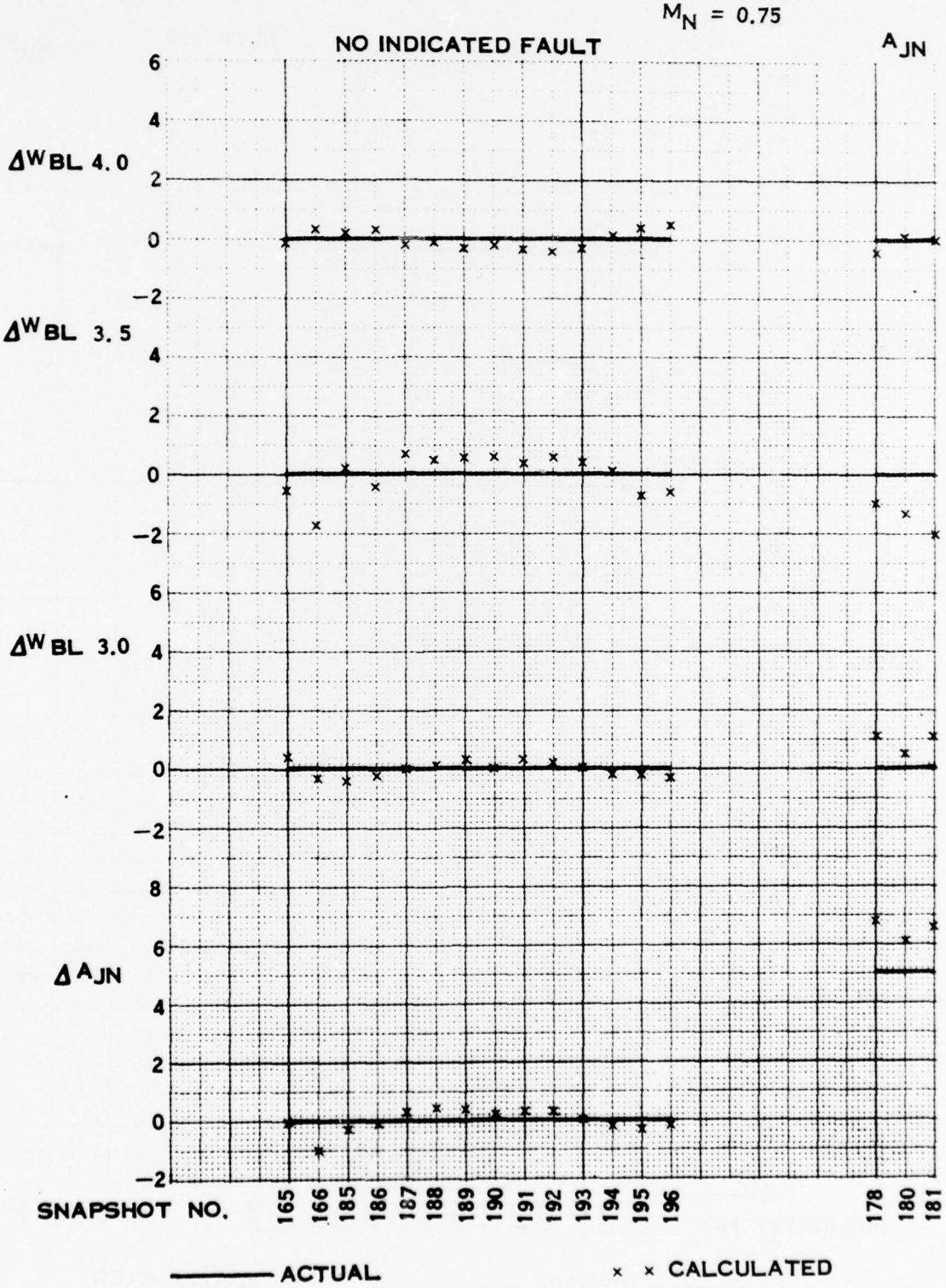

FIGURE B-19: DIAGNOSTIC RESULTS SYSTEM 2 TF30-P-408 MN=.075

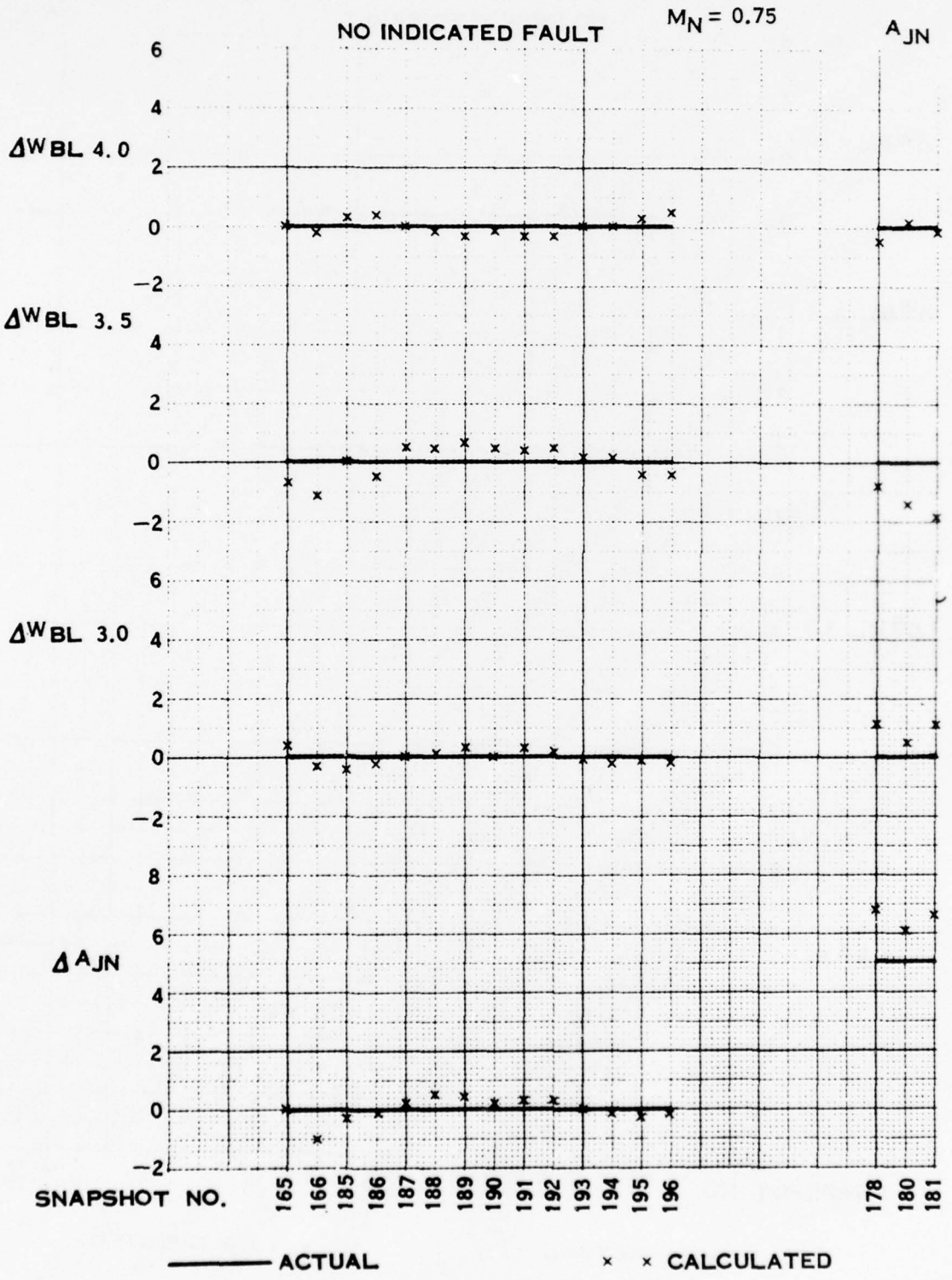

FIGURE B-20: DIAGNOSTIC RESULTS SYSTEM % TF30-P-408 MN=0.75

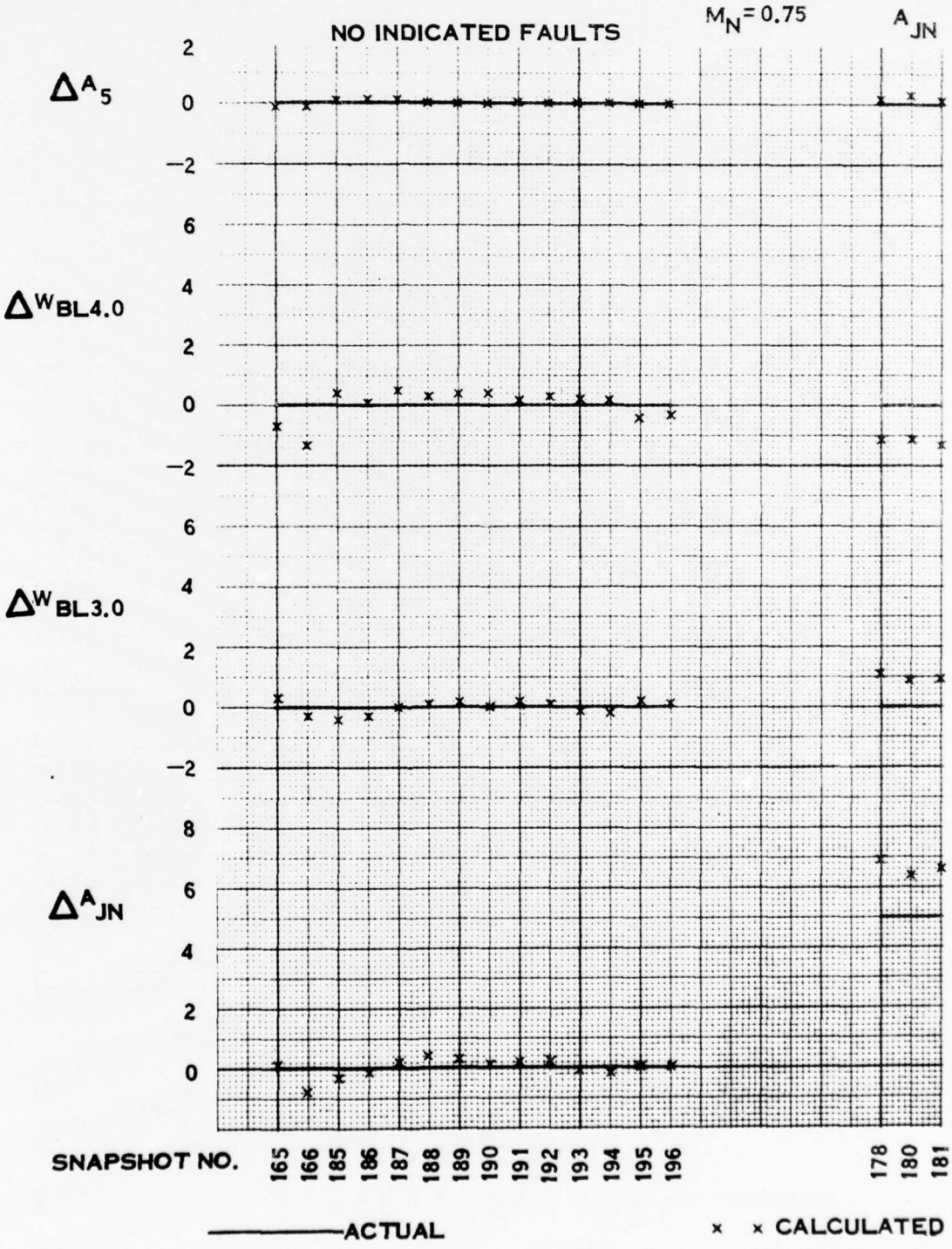

FIGURE B-21: DIAGNOSTIC RESULTS SYSTEM 7 TF30-P-408 MN=0.75

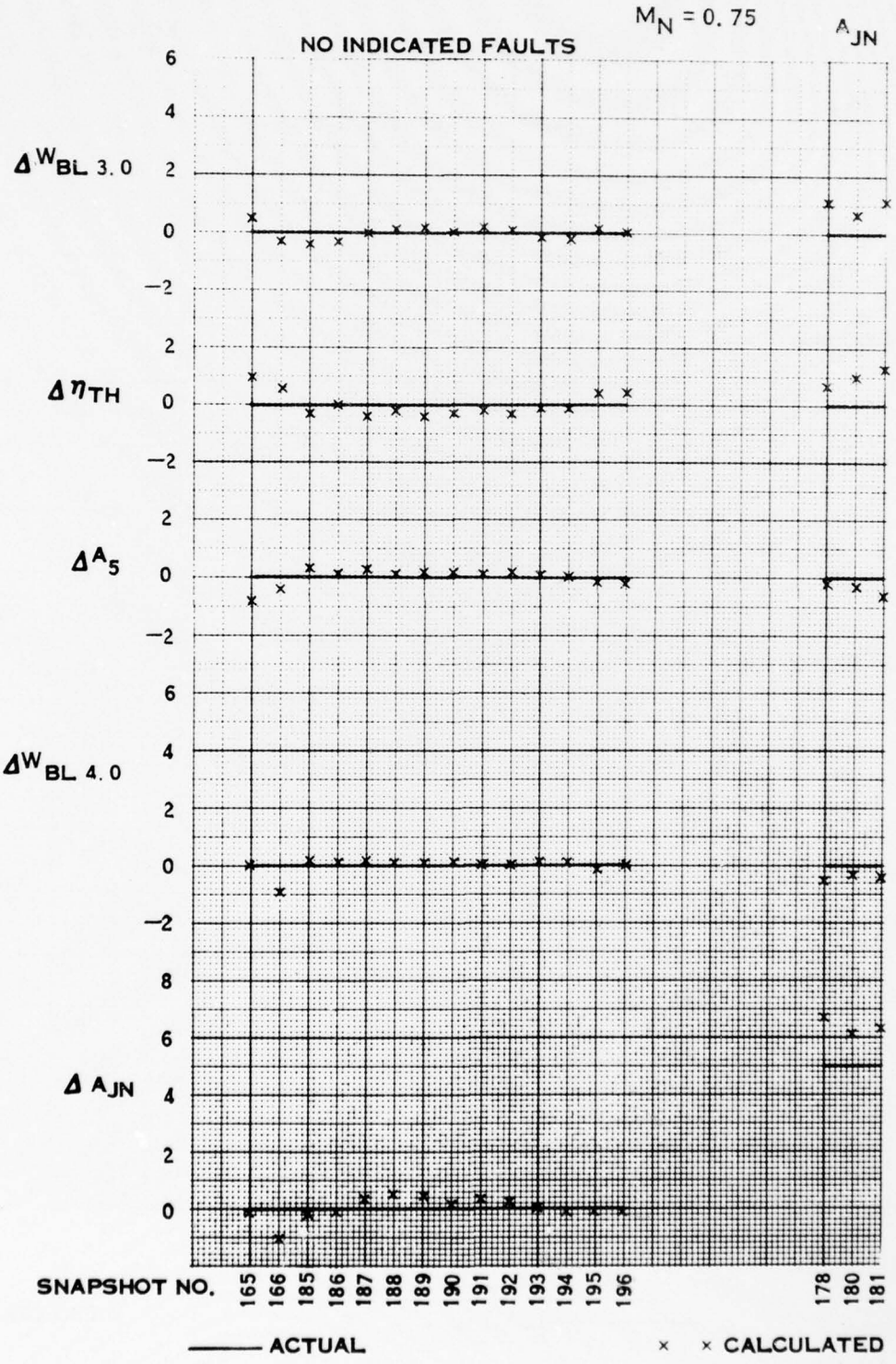

APPENDIX C

Variable Geometry Cycle Deck - Description and Status

A. GENERAL DESCRIPTION

This cycle deck has been written to conform to Aerospace Standard 681-C, which addresses Gas Turbine Engine Steady State Performance Presentation for Digital Computer Programs, and Aerospace Recommended Practice 755-A, concerning Gas Turbine Engine Performance Station Identification and Nomenclature. The specific gas turbine cycle simulated by this deck is a two-spool, T-fan[1], mixed-flow turbofan with afterburning. In addition, this cycle deck allows for variable area high and low pressure turbine (HPT and LPT) nozzles and variable exhaust nozzle (A8) area. Figure C-1 is a schematic diagram of the engine components showing the station identification numbers.

B. OVERALL OPERATION

Basically, this cycle deck consists of the thermodynamic equations of a two-spool, mixed-flow turbofan. These equations account for flow continuity, energy balance, speed matching, and pressure balance. In addition, the program is required to satisfy the requested HPT, LPT, and A-8 areas. The theromdynamic properties of air are obtained from GASTAB, which is a computerized gas table.

C. INPUTS

1. Design Inputs

This cycle deck has been written as a design or Parametric deck, so that any engine in the two-spool, T-fan, mixed-flow turbofan category can be simulated. To simulate a particular engine, the engine design point information must be provided to the program, operating in the Design Mode. The design point can be at any desired flight condition and must be at intermediate power, i.e., rating code = 50. Table C-I shows the required design point inputs.

Once a design run has been balanced, that is adjusted to obtain a static pressure balance at the mixer and adjusted to obtain the desired performance, a design deck is generated. This deck contains the "standard" inputs and the design point information required to use the deck in its Normal Mode.

2. User Inputs

Operating in its Normal Mode, the program accepts inputs, such as altitude and Mach number, horsepower and bleed air extraction,

---

[1] T-fan implies fan and low pressure compressor on low spool.

changes in component performance, changes in HPT, LPT, and exhaust nozzle areas, and rating code (ZRC), which is the power level input. The program can be operated to generate a single data point or to generage a "power series" at the given input conditions. The "power series" is controlled by a power code (ZPC) input. In all cases, a new input will supersede the standard input, and will remain until changed or until the standard deck is reloaded.

TABLE C-I

Design Point Inputs

1.	T2*	Fan Inlet Temperature
2.	P2*	Fan Inlet Total Pressure
3.	TAMB*	Ambient Temperature
4.	PAMB*	Ambient Pressure
5.	ZALT*	Altitude
6.	ZMN*	Flight Mach Number
7.	VA*	Flight Airspeed
8.	SERAM	Inlet Recovery Computation Method
9.	ZRR	Inlet Recovery (used only if SERAM = 1)
10.	SIM	Inlet Condition Input Selector
11.	W2	Inlet Airflow
12.	BPR	By-pass Ratio
13.	P13Q2	Outer Fan Pressure Ratio
14.	EFO	Outer Fan Efficiency
15.	P21Q2	Inner Fan Pressure Ratio
16.	EFI	Inner Fan Efficiency
17.	P23Q21	Low Pressure Compressor Pressure Ratio
18.	ECL	Low Pressure Compressor Efficiency

* Not all are required - value of SIM dictates requirements

19.	P3Q23	High Pressure Compressor Pressure Ratio
20.	ECH	High Pressure Compressor Efficiency
21.	WB22Q	Customer Bleed Air Extraction, LPC Dishcharge
22.	WB29Q	Customer Bleed Air Extraction, HPC Discharge
23.	T4	Burner Discharge Temperature
24.	EB	Burner Efficiency
25.	FHV	Fuel Heating Value
26.	ETH	High Pressure Turbine Efficiency
27.	ETL	Low Pressure Turbine Efficiency
28.	WBHV1Q	Turbine Cooling Flow, HPT First Vane
29.	WBHB1Q	Turbine Cooling Flow, HPT First Blade
30.	WBHV2Q	Turbine Cooling Flow, HPT Second Vane
31.	WBHB2Q	Turbine Cooling Flow, HPT Second Blade
32.	WBLV1Q	Turbine Cooling Flow, LPT First Vane
33.	WBLB1Q	Turbine Cooling Flow, LPT First Blade
34.	WBLV2Q	Turbine Cooling Flow, LPT Second Vane
35.	WBLB2Q	Turbine Cooling Flow, LPT Second Blade
36.	TMHV1	Maximum Allowable Turbine Metal Temperature, HPT First Vane
37.	TMHB1	Maximum Allowable Turbine Metal Temperature, HPT First Blade
38.	TMHV2	Maximum Allowable Turbine Metal Temperature, HPT Second Vane
39.	TMHB2	Maximum Allowable Turbine Metal Temperature, HPT Second Blade
40.	TMLV1	Maximum Allowable Turbine Metal Temperature, LPT First Vane
41.	TMLB1	Maximum Allowable Turbine Metal Temperature, LPT First Blade

43. TMLB2 Maximum Allowable Turbine Metal Temperature, LPT Second Blade

44. PF4 Burner Discharge Pattern Factor

45. RPFH High Pressure Turbine Rotating Pattern Factor

46. RPFL Low Pressure Turbine Rotating Pattern Factor

47. T7MAX Maximum Afterburner Discharge Temperature

48. EAB Afterburner Efficiency

49. XMAB Afterburner Mach Number

50. CD8 Exhaust Nozzle Discharge Coefficient

51. A8 Exhaust Nozzle Throat Area

52. XNHT High Pressure Rotor Speed

53. XNLT Low Pressure Rotor Speed

54. PWXH High Pressure Rotor Power Extraction

55. PWXL Low Pressure Rotor Power Extraction

56. DP16 Fan Duct Pressure Drop

57. DPB Burner Pressure Drop

58. DP56 Turbine Diffuser Pressure Drop

59. DPAB Afterburner Friction Pressure Drop

60. P61D6 Mixing Pressure Drop

61. XMN16 Fan Duct Mach Number

62. XMN6 Turbine Diffuser Mach Number

3. Variable Geometry Schedules

Another group of inputs are used to define the HPT, LPT, and A-8 area schedules. The area schedules are expressed as a function of rating code, and are at this point limited to three (3) linear segments, as shown in Figure C-2. Once a set of schedules has been determined, these schedules can be incorporated into the "standard" or design deck for convenient re-use at a later time. Any input area schedules will supersede the standard area schedules.

D. OUTPUT

The data generated by this cycle deck is output to the line printer and/or magnetic tape. There are three (3) different printer formats for a single data point. Format 1 is a complete listing of all inputs, all stored computed values, and a summary page of engine parameters at each station. The second format is just the summary page. The third format is just the Inlet Conditions and Overall Performance sections of the summary page. (Format 2 is the standard format).

In addition to the engine performance data, the summary page includes a matrix of Numerical Status Indicators (NSI's) which are warning messages. These warning messages include such things as improper or inconsistent inputs, iteration non-convergence, flight envelope exceedance, internal function or map exceedance, compressor surge, and insufficient or excess cooling flow messages (see Table C-II).

TABLE C-II

Numerical Status Indicator Listing

NSI	MESSAGE
0200	Illegal Altitude Input, Altitude reset to 0.
0201	Illegal Mach Number Input, Mach number reset to 0.
0202	Illegal Flight Speed Input, Flight Speed reset to 0.
0203	Illegal Ram Recovery Input, Ram Recovery reset to 1.
0204	Illegal Ram Recovery Selector, Ram Recovery Selector reset to 0.
0300	Illegal Power Code Input, Power series not executed
0500	Flight Envelope Exceedance
070X	Excess Cooling Flow, at station 4. (X-1)
1801	Exhaust Nozzle Function limit exceedance
1802	Fan Efficiency Function limit exceedance
1803	Compressor Efficiency Function limit exceedance
270X	Insufficient Cooling Flow, at station 4. (X-1)
7001	High Pressure Turbine Map Exceedance, Velocity Ratio >4.0

NSI	MESSAGE
7002	High Pressure Turbine Map Exceedance, Work Ratio >2.0
7003	High Pressure Turbine Map Exceedance, Referred Speed Ratio <.897
7004	High Pressure Turbine Map Exceedance, Referred Speed Ratio >1.11
7011	Low Pressure Turbine Map Exceedance, Velocity Ratio >4.0
7012	Low Pressure Turbine Map Exceedance, Work Ratio >2.0
7013	Low Pressure Turbine Map Exceedance, Referred Speed Ratio <.65
7014	Low Pressure Turbine Map Exceedance, Referred Speed Ratio >1.17
7051	Fan Map Exceedance, Referred Flow Ratio >1.10
7052	Fan Map Exceedance, Referred Flow Ratio <.35
7053	Fan Map Exceedance, Percent Fan Pressure Ratio >1.2
7054	Fan Map Exceedance, Percent Fan Pressure Ratio <.35
7061	Low Pressure Compressor Map Exceedance, Referred Flow Ratio >1.2
7062	Low Pressure Compressor Map Exceedance, Referred Flow Ratio <.45
7063	Low Pressure Compressor Map Exceedance, Percent LPC Pressure Ratio >1.2
7064	Low Pressure Compressor Map Exceedance, Percent LPC Pressure Ratio <.45
7071	High Pressure Compressor Map Exceedance, Referred Flow Ratio >1.2
7072	High Pressure Compressor Map Exceedance, Referred Flow Ratio <.45
7073	High Pressure Compressor Map Exceedance, Percent HPC Pressure Ratio >1.2

NSI	MESSAGE
7074	High Pressure Compressor Map Exceedance, Percent HPC Pressure Ratio <.45
7091	Fan Surge
7092	Low Pressure Compressor Surge
7093	High Pressure Compressor Surge
7100	Inlet Referred Flow > Maximum limit
7101	Fan Discharge Mach Number >.8
7110	High Pressure Turbine Pressure Ratio > Maximum limit
7111	Low Pressure Turbine Pressure Ratio > Maximum limit
9101	Non-convergence, A-8 iteration: DATA INVALID
9102	Non-convergence, FP4, FP44 iteration: DATA INVALID
9200	Illegal Inlet Conditions Input, Calculated Ram Recovery >1.: RUN NOT EXECUTED
9201	Illegal Inlet Mode Selection Input: RUN NOT EXECUTED
9300	Illegal Rating Code Input: RUN NOT EXECUTED
9301	Illegal Power Code Input: RUN NOT EXECUTED

E. FEATURES

Some of the features of this program which make it flexible are as follows. Each compressor and turbine are individually represented by performance maps. The compressor maps are; (a) referred speed as a function of pressure ratio and referred flow and, (b) efficiency as a function of pressure ratio and referred flow. The turbine maps are; (a) flow parameter as a function of pressure ratio and referred speed and, (b) efficiency as a function of velocity ratio and corrected work. These are stored as percentages of design so that the same maps can be used for many engines. Pressure drops are not considered to be constant. The fan duct, burner, diffuser, mixer, and afterburner friction pressure drops are computed as a function of the referred flow and the design value of the pressure drop, providing more realistic calculations. Also, the afterburner momentum pressure loss is computed as a function of afterburner Mach number and temperature rise. Whenever possible, the program coding was organized into

building blocks, that is a subroutine for a compressor, a burner, a turbine vane, a turbine blade, etc. This has been done to facilitate construction of other engine cycles without duplicate effort.

For purposes of identification, a program indicator code (IND) is included with the data. This six digit code, XXYYZZ is used to identify the cycle (XX) (i.e., two-spool, T-fan, mixed-turbofan augmented = 01), the specific design (YY), and the variable geometry schedules (ZZ) used to generate this data.

Another option within this program involves the number of turbine stages. Both the high and low pressure turbines have the option of being single or two-stage components independently.

F. PERIPHERAL CAPABILITIES

Once data has been written on magnetic tape, there are a number of ways to retreive desired information. One option is to list all runs on tape. The output of this option is one line printer line per run on tape showing the Case (or Run) number, the program indicator code, the day, date and time the run was generated, and the NSI array. It is also possible to output a chosen run or set of runs in any of the three data output formats.

Another tape feature which is available is called Tape Edit. This allows output of up to eight stored values (inputs or outputs) for all or any selected group of runs. The "editing" is accomplished by requesting that only runs which satisfy the editing criteria be output, and any stored value may be used as an editing criteria. Each editing criterial must be assigned a minimum and maximum value. For example, if there exists a tape of power series of many different engine designs, each run at many altitudes and Mach numbers, the user may request data within a specified band of altitudes, and within a specified range of thrusts. Up to five such editing criteria are available. In addition, editing on the maximum value of the NSI array and the program indicator code is available.

G. FURTHER EFFORTS

The building block approach to the coding of this deck allows for the creation of other gas turbine cycles with a minimum effort. All of the programming required for input/output and program control will remain essentially unchanged. The peripheral capabilities are independent of the cycle and are therefore available for use on any cycle.

The cycles which are planned to be developed in the immediate future are the (a) two-spool, unmixed-turbofan with duct burning and/or afterburning, (b) two-spool, mixed turbofan with afterburning, (c) two-spool, regenerative turboshaft with a free power turbine, and, (d) high bypass ratio turbofan.

Other features which are planned to be incorporated into this deck and all other cycle decks are (a) English or Metric units, (b) static pressure mismatching (for mixed flow systems) and, (c) automated sensitivities. Automated sensitivities implies that a peripheral program will be developed which can compare any single run on tape with any defined operating line (whose data is also on tape). This method of comparison is chosen by the user. For example, this program can be used to generate the sensitivity of specific fuel consumption at constant thrust of a particular design to a 1% change in a component efficiency.

H. VARIABLE GEOMETRY DATA FOR PARAMETER INTERRELATIONSHIPS STUDY

Variable geometry data from this cycle deck was supplied to Hamilton Standard Division, United Technologies Corporation for study using the parameter interrelationships method of gas path analysis.

This data represents an engine whose geometry schedules are designed for 30,000 ft., Mach 0.8 Cruise condition because the cruise condition is an appropriate choice for steady state gas path analysis. The geometry schedules were selected to provide installed performance gains. This is accomplished by maintaining the inlet design airflow while reducing thrust (thereby reducing or eliminating spillage drag) and by opening the exhaust nozzle to reduce boattail losses (aft end losses). Additionally, maintaining overall compression ratio tends to minimize uninstalled TSFC. The operating limits, by which the geometry schedules were restricted, are the compressor surge limits (15% reduction in surge margin), maximum turbine pressure ratio ($P4/P44$, $P44/P5$), maximum inlet referred flow (W2R), maximum burner discharge temperature (T4), and maximum fan discharge Mach number.

Figures C-8 through C-12 are plots of the engine performance data showing the fixed geometry and variable geometry operating lines plotted versus net thrust. The variable geometry data covers the range of 40 to 100% of intermediate net thrust. Figure C-8 shows that constant inlet referred flow is held, accomplishing reduced spillage drag. Figure C-9 shows uninstalled TSFC improvement from 70 to 100% thrust, while below 70% FN, uninstalled TSFC penalties are present. However, those lower power conditions are associated with the largest installation losses, so a net TSFC improvement may be realized. Figure C-13 shows the geometry schedules used to generate this data.

FIGURE C-1:
SCHEMATIC DIAGRAM
AND STATION IDENTIFICATION

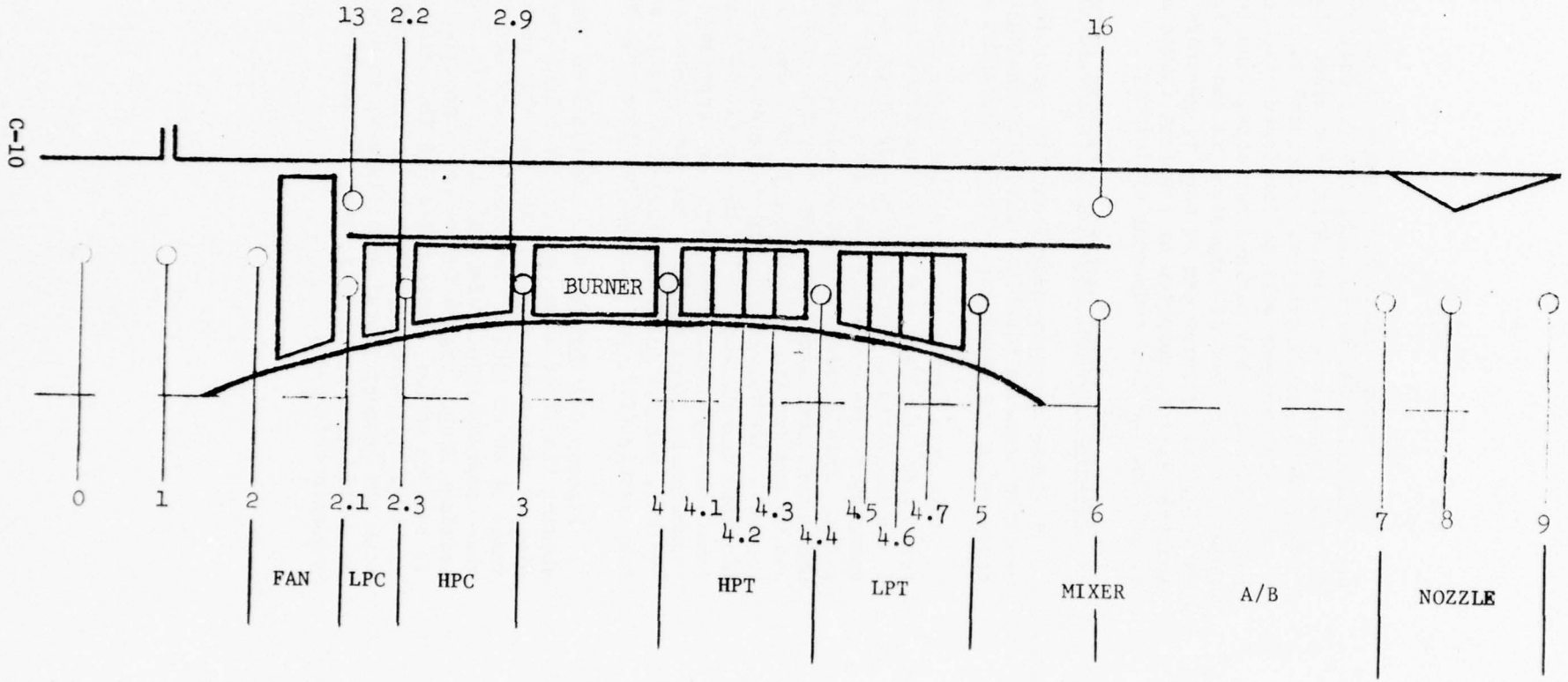

FIGURE C-2: EXAMPLE OF AREA SCHEDULES

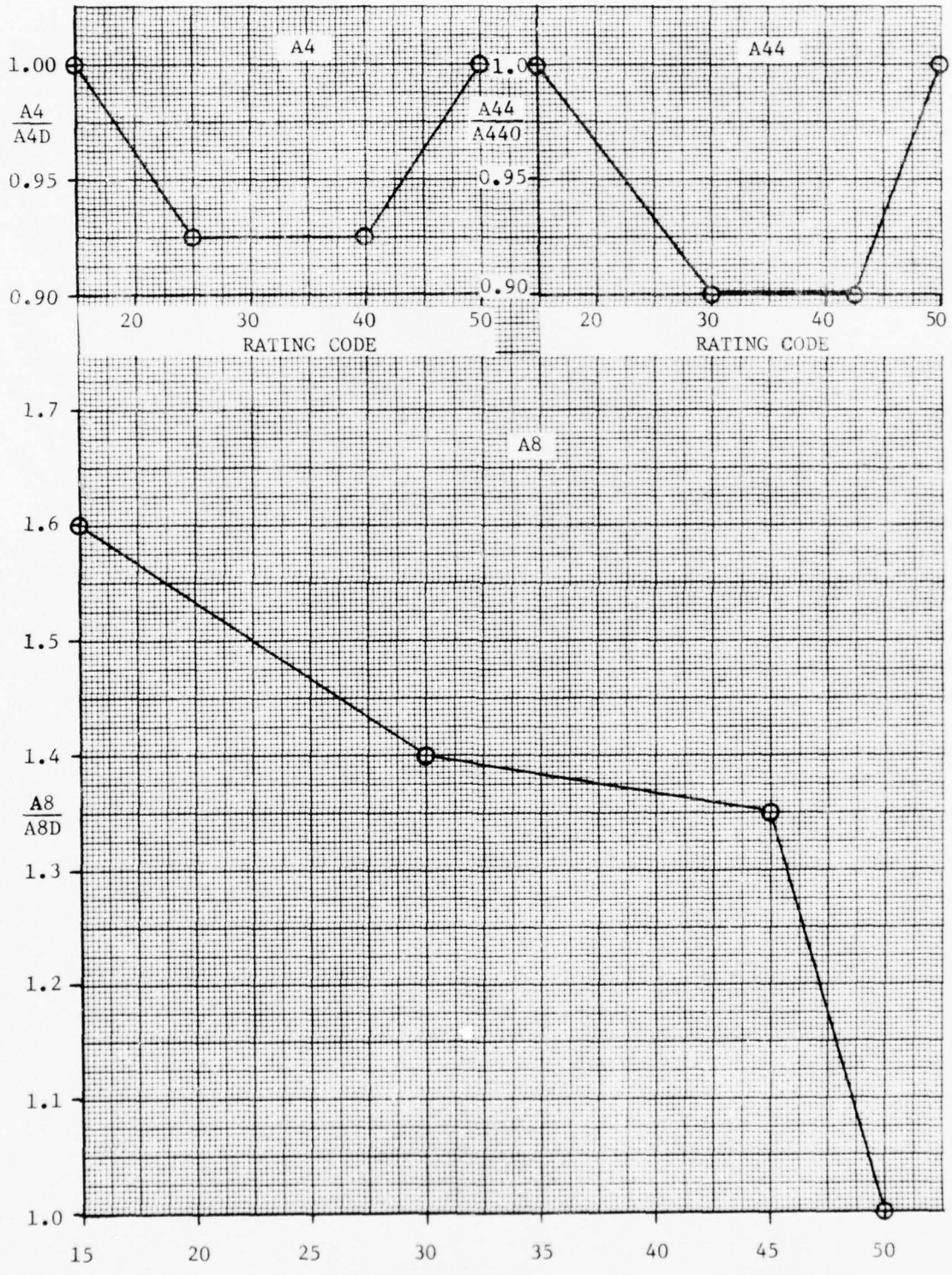

FIGURE C-3

* * * * * * * * * FIXED INPUTS AND OUTPUTS * * * * * * * * *

* * * * * FIXIN * * * * *

1 NIN : 102 2 NOUT : 108 3 IND : 010101
4 TITLE : '

5	CASE	: 50.0000	6	ZALT	: .000000	7	ZDTAMB	: .000000	8	ZDT1	: .000000	9	ZRR	: .000000
10	ZPWXH	: .000000	11	ZPAMB	: .000000	12	ZPC	: .000000	13		: .000000	14	ZP2	: .000000
15	ZRC	: 50.0000	16	SERAM	: 1.00000	17	SIM	: 1.00000	18	ZTAMB	: .000000	19	ZT2	: .000000
20		: .000000	21	ZWB29Q	: .000000	22	ZMN	: .000000	23		: .000000	24		: .000000
25		: .000000	26		: .000000	27		: .000000	28		: .000000	29		: .000000
30		: .000000	31		: .000000	32		: .000000	33		: .000000	34		: .000000
35		: .000000	36		: .000000	37		: .000000	38		: .000000	39		: .000000
40		: .000000	41		: .000000									

* * * * * FIXOUT * * * * *

1 CLASS :
2 IDENT : '

'**** UNCLASSIFIED ****'

VARIABLE GEOMETRY CYCLE DECK
NAVAL AIR PROPULSION TEST CENTER

3 NSI : 1801 8999 0 0 0 0 0 0 0 0 '

4	A8	: 374.464	5		: .000000	6		: .000000	7	FRAM	: .000000	8	FG9	: 13025.9
9		: .000000	10		: .000000	11		: .000000	12	FHV	: 18300.0	13	FN	: 13025.9
14	P3	: 367.375	15	P7	: 40.4363	16		: .000000	17	TSFC	: .751023	18		: .000000
19	T3	: 1454.85	20		: .000000	21	T7	: 1471.48	22		: .000000	23		: 9732.74
24	WFTBT	: 9782.74	25	W2	: 199.998	26	W7	: 202.716	27		: .000000	28	W23	: 99.2154
29	N2	: 10000.0	30		: .000000	31	N1	: 4999.98	32		: .000000	33	ALT	: .000000
34	ERAMA	: 1.00000	35	PAMB	: 14.6960	36		: .000000	37	P2	: 14.6960	38	TAMB	: 518.688
39	T2	: 518.688	40	MN	: .000000	41		: .000000	42		: .000000	43		: .000000
44		: .000000	45		: .000000	46		: .000000	47		: .000000	48		: .000000
49		: .000000	50		: .000000	51		: .000000	52		: .000000	53		: .000000
54		: .000000	55	DTAMB	: .000000	56	DT1	: .000000	57	CPC	: .000000	58	CRC	: 50.0000
59	WB29	: .000000	60	WB29Q	: .000000	61	HPXH	: .000000						

FIGURE C-4

VARIABLE INPUTS AND OUTPUTS

VARIN

1	VA	: •000000	2	ZWB22Q	: •000000	3	ZPWXL	: •000000	4		: •000000	5		: •000000
6		: •000000	7		: •000000	8		: •000000	9	ABMNDT	: 100•000	10	ZPHV	: 18300•0
11	DEFB	: •000000	12	DEFI	: •000000	13	DECL	: •000000	14	DECH	: •000000	15	DETH	: •000000
16	DETL	: •000000	17	DEB	: •000000	18	DEAB	: •000000	19		: •000000	20		: •000000
21	DA41	: •000000	22	DA43	: •000000	23	DA45	: •000000	24	DA47	: •000000	25	DAN	: •000000
26		: •000000	27		: •000000	28		: •000000	29		: •000000	30		: •000000

VARBUT

1	W13	: 100•783	2	BPR	: 1•01580	3	EF9	: •820009	4	P13Q2	: 2•99996	5	FRHP	: 7956•74
6	P13	: 44•0874	7	T13	: 750•373	8	H13	: 179•759	9	W21	: 99•2154	10	EFI	: •820009
11	P21Q2	: 2•99996	12	FIHP	: 7832•98	13	P21	: 44•0874	14	T21	: 750•373	15	H21	: 179•759
16	ECL	: •829999	17	P23Q21	: 1•34400	18	LPCHP	: 2680•45	19	P23	: 59•2535	20	T23	: 828•881
21	H23	: 198•853	22	TLPCHP	: 1847•02	23	WB22	: •000000	24	WB22Q	: •000000	25	ECH	: •839999
26	P3Q23	: 6•20005	27	HPCHP	: 2223•03	28		: •000000	29		: •000000	30	H3	: 357•280
31	W295	: 99•2154	32	WBHV1	: 8•92938	33	WBHB1	: 6•94507	34	WBHV2	: •000000	35	WBHB2	: •000000
36	WBLV1	: 4•46469	37	WBLB1	: 2•97546	38	WBLV2	: •000000	39	WBLB2	: •000000	40	WBTCA	: 23•3156
41	W3	: 75•8997	42	T4	: 3460•00	43	ETH	: •850000	44	ETL	: •860000	45	FAR4	: •358028E-01
46	W4	: 78•6172	47	P4	: 349•006	48	H4	: 974•548	49	P3D4	: •499995E-01	50	TMX1VH	: 3951•29
51	TM1V04	: 1•14488	52	GAM4	: 1•27401	53	GFP4	: •408558	54	A4CP	: 32•4316	55	WCHV1Q	: •881759E-01
56	W41	: 87•5466	57	FAR41	: •320341E-01	58	H41	: 911•589	59	T41	: 3274•81	60	TMX1RH	: 3196•30
61	WCHB1Q	: •678994E-01	62	H42D41	: 179•530	63	P42	: 118•209	64	W42	: 94•4916	65	FAR42	: •236099E-01
66	H42	: 704•457	67	T42	: 2613•50	68	FP42	: 40•8653	69	P4Q42	: 2•95245	70	TMX2VH	:-•999999E 07
71	GAM42	:-•999999E 07	72	GFP42	:-•999999E 07	73	A42	:-•999999E 07	74	WCHV2Q	:-•999999E 07	75	W43	:-•999999E 07
76	FAR43	:-•999999E 07	77	H43	:-•999999E 07	78	T43	:-•999999E 07	79	TMX2RH	:-•999999E 07	80	WCHB2Q	:-•999999E 07
81	H44D43	: •000000	82	P44	: 118•209	83	W44	:-•999999E 07	84	FAR44	:-•999999E 07	85	H44	:-•999999E 07
86	T44	:-•999999E 07	87	FP44	: 40•8653	88	P42Q44	:-•999999E 07	89	GAM44	: 1•29121	90	GFP44	: •410499
91	A44CP	: 99•5503	92	WCLV1Q	: •415628E-01	93	W45	: 98•9563	94	FAR45	: •282363E-01	95	H45	: 688•793
96	T45	: 2565•65	97	P45	: 118•209	98	WCLB1Q	: •262293E-01	99	H46D45	: 131•961	100	P46	: 44•0991
101	W46	: 101•933	102	FAR46	: •273892E-01	103	H46	: 551•005	104	T46	: 2104•86	105	FP46	: 106•046
106	P44Q46	: 2•68053	107	GAM46	:-•999999E 07	108	GFP46	:-•999999E 07	109	A46	:-•999999E 07	110	WCLV2Q	:-•999999E 07
111	W47	:-•999999E 07	112	FAR47	:-•999999E 07	113	H47	:-•999999E 07	114	T47	:-•999999E 07	115	H5D47	: •000000
116	P5	: 44•0991	117	W5	: 101•933	118	FAR5	: •273892E-01	119	H5	: 551•005	120	T5	: 2104•86
121	FP5	: 106•046	122	P46Q5	:-•999999E 07	123	W13R	: 40•4078	124	P16	: 43•2056	125	W5R	: 68•4304
126	P6	: 43•6581	127	W61	: 202•716	128	P611	: 42•5645	129	H61	: 366•435	130	FAR61	: •135872E-01
131	T61	: 1471•43	132	W61R	: 117•388	133	P611	: 40•4363	134	WCLB2Q	:-•999999E 07	135		: •980000
136		: •870000	137	H7	: 366•435	138	FAR7	: •135872E-01	139	WFAB	: •000000	140	P7D61	: •499989E-01
141	XT7	: •000000	142	GAM7	: 1•34232	143	R7	: 53•3442	144	GFP7	: •524031	145	CD8	: •980000
146	PRCB	: 1•25806	147	P7GAMB	: 2•75152	148	A8	: 374•464	149	CV	: •984357	150	TIAM	: 1136•72
151	HIAM	: 278•342	152	V18	: 2100•26	153	V8	: 2067•40	154	VMN	: •000000	155	WFQP3	: 26•6288
156	WFQP3R	: 26•6279	157	P8D2	: 24•9983	158	P8Q2	: 3•00075	159	P23Q2	: 4•03195	160	W2R	: 200•002
161	W21R	: 39•7793	162	W23R	: 31•1074	163	W3R	: 5•85504	164	W4R	: 8•55020	165	HPXHR2	: •000000
166	HPXLR2	: •000000	167	TMX1VL	: 2802•83	168	TMX1RL	: 2417•62	169	TMX2VL	:-•999999E 07	170	TMX2RL	:-•999999E 07
171	T1	: 518•683	172	P1	: 14•6360	173	P2QAMB	: 1•00000	174	WFER	: 9782•51	175	WFTSTR	: 9782•51
176	HPXL	: •000000	177	PB22	: 59•2535	178	TB22	: 828•881	179	PB29	: 367•375	180	TB29	: 1454•85
181	W2R2	: 9999•85	182	W2223	: 7910•44	183	N1R2	: 4999•89	184		: •000000	185		: •000000
186	HPTHP	: 2223•03	187	LPTHP	: 1847•02	188	WFEX	: 2•71743	189	WAB	: •200000	190	GAM16	: 1•39425
191	GAM8	: 1•30374	192	GAM61	: 1•34232	193	W16R	: 41•2324	194	W6R	: 69•1216	195	W611R	: 124•093
196	P8QT16	: •934471	197	P8QT4	: •974301	198	P8QT61	: •973600	199	P16S	: 42•5347	200	P6S	: 42•5361
201	FP4	: 13•2502	202	H44D41	: 179•530	203	H5D45	: 131•961	204	P4Q44	: 1•95245	205	P44Q5	: 1•68053
206	W2R41	: 174•746	207	N1445	: 98•7119	208	A4	: 32•4317	209	A44	: 99•5507	210		: •000000
211		: •000000	212		: •000000	213		: •000000	214		: •000000	215		: •000000
216		: •000000	217		: •000000	218		: •000000	219		: •000000	220		: •000000
221		: •000000	222		: •000000	223		: •000000	224		: •000000	225		: •000000
226		: •000000	227		: •000000	228		: •000000	229		: •000000	230		: •000000

FIGURE C-5

EXPANDED INPUTS AND OUTPUTS

EXPIN

1	W2DP	200.000	2	T2DP	518.688	3	P2DP	14.6960	4	P13Q2DP	3.00000	5	P21Q2DP	3.00000
6	P23Q21DP	1.34400	7	P3023DP	6.20000	8	EF8DP	.820000	9	EF1DP	.820000	10	ECLDP	.830000
11	ECHDP	.840000	12	BPRDP	1.01580	13	WB22QDP	.000000	14	WB29QDP	.000000	15	P4DP	349.008
16	P44DP	113.209	17	P48DP	44.0982	18	GAM4DP	1.27401	19	GAM44DP	1.29121	20	ETHDP	.850000
21	ETLDP	.860000	22	A4DP	32.4317	23	A44DP	99.5507	24	A8DP	374.468	25	T4MAX	3450.00
26	T7MAX	3600.00	27	CDP8	.193371E-02	28	CDP16	.122490E-04	29	CDP56	.213540E-05	30	CDPA8	.359765E-05
31	UP8D	.500000E-01	32	DP16D	.200000E-01	33	DP56D	.100000E-01	34	DPA8D	.500000E-01	35	WBHV1Q	.300000E-01
36	WBHB1Q	.700000E-01	37	WBHV2Q	.000000	38	WBHB2Q	.000000	39	WBLV1Q	.450000E-01	40	WBLB1Q	.300000E-01
41	WBLV2Q	.000000	42	WBLB2Q	.000000	43	TMHV1	2360.00	44	TMHB1	2260.00	45	TMHV2	.000000
46	TMHB2	.000000	47	TMLV1	2160.00	48	TMLB1	2060.00	49	TMLV2	.000000	50	TMLB2	.000000
51	PF4	.250000	52	RPFH	.600000E-01	53	RPFL	.300000E-01	54	NHT	1.00000	55	NLT	1.00000
56	EB	.980000	57	EAB	.870000	58	MABDP	.200000	59	CD8D	.980000	60	DPMIXD	.200000E-01
61	CDPMIX	.149840E-05	62	DAMFAC1	.500000	63	DAMFAC2	.500000E-01	64	DAMFAC3	1.00000	65	DAMFAC4	1.00000
66	DAMFAC5	.500000	67	T21DP	750.379	68	T23DP	828.887	69	T3DP	1454.86	70	GAM16D	1.39425
71	GAM6D	1.36574	72	GAM61D	1.34232	73	W16RD	41.2324	74	W6RD	69.1234	75	W611RD	124.094
76	PSQT16D	.984471	77	PSQT6D	.974301	78	PSQT61D	.973600	79	MN16	.150000	80	MN6	.200000
81	N2DP	10000.0	82	N1DP	5000.00	83	FP4D	13.2503	84	FP42D	40.8655	85	FP44D	40.8655
86	FP46D	106.049	87	FP5D	106.049	88	H44D41D	179.599	89	H5D45D	131.964	90	P4044D	1.95245
91	P44Q5D	1.68059	92	N2R41D	174.746	93	N1R45D	98.7123	94	T41D	3274.81	95	T45D	2565.65
96		2.97069	97		.200000	98		.500000	99		.000000	100		.000000

EXPOUT

1	T4RATE	1.00001	2	RAT18T	1.00001	3	PR23MQD	1.00001	4	W23MQD	1.00000	5	ECHMQD	.999998
6	XNH23MQD	1.00000	7	PR21MQD	1.00000	8	W21MQD	1.00001	9	ECLMQD	.999999	10	XNL21MQD	1.00001
11	VRTH	1.00000	12	WTH	1.00000	13	ETHMQD	1.00000	14	VRTL	.999996	15	WTL	1.00000
16	ETLMQD	1.00000	17	W2R2MQD	.999992	18	FPRMQD	.999986	19	EFMQD	1.00001	20	XNFR2MQD	.999996
21	P4Q44MQD	.999999	22	XNHQTMQD	1.00000	23	FP4MQD	1.00000	24	P44Q5MQD	.999962	25	XNLQTMQ4	.999996
26	FP44MQD	1.00000	27		.000000	28		.000000	29		.000000	30		.000000
31		.000000	32		.000000	33		.000000	34		.000000	35		.000000
36		.000000	37		.000000	38		.000000	39		.000000	40		.000000
41		.000000	42		.000000	43		.000000	44		.000000	45		.000000
46		.000000	47		.000000	48		.000000	49		.000000	50		.000000

FIGURE C-6

```
NSI: 1801 9999
       0    0
       0    0
       0    0
       0    0
```

VARIABLE GEOMETRY CYCLE DECK
NAVAL AIR PROPULSION TEST CENTER
**** UNCLASSIFIED ****

```
RUN :    50.00
IND :  010101
DAY :     TUE
DATE: 04/08/75
TIME: 18:59:01
```

********** I N L E T C O N D I T I O N S **********

ALT	: .000000	TAMB	: 518.688	PAMB	: 14.6960	ERAMA	: 1.00000	P2QAMB:	1.00000	CRC	: 50.0000
		T1	: 518.688	P1	: 14.6960	MN	: .000000				
		T2	: 518.688	P2	: 14.6960	VA	: .000000				

******* C O M P O N E N T P E R F O R M A N C E *******

FAN OUTER		LOW COMP		BURNER		HPT VANE 1		HPT VANE 2		LPT VANE 1		LPT VANE 2	
W13	: 100.783	W23	: 99.2154	W4	: 78.6172	A4	: 32.4317	A42	:	A44	: 99.5507	A46	:
W13R	: 40.4078	W23R	: 31.1074	W4R	: 8.55020	GAM4	: 1.27401	GAM42	:	GAM44	: 1.29121	GAM46	:
P13	: 44.0874	P23	: 59.2535	P4	: 349.006	GFP4	: .408558	GFP42	:	GFP44	: .410499	GFP46	:
P13Q2	: 2.99996	P23Q21	: 1.34400	P3D4	: .049999	W41	: 87.5466	W43	:	W45	: 98.9563	W47	:
T13	: 750.373	T23	: 838.881	T4	: 3460.00	T41	: 3274.81	T43	:	T45	: 2565.65	T47	:
H13	: 179.759	H23	: 198.853	H4	: 974.548	H41	: 911.589	H43	:	H45	: 688.793	H47	:
EFB	: .820009	ECL	: .829999	FAR4	: .035803	FAR41	: .032034	FAR43	:	FAR45	: .028236	FAR47	:
FGHP	: 7956.74	LPCHP	: 2680.45	WFE	: 9782.74	WCHV1Q	: .088176	WCHV2Q	:	WCLV1Q	: .041563	WCLV2Q	:
				WFER	: 9782.51	WBHV1Q	: .090000	WBHV2Q	: .000000	WBLV1Q	: .045000	WBLV2Q	: .000000
				FP4	: 13.2502								

FAN INNER		HIGH COMP		HPT BLADE 1		HPT BLADE 2		LPT BLADE 1		LPT BLADE 2	
W21	: 99.2154	W3	: 75.8997	W42	: 94.4916	W44	:	W46	: 101.933	W5	: 101.933
W21R	: 39.7793	W3R	: 5.08504	FP42	: 40.8653	FP44	: 40.8653	FP46	: 106.046	FP5	: 106.046
P21	: 44.0874	P3	: 367.375	P42	: 118.209	P44	: 118.209	P46	: 44.0991	P5	: 44.0991
P21Q2	: 2.99996	P3Q23	: 6.20005	P4Q42	: 2.95245	P42Q44	:	P44Q46	: 2.68053	P46Q5	:
T21	: 750.373	T3	: 1454.85	T42	: 2613.50	T44	:	T46	: 2104.86	T5	: 2104.86
H21	: 179.759	H3	: 357.280	H42	: 704.457	H44	:	H46	: 551.005	H5	: 551.005
EFI	: .820009	ECH	: .839999	FAR42	: .029610	FAR44	:	FAR46	: .027389	FAR5	: .027389
FIHP	: 7832.98	HPCHP	: 22238.3	WCHB1Q	: .067899	WCHB2Q	:	WCLB1Q	: .026229	WCLB2Q	:
				WBHB1Q	: .070000	WBHB2Q	: .000000	WBLB1Q	: .030000	WBLB2Q	: .000000
				ETH	: .850000	ETH	: .850000	ETL	: .860000	ETL	: .860000
				H42D41	: 179.590	H44D43	: .000000	H46D45	: 131.961	H5D47	: .000000

MIXER		AFTERBURNER		NOZZLE		BLEED		HP	
W61	: 202.716	W7	: 202.716	P7QAMB	: 2.75152	WB22	: .000000	WPXH	: .000000
P61	: 42.5645	P7	: 40.4363	PRC8	: 1.85806	WB22Q	: .000000	WPXL	: .000000
T61	: 1471.48	T7	: 1471.48	A8	: 374.464	WB29	: .000000	WPXHR2	: .000000
H61	: 366.435	H7	: 366.435	A9	: 374.464	WB29Q	: .000000	WPXLR2	: .000000
P16	: 43.2056	FAB	: .870000	CV	: .984357	PB22	: 59.2535		
P6	: 43.6581	WFAB	: .000000	V9	: 2067.40	TB22	: 828.881		
FAR61	: .013587	FAR7	: .013587	CD8	: .980000	PB29	: 367.375		
P16S	: 42.5347	P7D61	: .049999			TB29	: 1454.85		
P6S	: 42.8341	MAB	: .200000						

********** P E R F O R M A N C E **********

FGG	: 13025.9	N1	: 4999.98	N2	: 199.998	P3Q2	: 24.9983	WFTOTR: 9782.51
FN	: 13025.9	N1R2	: 4999.89	N2R	: 200.002	P5Q2	: 3.00075	
FRAM	: .000000	N2	: 10000.0	BPR	: 1.01580	P23Q2	: 4.03195	
TSFC	: .751023	N2R2	: 9999.86	HPTHP	: 22238.3	WFQP3	: 26.6288	
WFTOT	: 9782.74	N2R23	: 7310.44	LPTHP	: 18470.2	WFQP3R	: 26.6279	

FIGURE C-7

```
NSI: 1801 9999
     0    0
     0    0
     0    0
     0    0
```

VARIABLE GEOMETRY CYCLE DECK
NAVAL AIR PROPULSION TEST CENTER
**** UNCLASSIFIED ****

RUN : 50.00
IND : 010101
DAY : TUE
DATE: 04/08/75
TIME: 18:59:01

* * * * * * * * * * * I N L E T C O N D I T I O N S * * * * * * * * * * *

ALT	: .000000	TAMB	: 518.688	PAMB	: 14.6960	ERAMA	: 1.00000	P2QAMB: 1.00000	CRC	: 50.0000
		T1	: 518.688	P1	: 14.6960	MN	: .000000			
		T2	: 518.688	P2	: 14.6960	VA	: .000000			

* * * * * * * * * * * * * * * P E R F O R M A N C E * * * * * * * * * * * * * *

FG9	: 13025.9	N1	: 4999.98	W2	: 199.998	P3Q2	: 24.9583	WFTOTR: 9782.51	
FN	: 13025.9	N1R2	: 4999.89	W2R	: 200.002	P5Q2	: 3.00075		
FRAM	: .000000	N2	: 10000.0	BPR	: 1.01580	P23Q2	: 4.03195		
TSFC	: .751023	N2R2	: 9999.85	HPTHP	: 22238.3	WFQP3	: 26.6288		
WFTOT	: 9782.74	N2R23	: 7910.44	LPTHP	: 18470.2	WFQP3R	: 26.6279		

```
NSI:  0    0
      0    0
      0    0
      0    0
      0    0
```

VARIABLE GEOMETRY CYCLE DECK
NAVAL AIR PROPULSION TEST CENTER
**** UNCLASSIFIED ****

RUN : 51.00
IND : 010101
DAY : TUE
DATE: 04/08/75
TIME: 19:00:08

* * * * * * * * * * * I N L E T C O N D I T I O N S * * * * * * * * * * *

ALT	: .000000	TAMB	: 518.688	PAMB	: 14.6960	ERAMA	: 1.00000	P2QAMB: 1.00000	CRC	: 48.0000
		T1	: 518.688	P1	: 14.6960	MN	: .000000			
		T2	: 518.688	P2	: 14.6960	VA	: .000000			

* * * * * * * * * * * * * * * P E R F O R M A N C E * * * * * * * * * * * * * *

FG9	: 12246.5	N1	: 4892.25	W2	: 194.784	P3Q2	: 23.6397	WFTOTR: 9023.04	
FN	: 12246.5	N1R2	: 4892.16	W2R	: 194.788	P5Q2	: 2.86625		
FRAM	: .000000	N2	: 9884.70	BPR	: 1.04758	P23Q2	: 3.84441		
TSFC	: .736800	N2R2	: 9884.53	HPTHP	: 20774.8	WFQP3	: 25.9730		
WFTOT	: 9023.26	N2R23	: 7895.26	LPTHP	: 16983.5	WFQP3R	: 25.9721		

```
NSI: 1801    0
     0    0
     0    0
     0    0
     0    0
```

VARIABLE GEOMETRY CYCLE DECK
NAVAL AIR PROPULSION TEST CENTER
**** UNCLASSIFIED ****

RUN : 52.00
IND : 010101
DAY : TUE
DATE: 04/08/75
TIME: 19:01:00

* * * * * * * * * * * I N L E T C O N D I T I O N S * * * * * * * * * * *

ALT	: .000000	TAMB	: 518.688	PAMB	: 14.6960	ERAMA	: 1.00000	P2QAMB: 1.00000	CRC	: 46.0000
		T1	: 518.688	P1	: 14.6960	MN	: .000000			
		T2	: 518.688	P2	: 14.6960	VA	: .000000			

* * * * * * * * * * * * * * * P E R F O R M A N C E * * * * * * * * * * * * * *

FG9	: 11162.5	N1	: 4713.82	W2	: 186.301	P3Q2	: 21.8515	WFTOTR: 8093.87	
FN	: 11162.5	N1R2	: 4713.74	W2R	: 186.304	P5Q2	: 2.68732		
FRAM	: .000000	N2	: 9756.51	BPR	: 1.08401	P23Q2	: 3.57339		
TSFC	: .725020	N2R2	: 9756.34	HPTHP	: 18979.5	WFQP3	: 25.2018		
WFTOT	: 8093.96	N2R23	: 7888.28	LPTHP	: 15084.4	WFQP3R	: 25.2009		

FIGURE C-8: INLET REFERRED FLOW VERSUS NET THRUST, 30K, M_n = .8

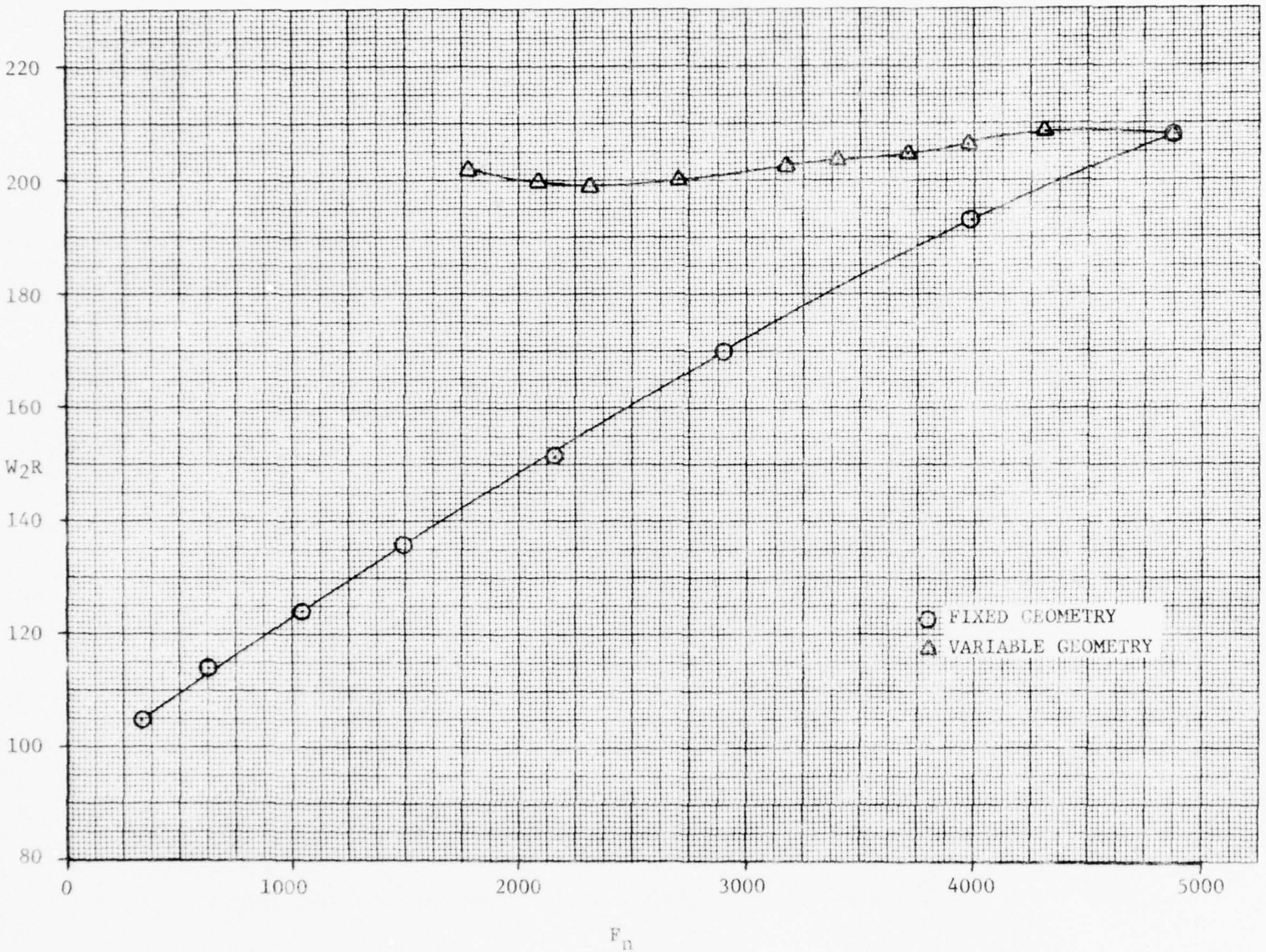

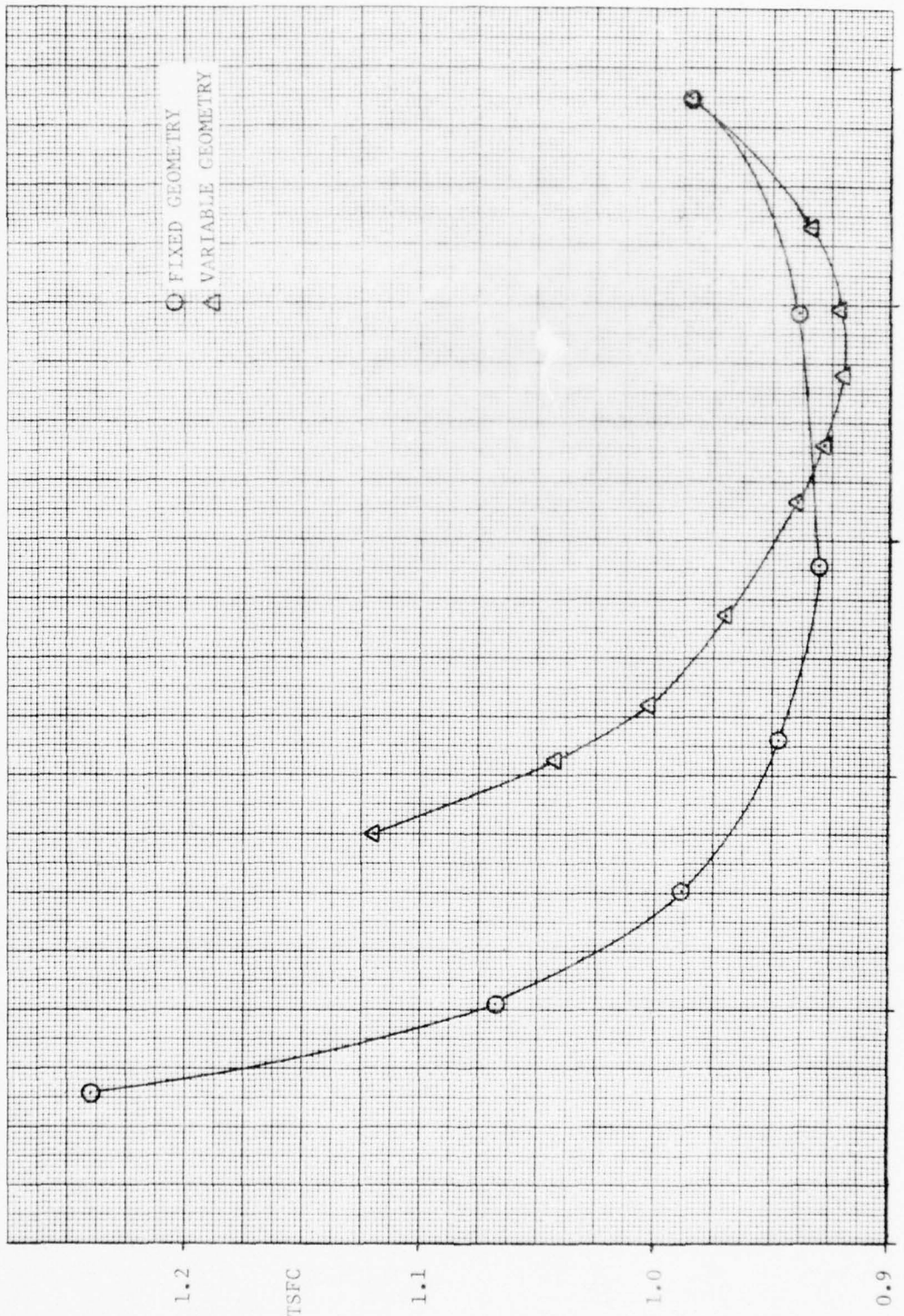

FIGURE C-9: THRUST SPECIFIC FUEL CONSUMPTION VERSUS NET THRUST, 30K, Mn = .8

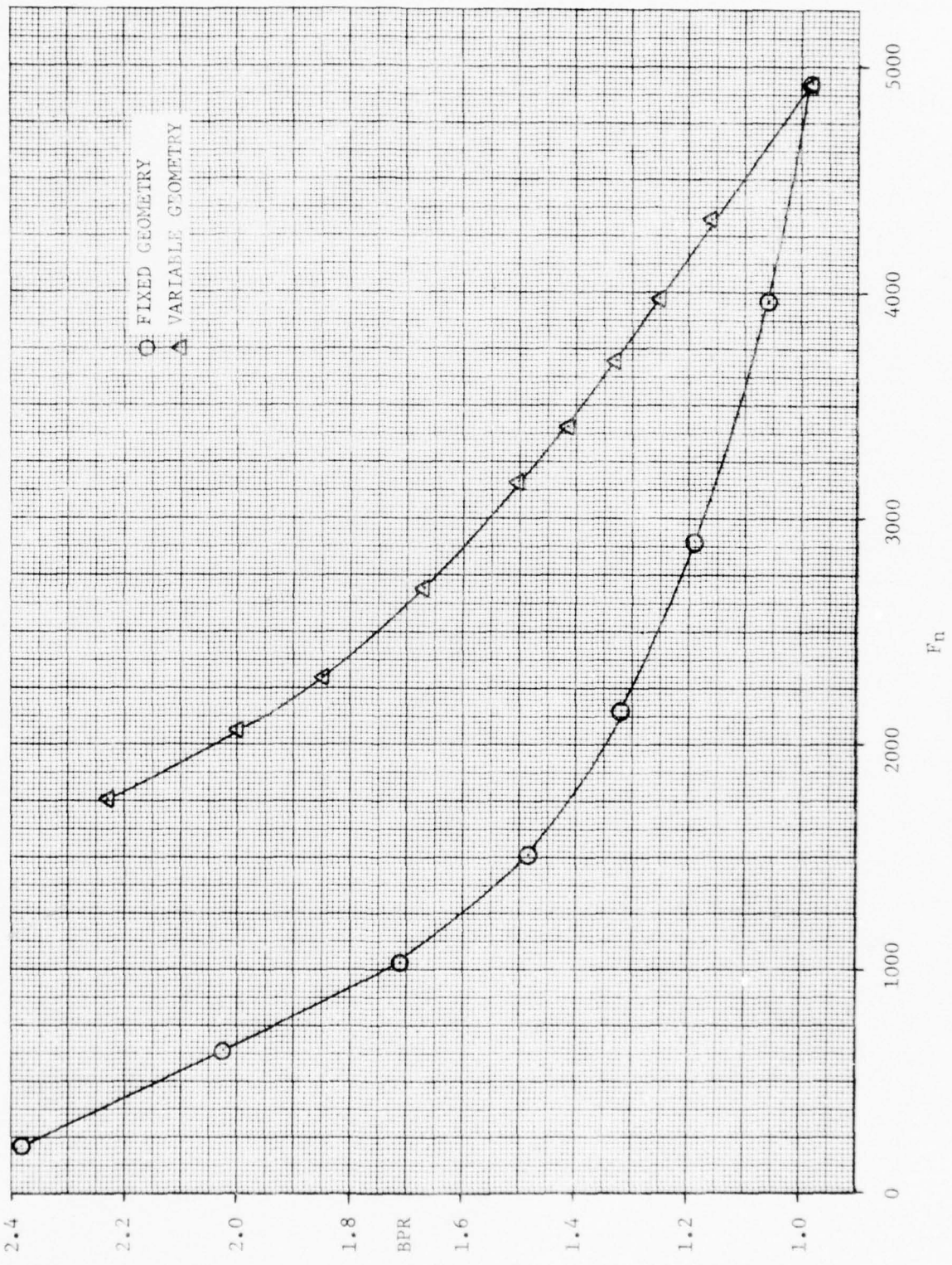

FIGURE C-10: BYPSSS RATIO VERSUS NET THRUST, 30K, M_n = .8

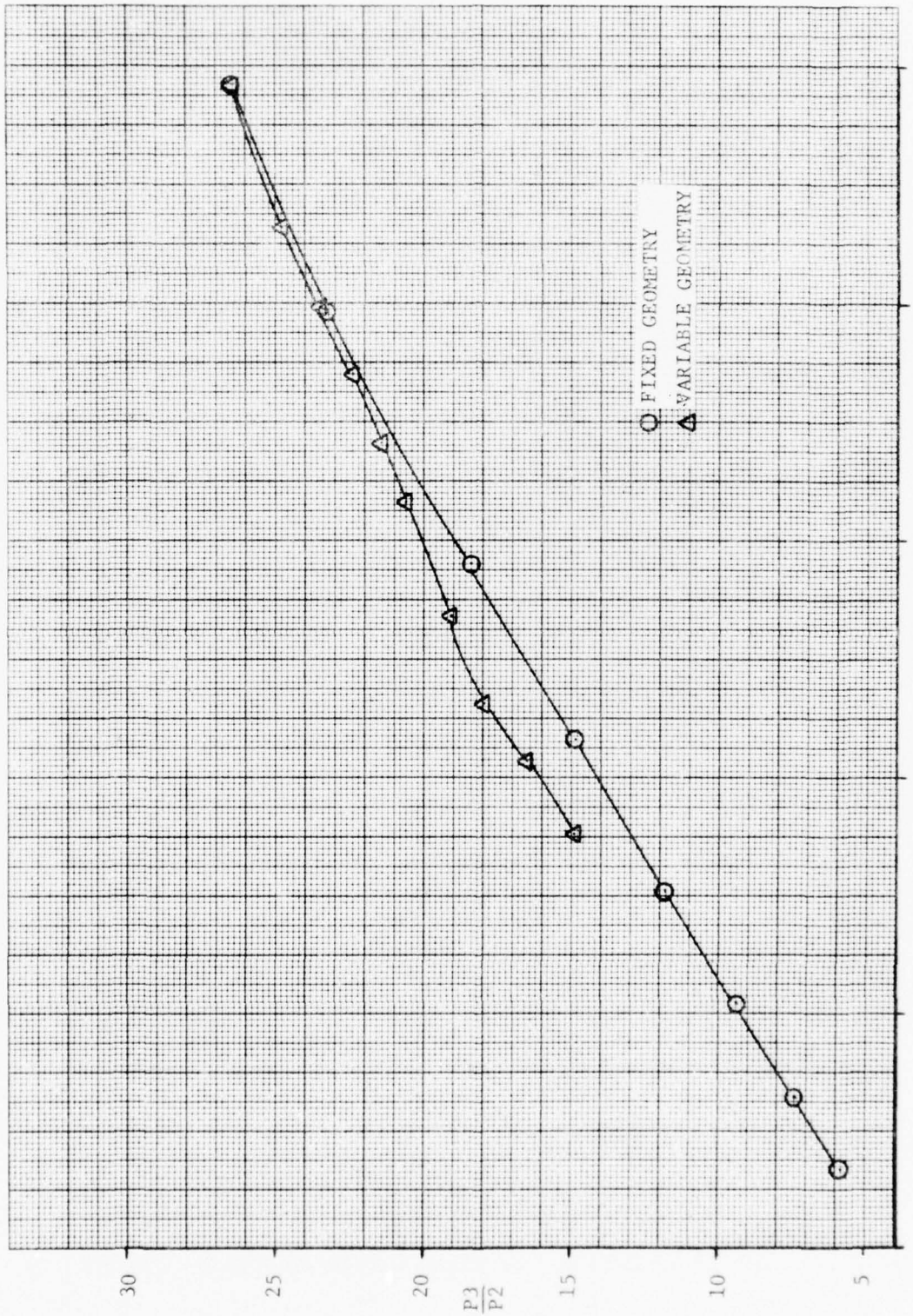

FIGURE C-11: OVERALL COMPRESSION RATIO VERSUS NET THRUST, 30K, M_n = .8

FIGURE C-12: BURNER DISCHARGE TEMPERATURE VERSUS NET THRUST, 30K, M_n = .8

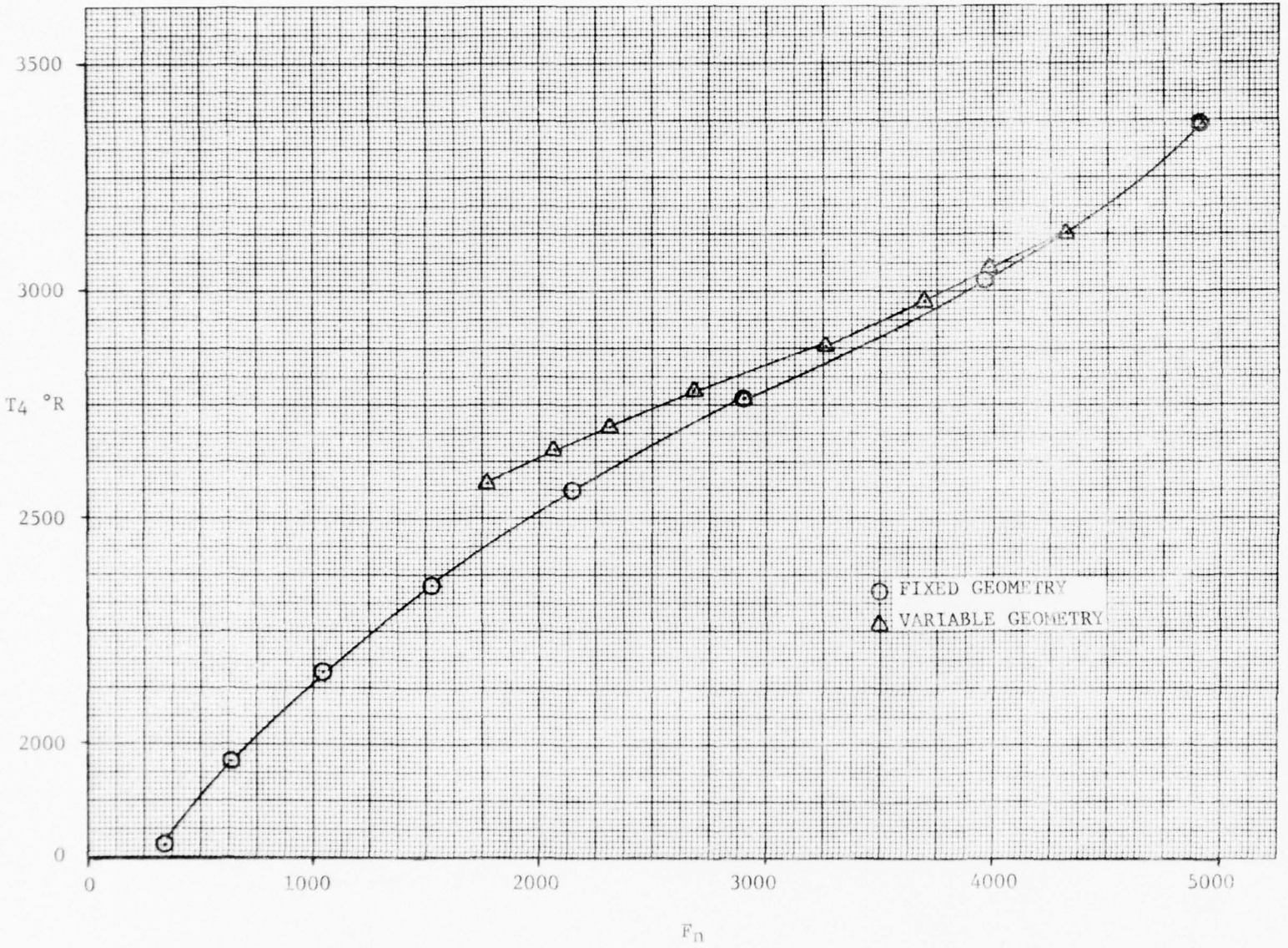

FIGURE C-13: VARIABLE GEOMETRY SCHEDULES FOR 30K, M_n = .8 CRUISE

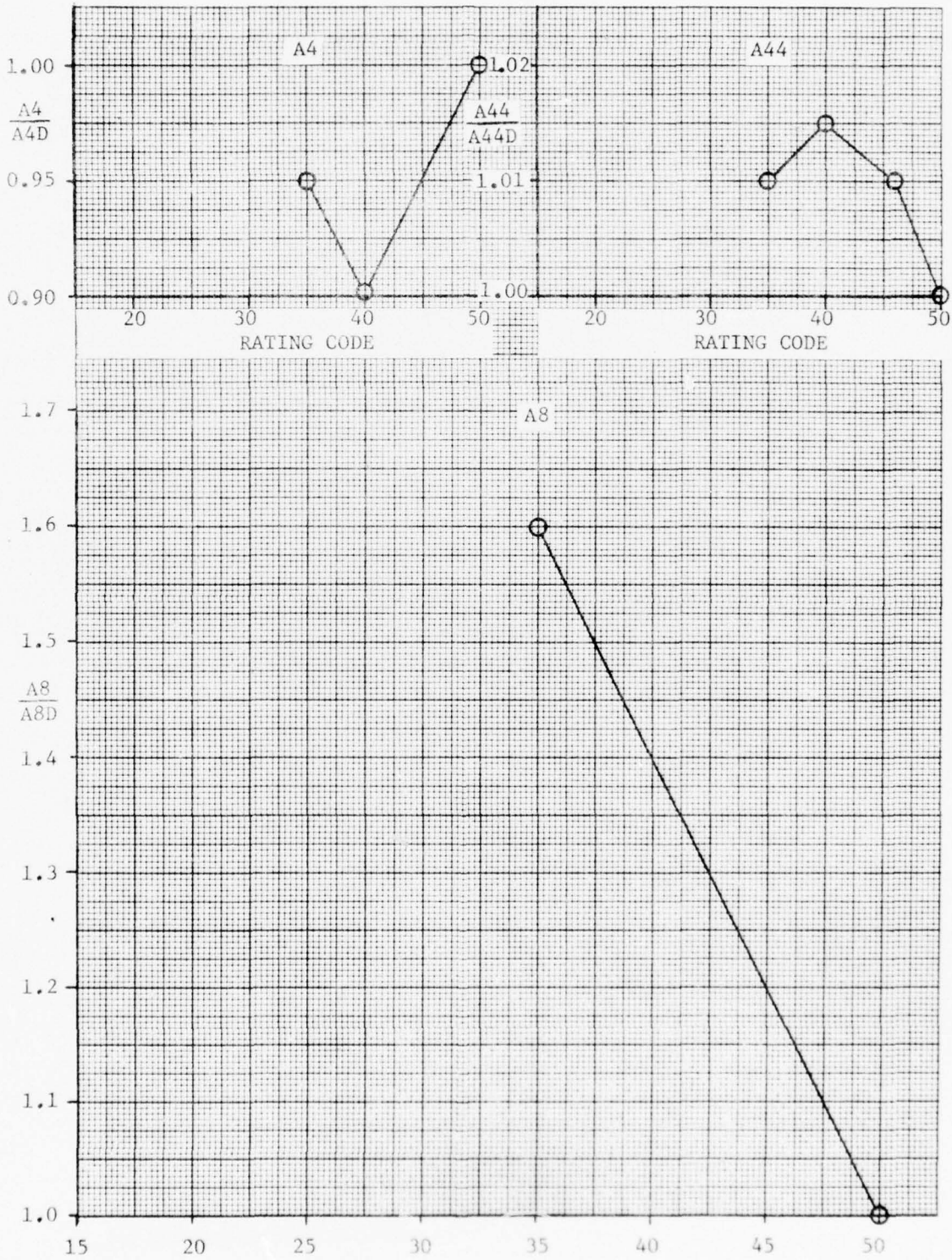

APPENDIX D

Sensitivity Study of TEDD Program

A. INTRODUCTION

This study was conducted on the TEDD Phase II program to determine the effects of parameter errors on the diagnostic capabilities of the system and to get an indication of which parameters are the most critical and what measurement accuracies are required. The parameters studies were the ones used in the steady-state performance analysis, plus turbine blade temperature (pyrometer output), which was used in the turbine life subroutines. The other TEDD parameters were used mostly in simple limit exceedance checks (such as oil temperature and pressure, fuel pressure, etc.), or for on-off type indications (fuel control selector switch, squat switch, 12th stage bleed, etc.), where extreme accuracy is not as important.

B. MEASUREMENT ERROR

Before presenting the results of the sensitivity study, a brief discussion of parameter measurement error is in order. Measurement error has two types of components, fixed error and random error. Random error (non-repeatability) is seen in repeated measurements, which do not and are not expected to agree exactly, for various reasons. The variation between repeated measurements is called "precision error". The standard deviation is used as a measure of the precision error. A large standard deviation means large scatter in the measurements. Data smoothing techniques can be used to minimize the effects of random error. A statistical analysis of TEDD Phase II data will be presented later.

The constant or systematic error is known as bias. In repeated measurements, each measurement has the same bias. Bias can be categorized into various classes. Known biases may be eliminated by calibration, but unknown biases are not correctible. A comprehensive study of measurement error in gas turbine engines is provided in Reference D-1.

The absolute level of accuracy becomes relatively unimportant when a differential or trending technique is used for diagnosis. In this approach, a custom baseline is obtained for each engine using the actual engine sensors and total diagnostic system, and the deltas or changes from the original values are used for diagnosis. This method eliminates the effect of bias errors, as well as engine to engine variations.

The above (delta) approach was used for the TEDD performance analysis. The absolute measurement accuracy is important, however, for

other applications, such as in critical limit exceedance checks (RPM, turbine inlet temperature) and in computations such as the turbine life subroutines.

C. TURBINE LIFE SUBROUTINES

The first sensitivity analysis performed was for turbine blade temperature, as utilized in the TEDD turbine erosion life and turbine creep life diagnostic subroutines. Calculations of turbine life were made at several different temperature levels and with plus or minus errors (variations) from these levels. For each temperature variation, the change in calculated turbine life was expressed as a percentage (plus or minus) change from the original level. The results are shown in Figures D-1 and D-2. It can be seen that these computations are quite sensitive to any error in turbine blade temperature. For erosion life, this sensitivity is as high as 1.2% computation error per degree temperature error, or 48% increase in calculated turbine erosion life at -40°F temperature error. The creep life calculations is even more sensitive to temperature error, up to a maximum of 56% increase in calculated turbine life at -15°F temperature error. These calculated turbine life values include a factor of safety of 70% for creep life and 90% for erosion life. Although, they have not been evaluated experimentally to compare with the actual engine part conditions, they illustrate some of the difficulties involved in making accurate turbine life calculations. Besides the problem of measurement accuracy (absolute accuracy), there are temperature variations from blade to blade and gradients along each blade. The creep life calculation also has an rpm input, but this can be measured more accurately, and any contribution to the life computation error has been found to be relatively small.

D. STEADY-STATE PERFORMANCE ANALYSIS

The major portion of this sensitivity study dealt with the TEDD Steady-State Performance Analysis. This study was made using the TF30-P-408 engine performance deck baselines and deck fault data processed through the TEDD Performance Analysis Program. For each of the eleven diagnosable faults, data was processed with errors input to each of the twelve different performance parameters used, in $\pm$1% increments to $\pm$5%. Errors greater than $\pm$5% were not considered, since they are larger than normal parameter inaccuracies, and in most cases, can be detected by the instrumentation check portion of the program. In fact, this instrumentation check had to be removed from the program for this study, since it could even detect smaller errors.

The engine operating condition chosen was sea level static, standard day, with a power setting of 2200°R turbine inlet temperature, which is approximately midway in the engine pressure ratio (ERP) band where performance analysis is done (ERP = 1.6 to maximum power).

Table D-I identifies the eleven faults analyzed and the fault levels used for this study. Table D-II lists the measured performance parameters used in the diagnosis.

TABLE D-I

Performance Fault Identification and Level

LPCE	=	Low Pressure Compressor Efficiency (6% Decrease)
HPCE	=	High Pressure Compressor Efficiency (6% Decrease)
HPTE	=	High Pressure Turbine Efficiency (6% Decrease)
LPTE	=	Low Pressure Turbine Efficiency (6% Decrease)
HPTA	=	High Pressure Turbine (Nozzle) Area (3% Increase)
LPTA	=	Low Pressure Turbine (Nozzle) Area (3% Increase)
ANZ+	=	Exhause Nozzle Area Increase (5%)
ANZ-	=	Exhaust Nozzle Area Decrease (4%)
BL09	=	Ninth Stage Bleed Flow (4 lb/sec)
BL12	=	Twelfth Stage Bleed Flow (5 lb/sec)
BL16	=	Sixteenth Stage Bleed Flow (3 lb/sec)

TABLE D-II

Measured Performance Parameters

T_{T2}	Inlet Air Total Temperature
P_{T2}	Inlet Air Total Pressure
T_{T3}	Low Pressure Comp. Disch. Total Temperature
P_{T3}	Low Pressure Comp. Disch. Total Pressure
T_{T4}	High Pressure Comp. Disch. Total Temperature
P_{T4}	High Pressure Comp. Disch. Total Pressure
P_b	Burner Pressure
T_{T7}	Low Pressure Turbine Disch. Total Temperature
P_{T7}	Low Pressure Turbine Disch. Total Pressure
N1	Low Pressure Rotor Speed
N2	High Pressure Rotor Speed
W_f	Fuel Flow

The results of this study are expressed in the series of plots shown in Figures D-3 through D-14. Each figure shows the effect of error in a given parameter on the diagnostic results for each of the

faults analyzed. The diagnostic program provides a measure of the accuracy of the fault signature match called Confidence Factor. In the upper plot of Figures D-3 through D-14, the sensitivity study results were expressed in terms of percent parameter error versus percent decrease in the Confidence Factor from the zero error factor (which in most cases was over 90%). Also shown in the lower plot of each figure is the effect of parameter error on percent change in calculated fault level, which is used in the calculation of Confidence Factor.

The results shown in Figures D-3 through D-14 are summarized in Table D-III. The parameter error criteria used was a 10% allowable decrease in Confidence Factor. Using this criteria, the smallest parameter error (+ or -) that would cause this 10% decrease was determined from the plots for each parameter and each fault. These allowable errors are listed in Table D-III, with the average allowable error computed for each parameter, and the parameters ranked in order of average allowable error (sensitivity). It is seen that, percentage-wise, errors in N2 and N1 will affect the accuracy of the diagnostic results the most, with average allowable errors of 0.48% and 0.65%, respectively. These average allowable errors only serve to provide an overall measure and ranking of parameters. The sensitivity of each parameter can vary considerably with each fault, and the required accuracy for each parameter must be bases upon the most sensitive case. However, this ranking by average allowable error is very similar to a ranking by smallest parameter error to cause a 10% decrease in Confidence Factor. These figures, ranging from 0.1% for N2 to 1.7% for T_2, are listed in the last column of Table D-III.

The results show T_2 to be the least sensitive parameter, but this is due to the basis used, and the actual T_2 error involved is not large. It should be noted that the parameter errors introducted were in terms of percent of point, in the measured engineering units, i.e., in the case of T_2, the point value is 59°F, and a 1% error represents a 0.59°F error. At an inlet temperature condition of 12°F, a 0.59° error would be a 4.9% of point. For the performance analysis computations, T_2 is converted from °F to the absolute temperature in °R. Now the same 0.59° error becomes only 0.11% of point in terms of the absolute temperature (519°R), so the percent error is considerably reduced. The same is true of T_3 and T_4, but these temperatures are at higher levels, so the conversion to absolute temperature has a lesser, but still significant effect.

In order to bring these percent error numbers into perspective, Table D-IV is presented. This lists the actual value of each parameter at the sea level static, standard day engine operating condition chosen and the engineering unit equivalent of a 1% of point error.

TABLE D-III

Allowable Parameter Errors For 10% Decrease In Confidence Factor

Fault No.	1	2	3	4	5	6	7	8	9	10	11		
	LPCE	HPCE	HPTE	LPTE	HPTA	LPTA	ANZ+	ANZ-	BL09	BL12	BL16	AVG.	MIN.
N2	0.3%	1.2%	1.0%	0.3%	0.2%	0.4%	0.5%	0.3%	0.1%	0.8%	0.2%	0.48%	0.1%
N1	0.8	1.3	0.8	0.4	0.2	0.2	0.6	0.6	1.1	0.7	0.5	0.65	0.2
P_{T7}	2.0	1.8	1.7	0.6	0.7	0.3	0.9	0.7	0.8	0.8	0.8	1.01	0.3
P_{T2}	1.3	2.2	2.5	0.7	0.4	0.6	1.3	1.0	0.7	1.1	0.6	1.13	0.4
P_{T4}	1.4	1.9	1.4	0.6	0.8	0.7	0.8	1.1	2.2	1.1	1.2	1.20	0.6
W_f	1.7	2.6	2.1	2.0	0.9	1.1	1.6	1.4	0.7	2.3	1.7	1.65	0.7
T_{T4}	4.1	2.7	3.8	0.6	1.0	0.6	2.5	2.9	2.3	2.3	1.7	2.23	0.6
P_B	2.4	6.3	4.6	1.2	1.2	1.0	-	0.8	1.6	2.0	1.5	2.26	0.8
P_{T3}	3.4	1.9	4.4	2.7	1.6	2.0	1.4	1.4	3.3	-	1.5	2.36	1.4
T_{T3}	5.1	4.5	4.8	1.1	0.4	0.8	3.3	3.9	3.6	5.4	2.2	3.19	0.4
T_{T7}	3.2	5.4	6.6	5.6	1.4	4.8	1.5	1.6	4.8	4.8	1.9	3.78	1.4
T_{T2}	6.4	11.2	11.5	2.2	1.7	2.3	5.1	4.2	2.5	6.0	3.3	5.13	1.7

TABLE D-IV

Sea Level Static Standard Day Values

Parameter	Point Value at T5=2200°R	1% Error ≈
N2	13,701 rpm	137 rpm
N1	8,951 rpm	90 rpm
P_{T7}	60.52" HgA	0.61" Hg
P_{T2}	29.92" HgA	0.30" Hg
P_{T4}	435.03" HgA	4.35" Hg
W_f	5914 pph	59 pph
T_{T4}	761°F	7.6°
$P_B(P_{T5})$	201.21 psia	2.0 psi
P_{T3}	153.76" HgA	1.54" Hg
T_{T3}	407°F	4.1°
T_{T7}	967°F	9.7°
T_{T2}	59°F	0.59°

The Table D-IV data is deck baseline data with no faults, so the point value will vary somewhat, depending on the fault, but the 1% column is a good approximation of the magnitude of the errors involved.

It is of interest to analyze the TEDD Phase II performance parameter data for repeatability. This information is readily available from the TEDD steady-state Calibration and Data Analysis Program which statistically examined the data to identify problem areas. Table D-V shows data taken at a steady-state operating condition. This data reading consists of 200 consecutive samples on each channel, for which an average, standard deviation, and statistical average are computed.

TABLE D-V

Statistical Analysis of TEDD Phase II Data

Parameter	[redacted] Average	Standard Deviation(s)	Statistical Average
N2	13,578 rpm	40.4**	13,575
N1	8,755	9.8**	8,754
P_{T7}	59.47" HgA	0.05	59.47
P_{T2}	29.80" HgA	0.17**	29.81
P_{T4}	415.1" HgA	0.58	415.1
W_f	1110 cps *	5.1**	1111
T_{T4}	708.9°F	4.0**	709.1
P_B	187.9 psia	0.44	188.0
P_{T3}	148.9" HgA	0.13	148.9
T_{T3}	393.8°F	7.3**	394.0
T_{T7}	1035.2°F	3.9	1035.3
T_{T2}	60.6°F	2.1**	60.6

* Flowmeter output signal
** Repeatability unsatisfactory without data smoothing

The average is a mathematical average of 200 consecutive samples. The standard deviation is estimated by S as follows:

$$S = \left[\frac{\sum_{i=1}^{n} (X_i - \bar{X})^2}{n-1} \right]^{1/2}$$

Where X_i is the ith sample, $\bar{X}$ is the mean of n samples

Statistically, if the sample is random (if it has no periodic noise), 95% of all samples will fall within a band, centered on the mean, which is approximately 4S wide. Any samples which fall outside this band may be considered insignificant, and may be ignored. The statistical average is a new mean computed from the points remaining after

all insignificant points are rejected. Ignoring the insignificant samples (5%), the data scatter is approximately $\pm$ 2S. Comparing the actual scatter shown in Table D-V with the maximum allowable % error shown in the last column of Table D-III, it is seen that the parameters N2, N1, P_{T3}, W_f, T_{T4}, T_{T3} and T_{T2} had too much scatter to use the raw data without smoothing. The limited moving average smoothing technique employed in TEDD Phase II reduced the scatter in the performance analysis results. However, further investigation was required in this area, as described in Appendix A.

The characteristics of the sensitivity plots in Figures D-3 through D-14, are unique to the TEDD Steady-State Performance Analysis Program. Occasional anomalies such as a large change in slope or a reversal can be caused by changeover from one range to another or other aspects of the analysis approach. If a plot flattens out at higher error levels, i.e., no more decrease in Confidence Factor with increasing error, this is due to the "saturation" (reaching 100%) of the various individual Confidence Values computed which use the subject parameter, plus the non-use of this parameter in the average fault level computation. In actual use, the instrumentation check portion of the program would have identified the problem of bad instrumentation before most of these error values were reached. To fully explain the plot characteristics, the details of the analysis program must be understood (Reference D-2), but this is not necessary to use the data.

The calculated fault level (lower plot of Figures D-3 through D-14) is determined by the program just prior to the Confidence Factor, and the results of the fault level calculation affect the Confidence Factor. For most of the faults only 3 or 4 curves are used for fault level calculation. These curves have been pre-selected for each fault as exhibiting large and linear changes with increasing fault level. Thus, some parameters are not used for some fault level calculations; and therefore, error in these parameters will not affect these calculations, and there is no corresponding curve shown for that fault. Since an error in calculated fault will cause an error in Confidence Factor, it is generally true that the larger the change in calculated fault level, the larger the decrease in Confidence Factor tends to be.

An area where the program was not fully refined, was in faults No. 4, 5, and 6; and this had an effect on the results in these cases. For these faults, all or substantially all of the 23 curves were used to calculate fault level, instead of selecting a representative few. In addition, all 23 curves (rather than a selected group) were used to calculate Confidence Factor. As a result, these three faults show up as being the most sensitive to parameter error in the majority of cases. An example is seen in Figure D-12 (T_{T3}). This parameter is not used to determine the calculated fault level for any fault except these three, and with further program refinement would not be used in these cases

either. This parameter is relatively insensitive to changes in engine condition due to these faults, so conversely, if it is utilized in the diagnosis, an error or change in this parameter would falsely indicate a relatively large change in the engine. This shows the importance of proper selection of curves. Making this correction in the program would increase many of the allowable errors to some extent.

E. SUMMARY

This sensitivity study is an indication of the kinds of accuracies required for the most critical parameters used on the TEDD/TF30-P-408 system. In addressing accuracy, both the absolute accuracy and the repeatability were considered. The absolute accuracy is important in calculations such as turbine life and in critical limit exceedances. However, in the delta approach used for steady state performance analysis, it is not the absolute accuracy but the data repeatability that is most important, and this can be significantly improved by data smoothing techniques. The accuracies (repeatabilities) required are subject to variation depending on the type of engine, the faults to be analyzed, and the type of diagnostic system. For any given engine/diagnostic system the required accuracy also can vary with engine flight conditon, power setting, level of fault detection desired, and multiplicity of faults. Also, these results reflect only the error in single parameters and not a combination of error in different parameters.

Two parameters which were not included in this TEDD/TF30-P-408 study, but will be important for advanced engines, for performance analysis and/or limit exceedance monitoring, are position measurement (variable compressor, turbine and nozzle; power lever) and turbine inlet temperature.

REFERENCES

D-1 REPORT - Abernethy, Dr. R. B. et. al., and Thompson, J. W. Jr., "Handbook, Uncertainty in Gas Turbine Measurements", Arnold Engineering Development Center, AEDC-TR-73-5 of February 1973

D-2 REPORT - van Gelder, F. M., "Turbine Engine Diagnostic Development Phase II Report", Naval Air Propulsion Test Center, NAPTC-PE-29 of March 1974

FIGURE D-1: SENSITIVITY OF TURBINE EROSION LIFE COMPUTATION TO TURBINE BLADE TEMPERATURE ERROR

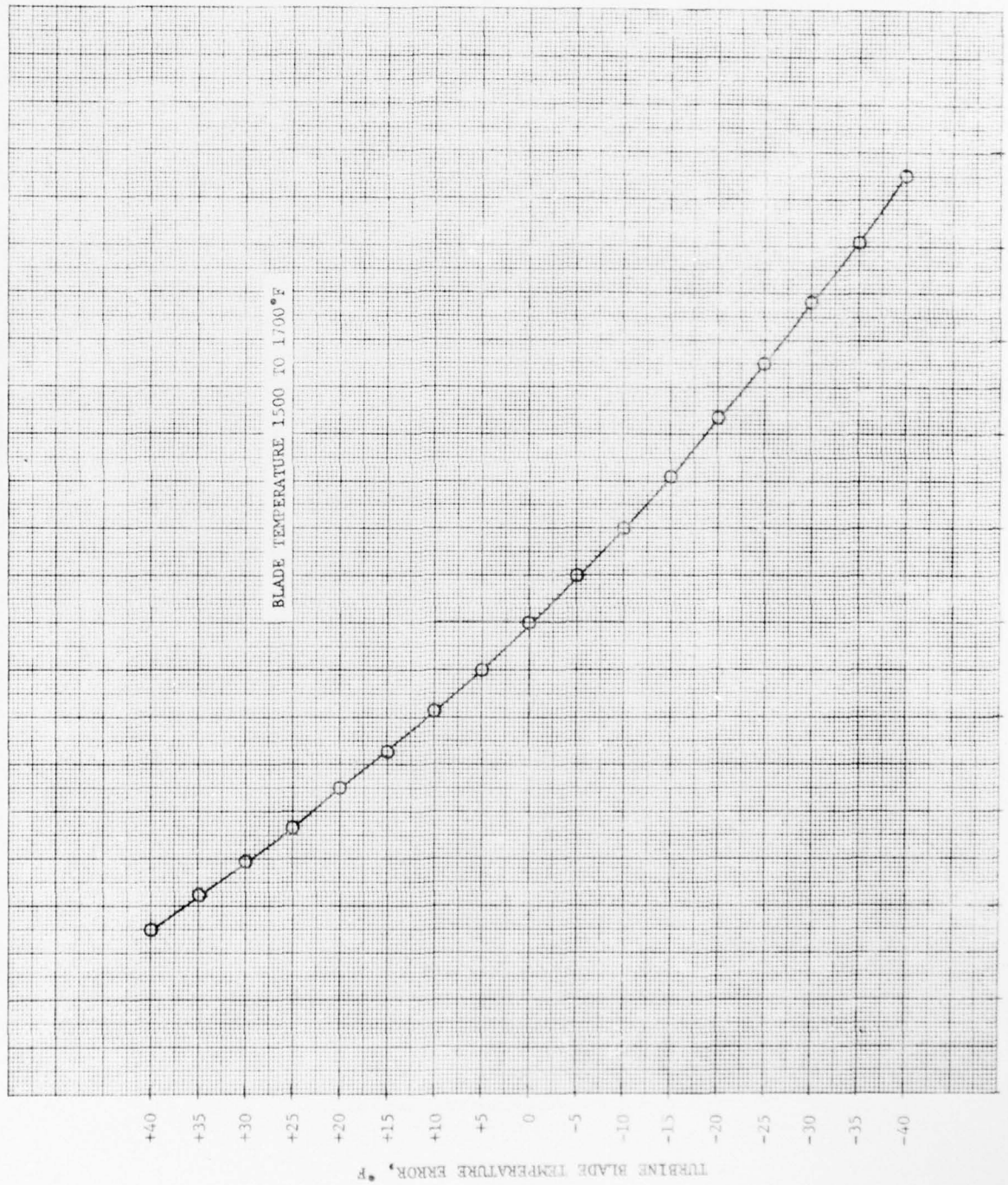

FIGURE D-2: SENSITIVITY OF TURBINE CREEP LIFE COMPUTATION TO TURBINE BLADE TEMPERATURE ERROR

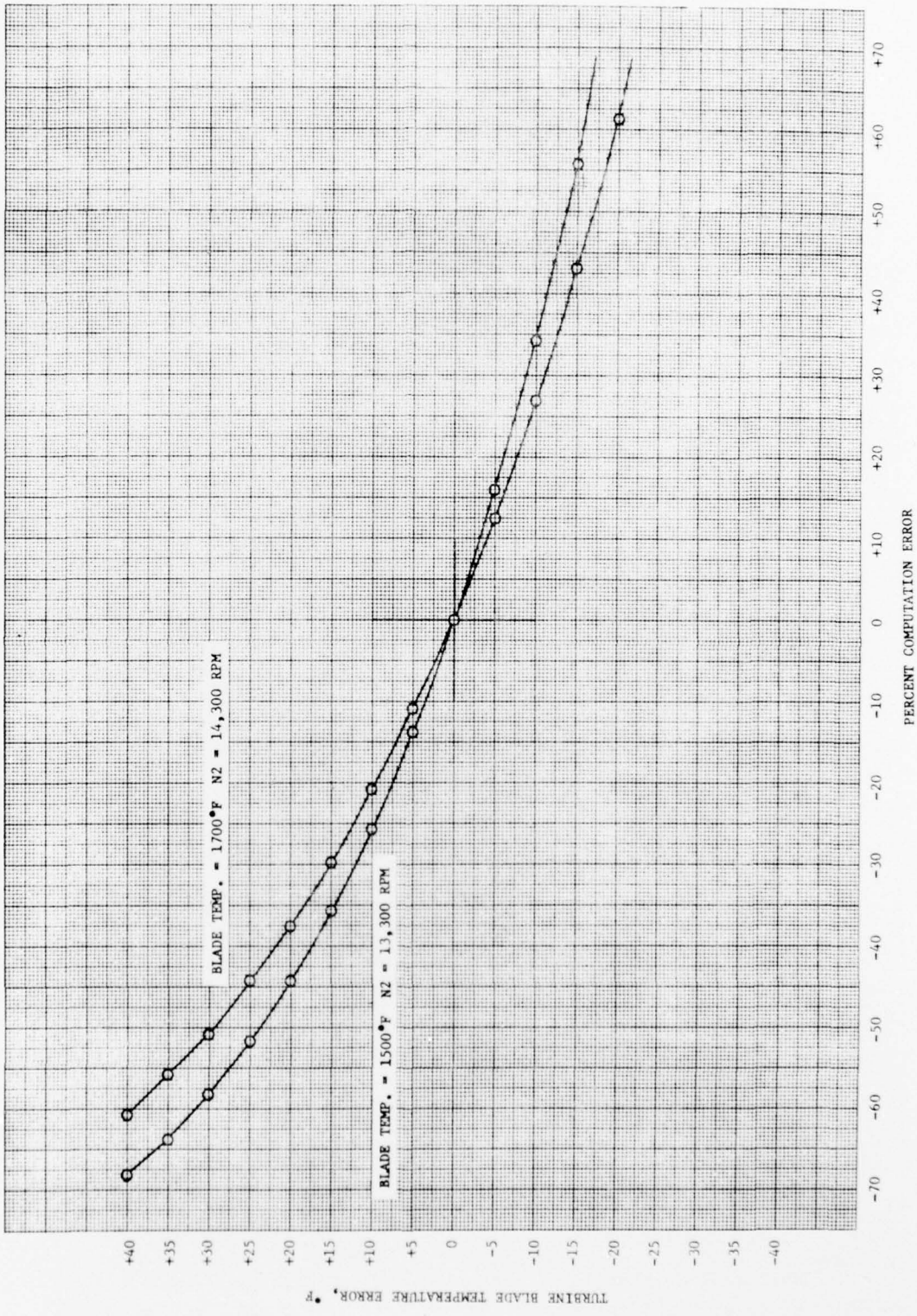

FIGURE D-3

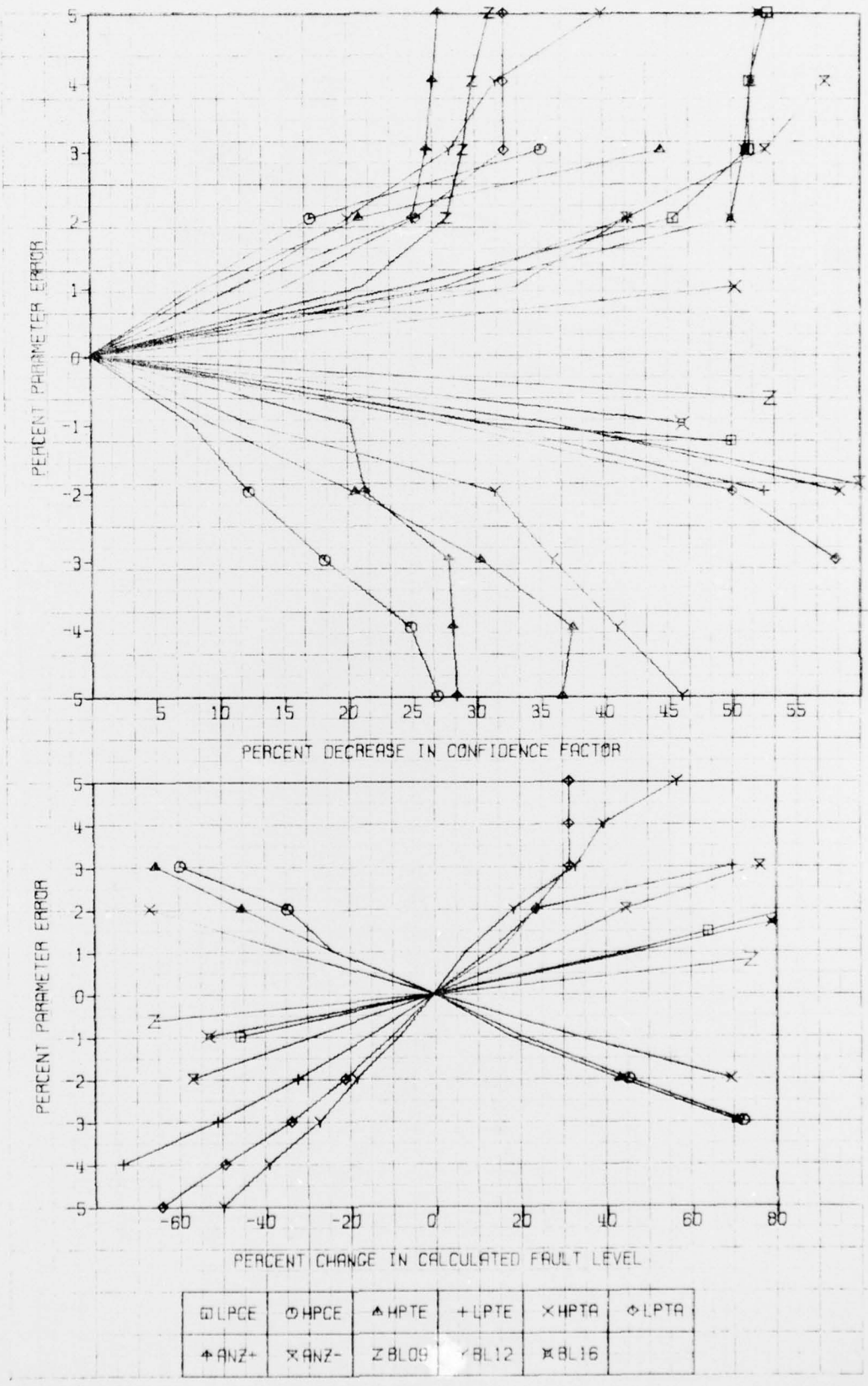
PERCENT PARAMETER ERROR
PERCENT DECREASE IN CONFIDENCE FACTOR
PERCENT PARAMETER ERROR
PERCENT CHANGE IN CALCULATED FAULT LEVEL
LPCE
HPCE
HPTE
LPTE
HPTA
LPTA
ANZ+
ANZ-
BL09
BL12
BL16

FIGURE D-4

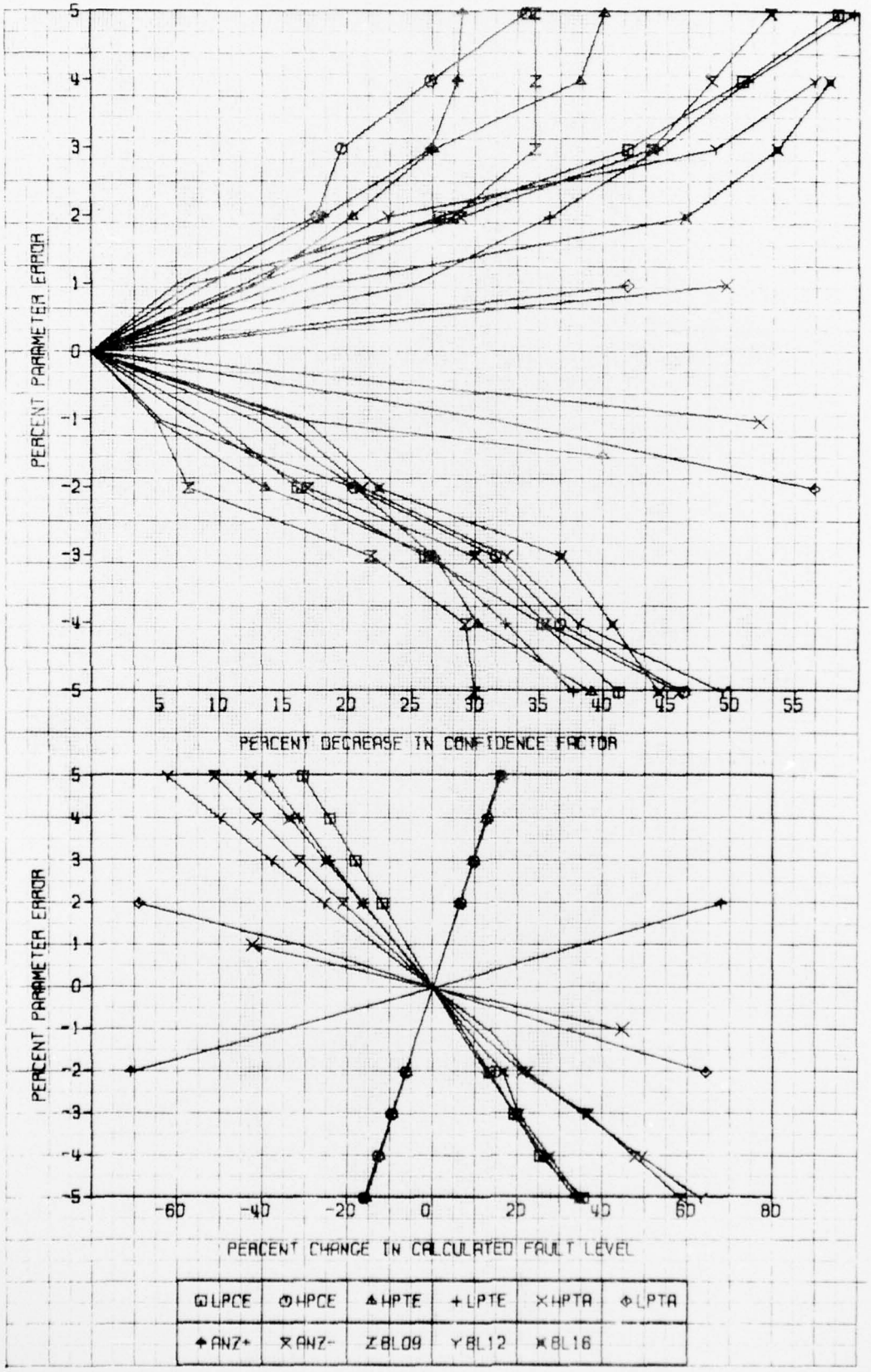
PERCENT PARAMETER ERROR
PERCENT DECREASE IN CONFIDENCE FACTOR
PERCENT PARAMETER ERROR
PERCENT CHANGE IN CALCULATED FAULT LEVEL
LPCE
HPCE
HPTE
LPTE
HPTA
LPTA
ANZ+
ANZ-
BL09
BL12
BL16

N1

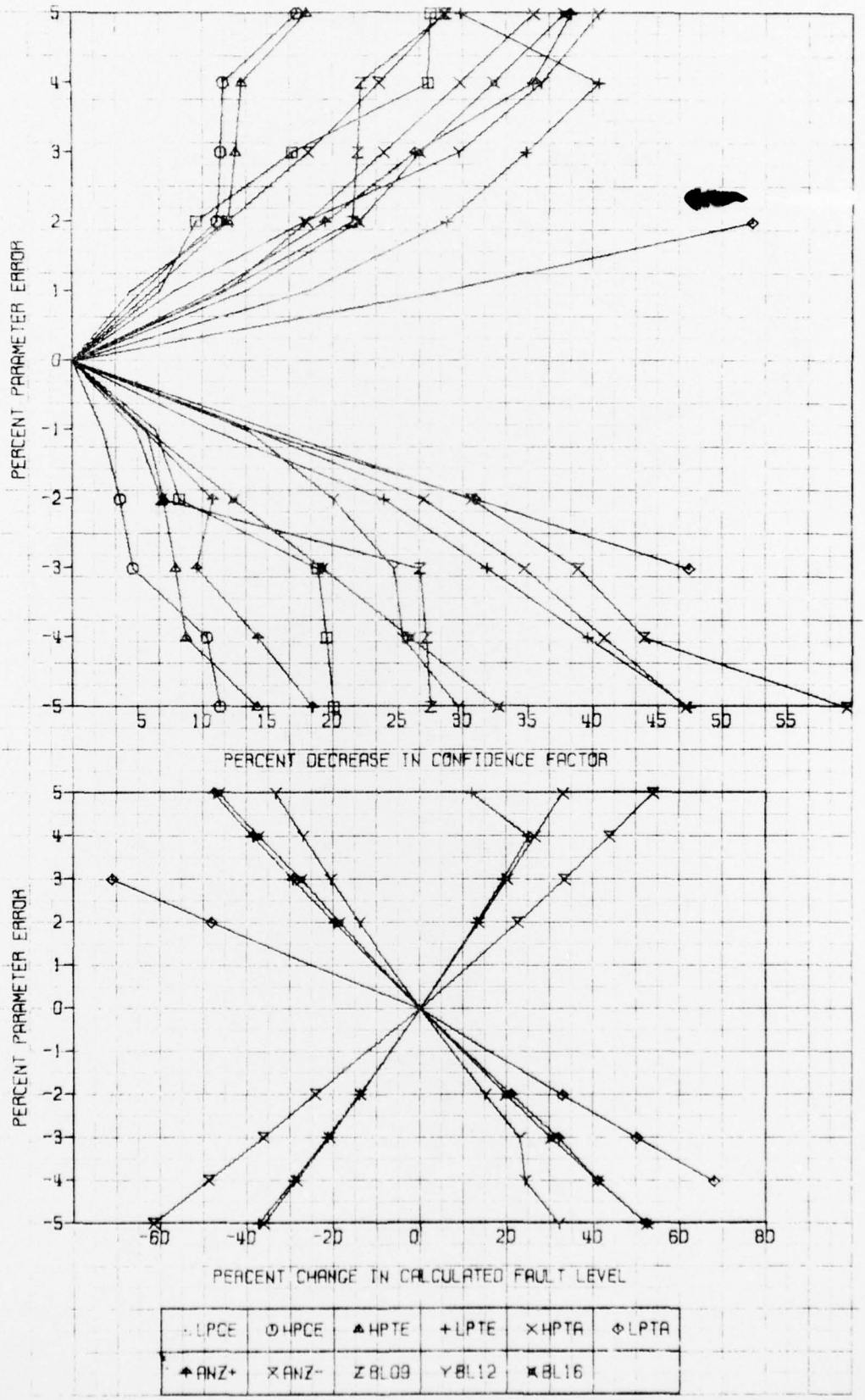
PERCENT PARAMETER ERROR
PERCENT DECREASE IN CONFIDENCE FACTOR
PERCENT PARAMETER ERROR
PERCENT CHANGE IN CALCULATED FAULT LEVEL
LPCE
HPCE
HPTE
LPTE
HPTA
LPTA
ANZ+
ANZ-
BL09
BL12
BL16

PT7

FIGURE D-6

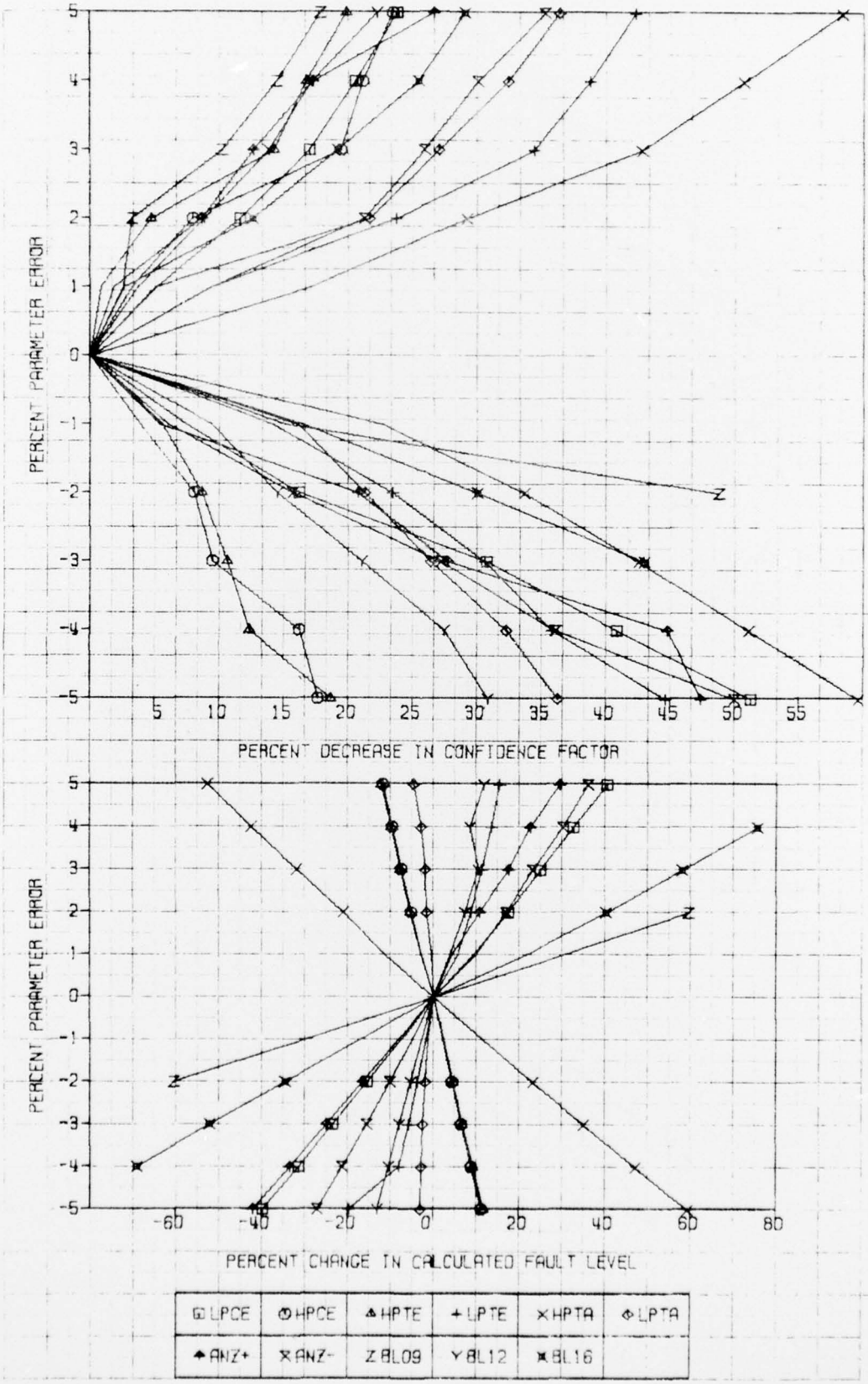

PT2

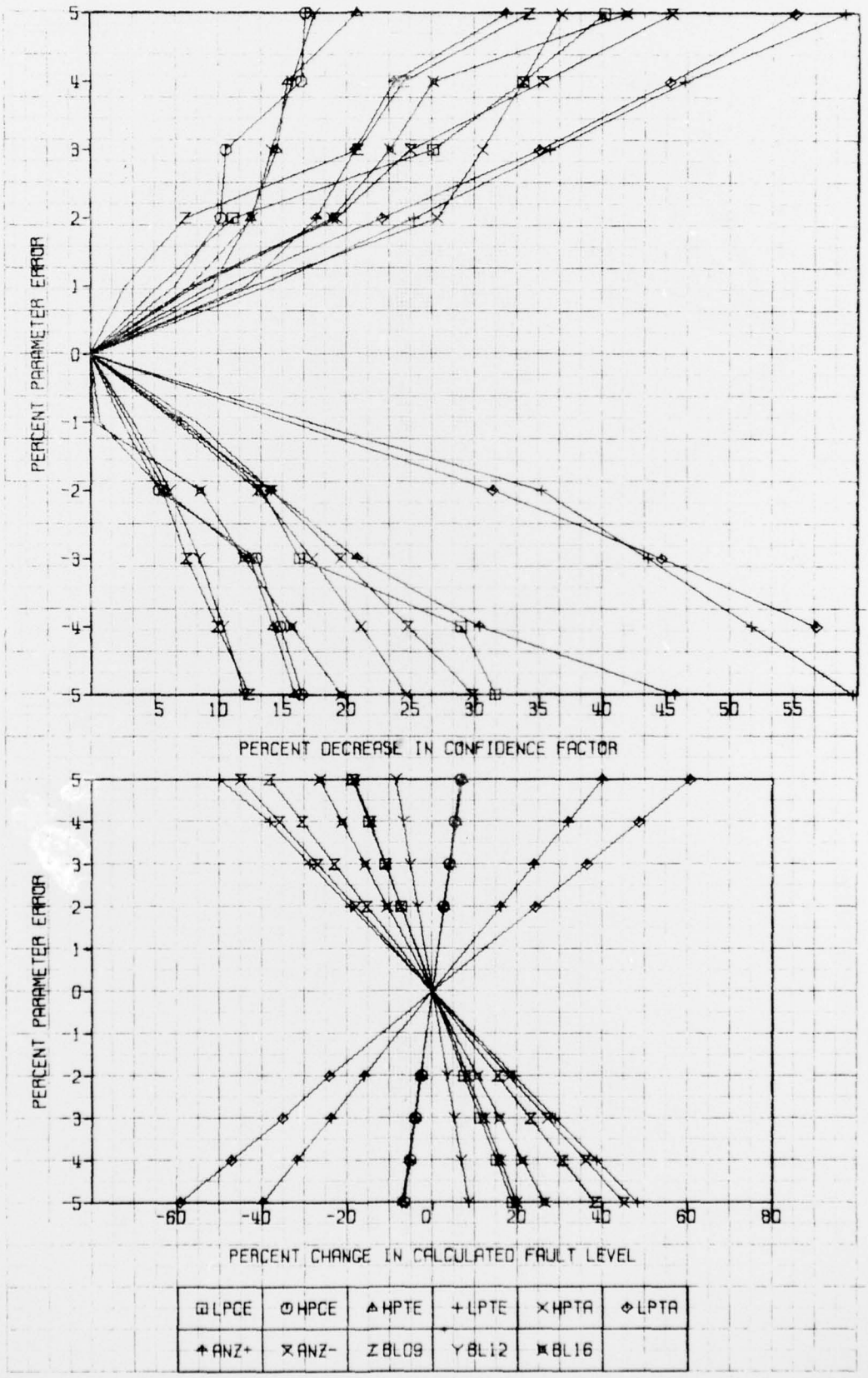
PERCENT PARAMETER ERROR
PERCENT DECREASE IN CONFIDENCE FACTOR
PERCENT PARAMETER ERROR
PERCENT CHANGE IN CALCULATED FAULT LEVEL
LPCE
HPCE
HPTE
LPTE
HPTA
LPTA
ANZ+
ANZ-
BL09
BL12
BL16

FIGURE D-8

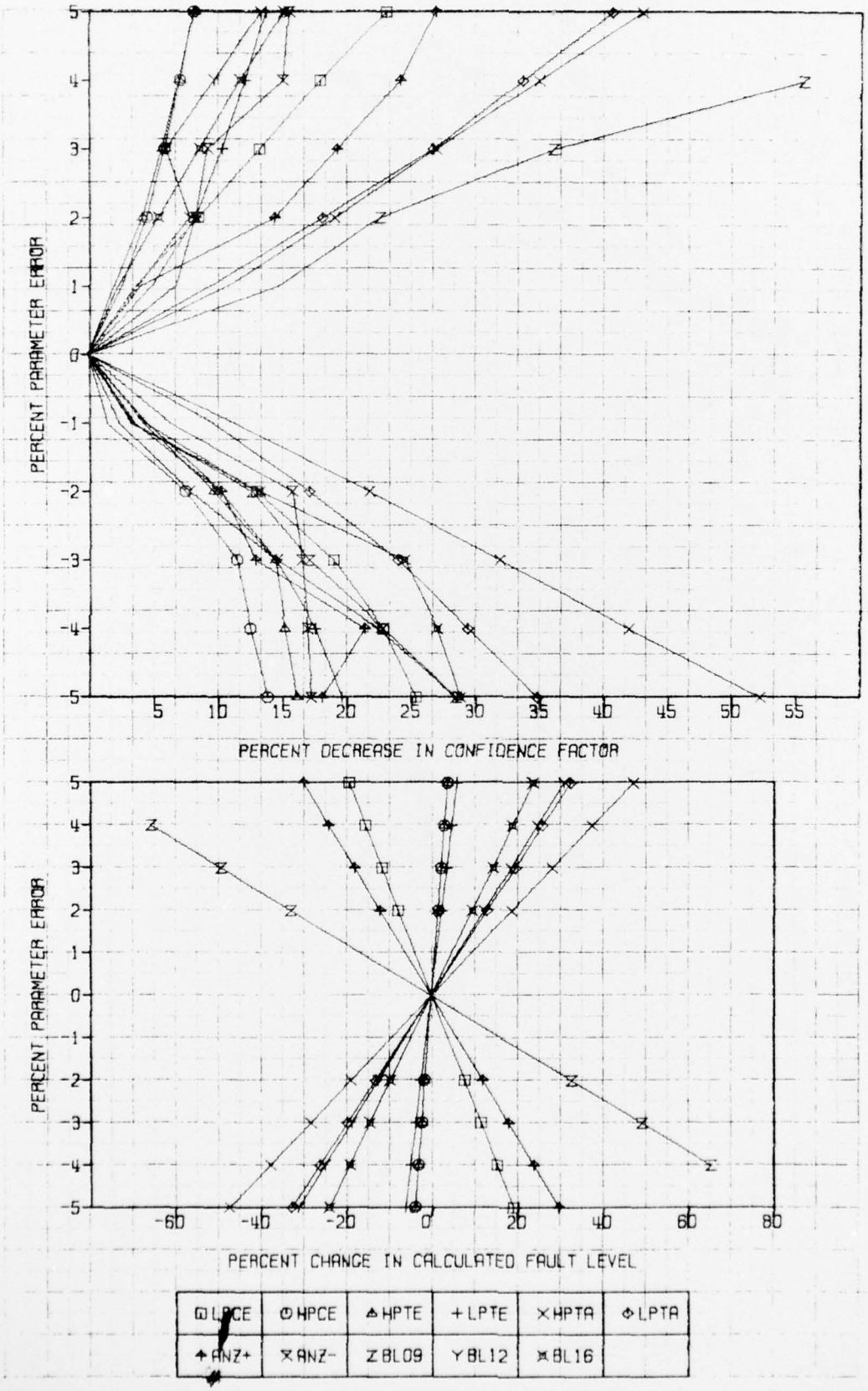
PERCENT PARAMETER ERROR
PERCENT DECREASE IN CONFIDENCE FACTOR
PERCENT PARAMETER ERROR
PERCENT CHANGE IN CALCULATED FAULT LEVEL
LPCE
HPCE
HPTE
LPTE
HPTA
LPTA
ANZ+
ANZ-
BL09
BL12
BL16

WF

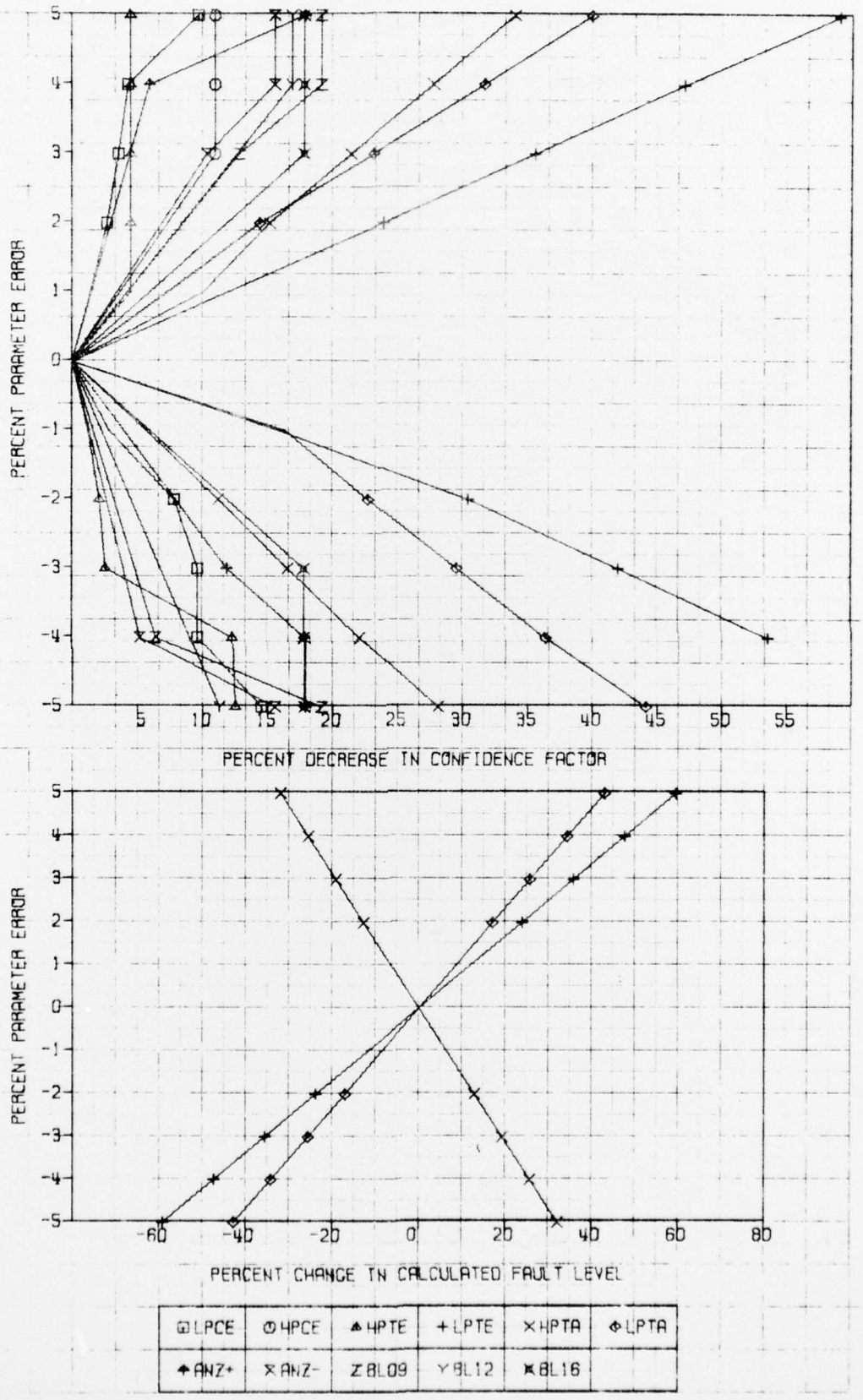
PERCENT PARAMETER ERROR
PERCENT DECREASE IN CONFIDENCE FACTOR
PERCENT PARAMETER ERROR
PERCENT CHANGE IN CALCULATED FAULT LEVEL
LPCE
HPCE
HPTE
LPTE
HPTA
LPTA
ANZ+
ANZ-
BL09
BL12
BL16

TT4

FIGURE D-10

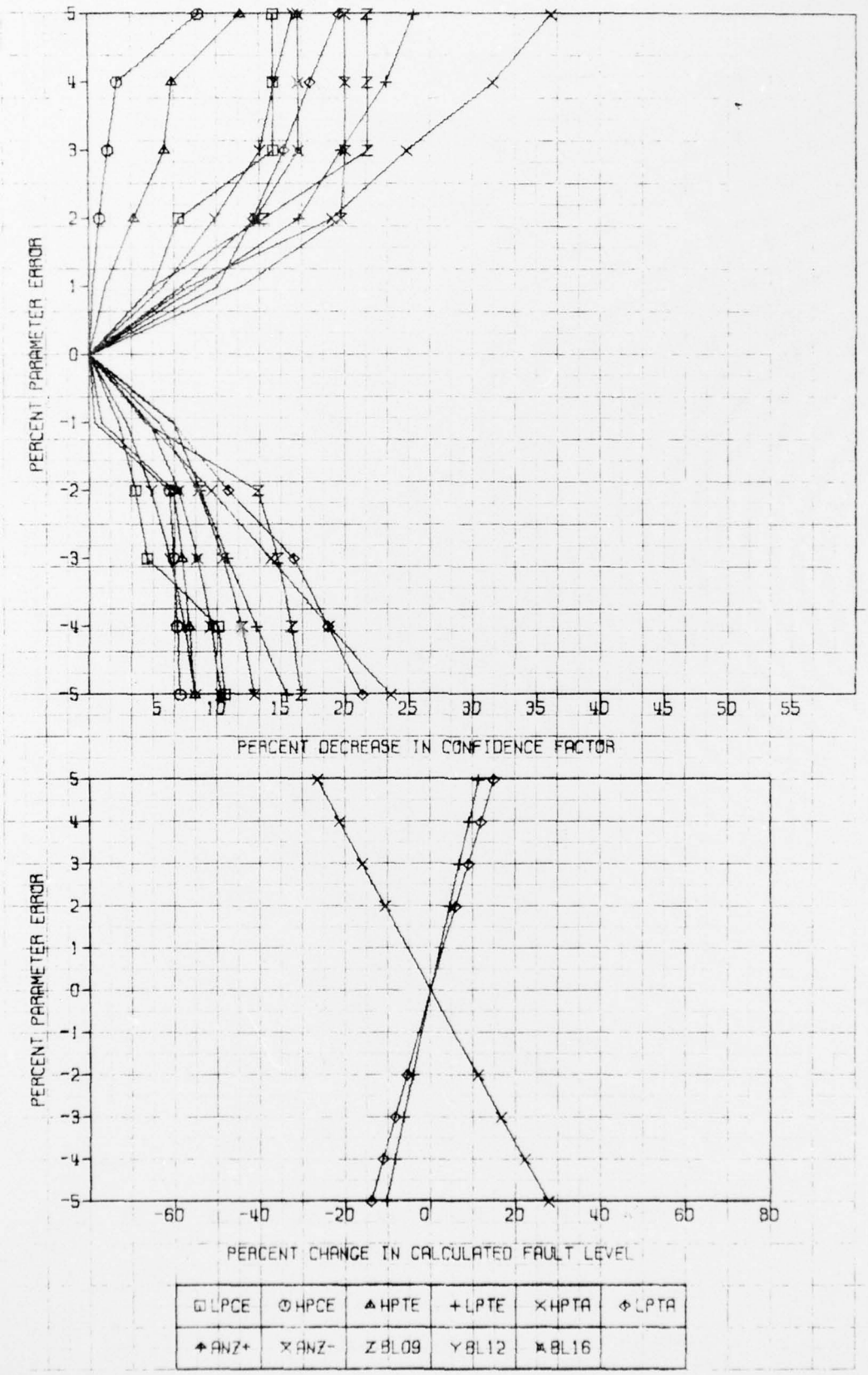

PB

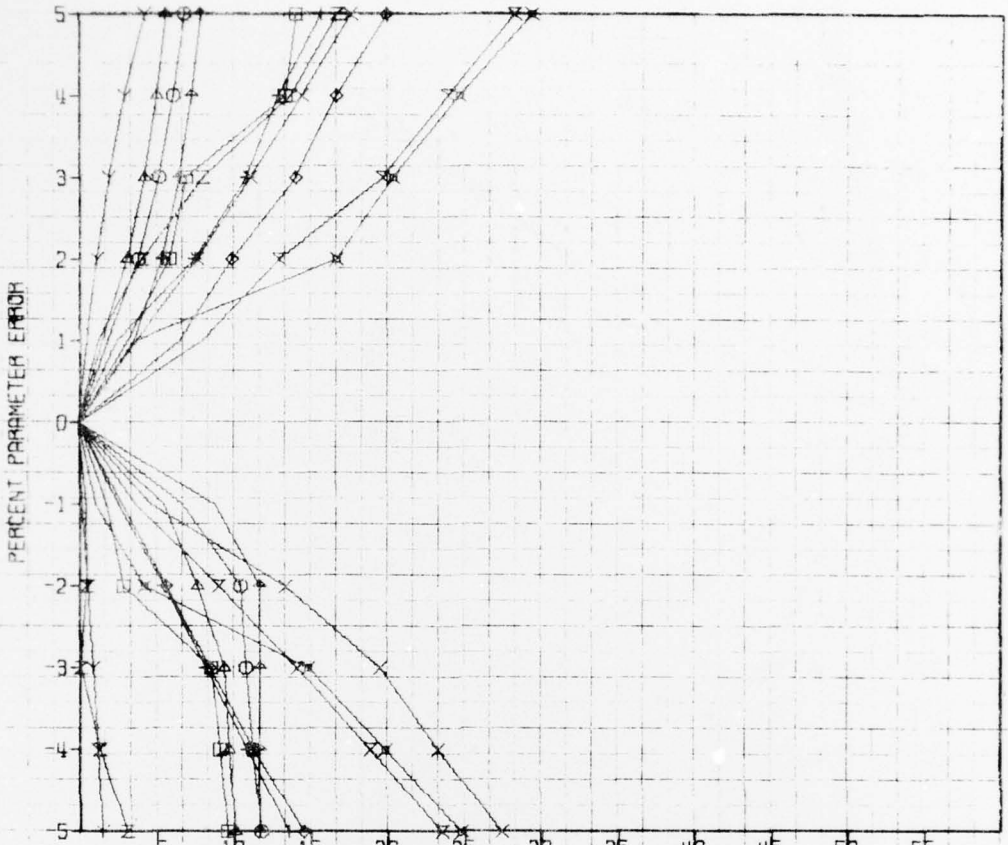

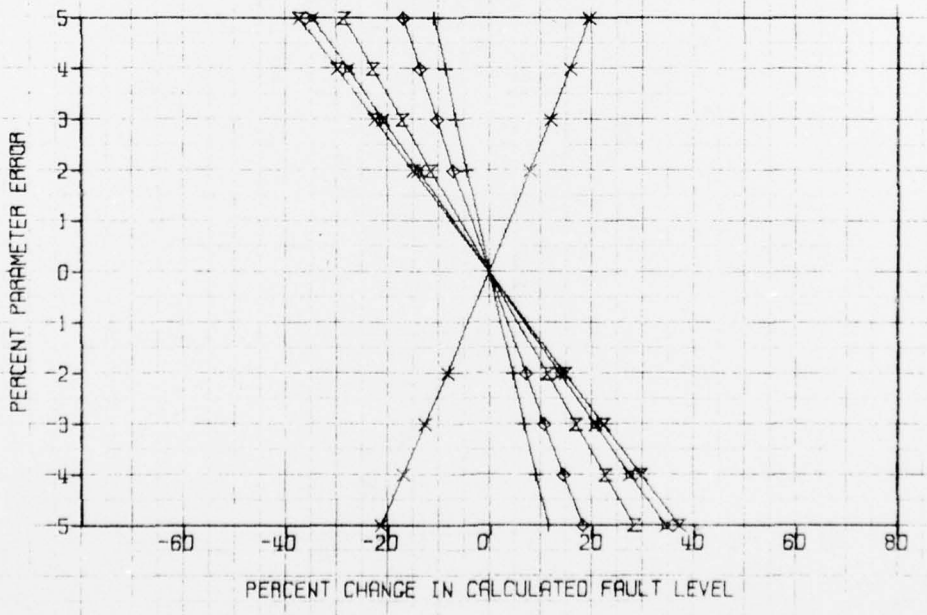

□ LPCE	Ø HPCE	△ HPTE	+ LPTE	× HPTA	◇ LPTA
✦ ANZ+	⧖ ANZ-	Z BL09	Y BL12	⧓ BL16	

FIGURE D-12

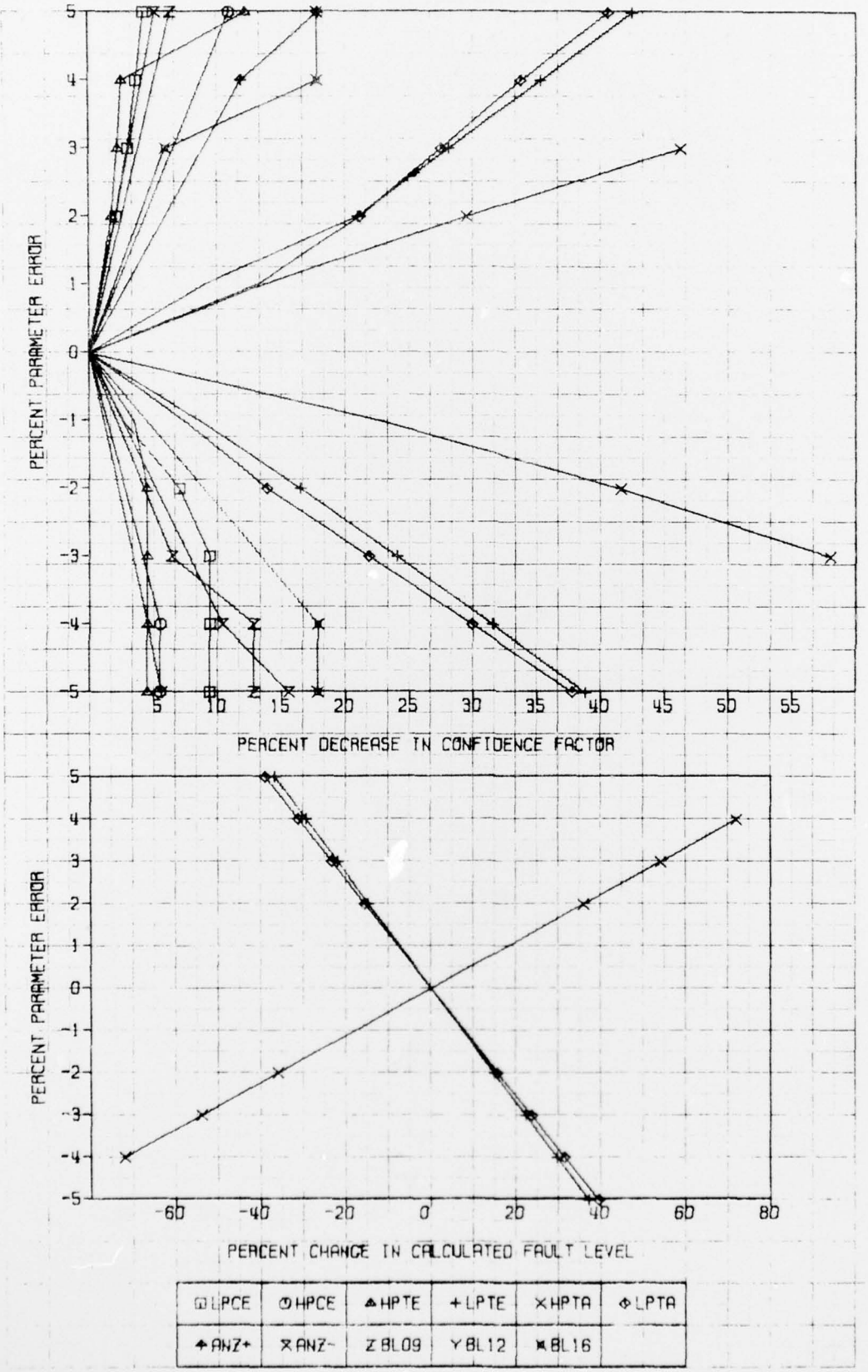

TT3

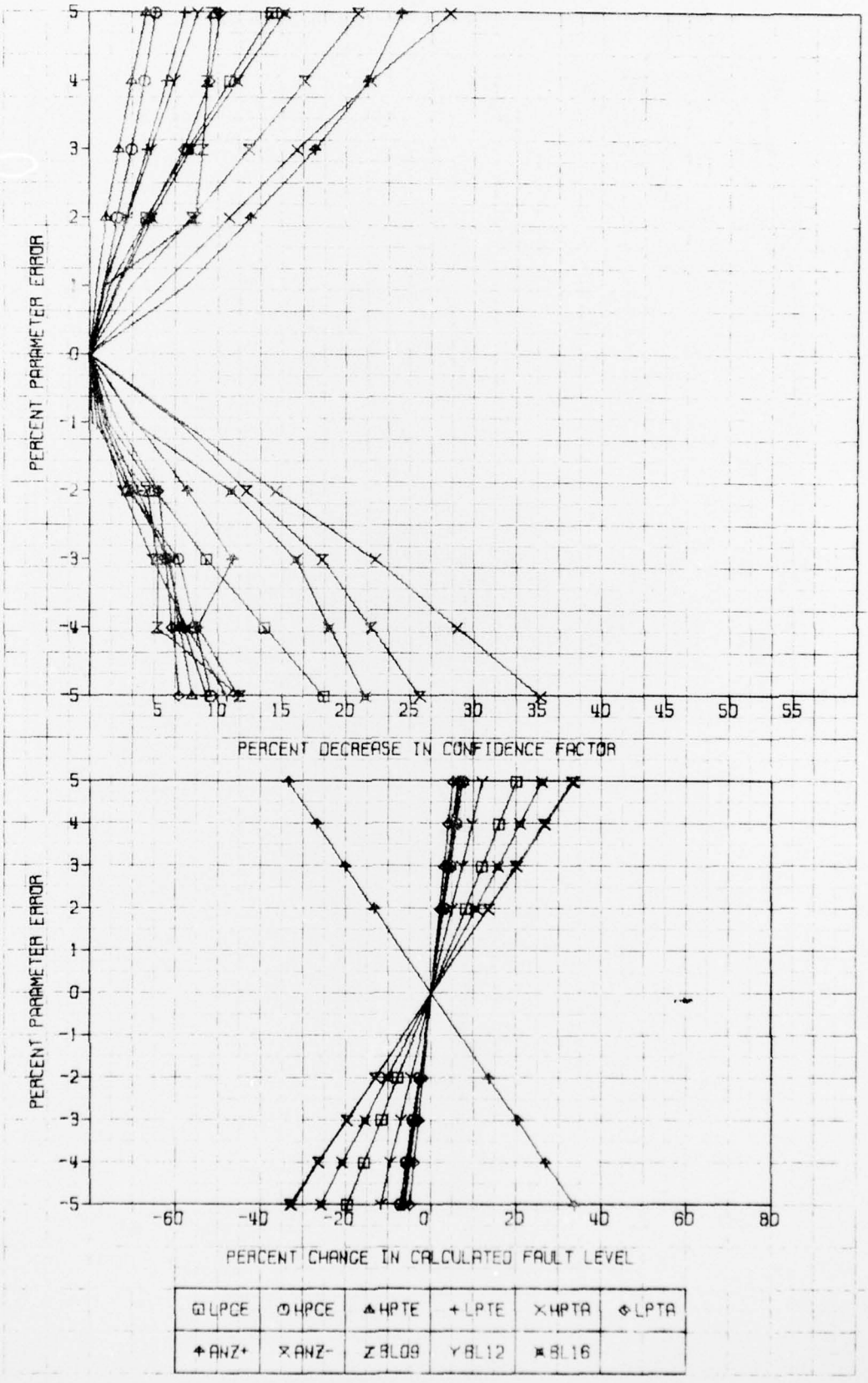
PERCENT PARAMETER ERROR
PERCENT DECREASE IN CONFIDENCE FACTOR
PERCENT PARAMETER ERROR
PERCENT CHANGE IN CALCULATED FAULT LEVEL
LPCE
4PCE
4PTE
LPTE
4PTA
LPTA
ANZ+
ANZ-
BL09
BL12
BL16

FIGURE D-14

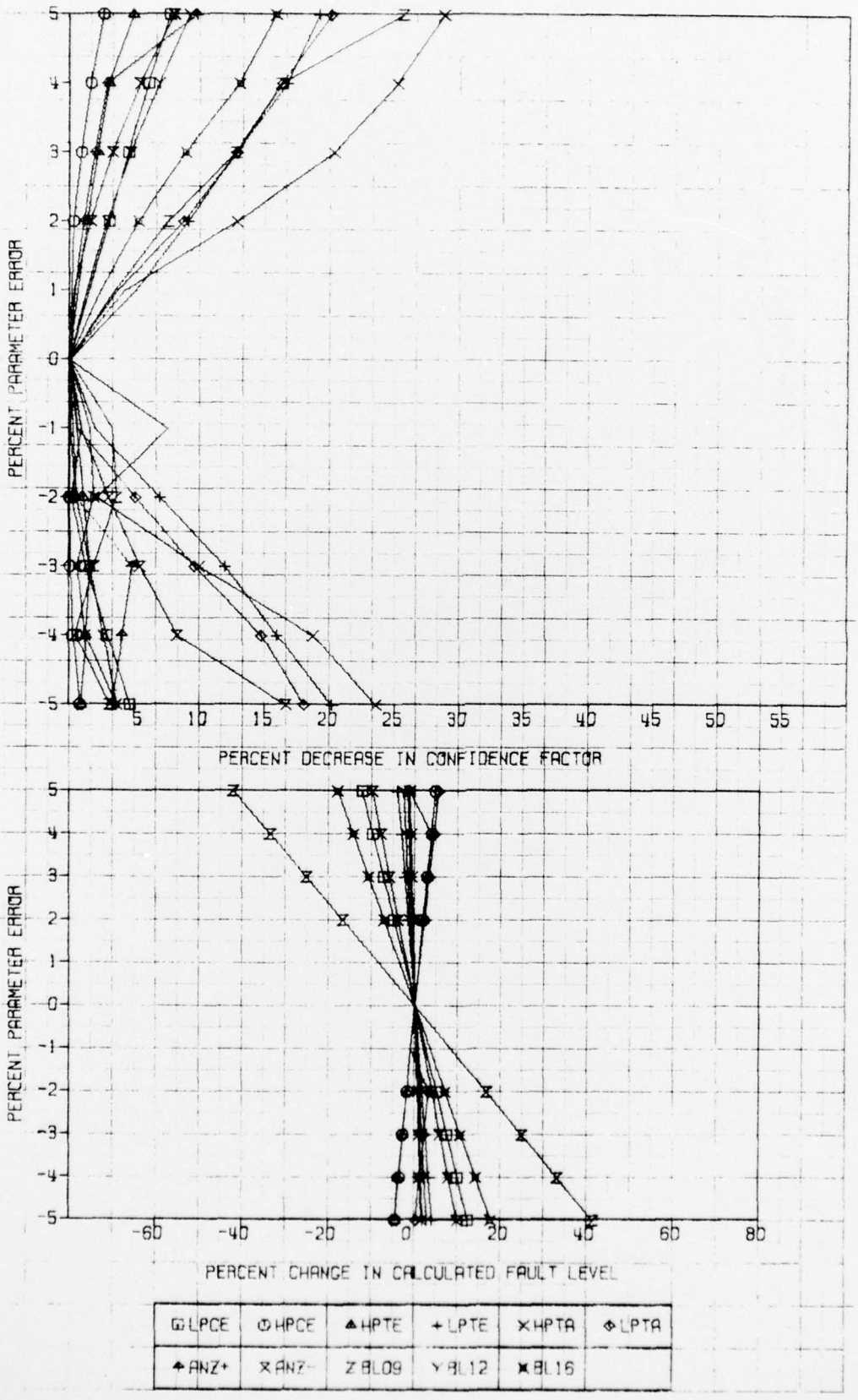
PERCENT PARAMETER ERROR
PERCENT DECREASE IN CONFIDENCE FACTOR
PERCENT PARAMETER ERROR
PERCENT CHANGE IN CALCULATED FAULT LEVEL
LPCE
HPCE
HPTE
LPTE
HPTA
LPTA
ANZ+
ANZ-
BL09
BL12
BL16

DISTRIBUTION LIST

Activity	Copies
Naval Air Systems Command (AIR-954), Washington, D.C. 20361	12
Intra-command Addressees:	
AIR-03E (1) AIR-330 (2) AIR-330C (2) AIR-340 (1) AIR-340D (1) AIR-340E (1) AIR-53632 (1) AIR-5343	
Defense Documentation Center for Scientific and Technical Information (DDC), Building No. 5, Cameron Station, Alexandria, Virginia 22314	12
Naval Air Engineering Center, Lakehurst, N.J. 08733	1
Naval Air Development Center (VT1), Warminster, Pennsylvania 18974	1
Naval Ship Engineering Center, Philadelphia Division (SEC 6700) Philadelphia, Pennsylvania 19112	1
Naval Air Test Center, Service Test Division, Patuxent River, Md 20670	1
Naval Air Test Center, Flight Test Division, Patuxent River, Md 20670	1
Director, Test Activities (AIR-06T), Naval Air Systems Command, Patuxent River, Maryland 20670	1
Naval Postgraduate School, Monterey, California 93940	2
Naval Safety Center, Naval Air Station, Norfolk, Virginia 23511	1
Federal Aviation Administration, Administrative Standards Division (MS-110), 800 Independence Avenue, S.W., Washington, D.C. 20590	1
Commanding General, U.S. Army Aviation Systems Command (AMSAV-ERS), 12th and Spruce Sts., St. Louis, Missouri 63166	1
Director, Eustis Directorate, U.S. Army Air Mobility Research and Development Laboratory (SAVDL-EU-AS), Fort Eustis, Virginia 23604	1
Commander, Air Force Wright Aeronautical Laboratories (AFFDL), Wright Patterson Air Force Base, Ohio 45433	1
Commander, Air Force Wright Aeronautical Laboratories (AFAPL-TBP, K. Hamilton), Wright Patterson Air Force Base, Ohio 45433	1
Commanding General, U.S. Army Materiel Command (AMC-RD-FS), Building No. T-7, Washington, D.C. 20315	1
Commander, U.S. Army Electronics Command (AMSEL-VL-S), Fort Monmouth, New Jersey 07716	1
Headquarters, Air Training Command (LGMAA), Randolph Air Force Base, Texas 78148	1
Lewis Research Center, National Aeronautics and Space Administration, 21000 Brookpark Road, Cleveland, Ohio 44135	1